Fabrication, Modification, and Evaluation of Modular, Gelatin-Based Microcarriers for the Delivery of Progenitor Cells in Bone Tissue Engineering Applications

by

Chukwuma Ernest Nweke

A dissertation submitted in partial fulfillment
of the requirements for the degree of
Doctor of Philosophy
(Macromolecular Science and Engineering)
in the University of Michigan
2022

Doctoral Committee:

Professor Jan Stegemann, Chair
Professor David Kohn
Professor Brian Love
Professor Geeta Mehta

Chukwuma E. Nweke

nwekec@umich.edu

ORCID iD: 0000-0002-6986-5067

Dedication

This dissertation is dedicated to my family, for their unwavering love and support. If not for their wisdom and patient guidance, I would not be here today.

Acknowledgements

I would like to first thank my doctoral advisor, Dr. Jan P. Stegemann. Your consistent accommodation and insight have been indispensable in my journey as a developing researcher. I'm forever appreciative of the many experiences and opportunities that I've been exposed to as a member of the CMITE lab. They have been instrumental in my progress in the face of what sometimes felt like impassable obstacles. I would also thank the rest of my committee, Drs. David Kohn, Brian Love, and Geeta Mehta for availing me of their time and knowledge as my project has taken shape. Thankfully, I've had the great fortune to work alongside several skilled researchers, like Dr. Gopinath Tiruchinapalli, Dr. Brandan Walters, Dr. Ramkumar Annamalai, Dr. Nicholas Schott, Dr. Eric Hobson, and Nicole Friend. Their collective scientific expertise has been incalculably beneficial to me throughout the years. And finally, I want to recognize funding sources like the Rackham Merit Fellowship Program and the Tissue Engineering and Regeneration T32 Training Grant Program, without which I would not have been able to complete this work.

Table of Contents

List of Figures

Abstract

Complete regeneration of large bone defects is constrained by metabolite diffusion and spatiotemporal limits to osteogenic cue distribution. Macroscale bone filler osseointegration is relatedly hampered by limited cytocompatibility and infill of large voids. In this project, cellularizable, injectable microcarriers were thus developed with the goal of creating a mechanobiologically osteogenic bone filler material. Gelatin-based microcarriers (GmC) crosslinked with genipin were emulsified and the effect of impeller geometry and stirring rate on microparticle morphology were examined. GmC were seeded at varying densities with mesenchymal stromal cells (MSC) and were evaluated physically and biologically. The effect of GmC matrix composition was examined by varying gelatin concentration and exogenous addition of hydroxyapatite (HA) and/or solution-mineralization. Suspension culture of GmC in a fibrin carrier gel was examined to determine the effect on MSC localization and phenotype, and as a model of GmC delivery.

In a first study, GmC size was modulated to produce microparticles suitable for injectable delivery. Seeding density of MSC was modulated to maximize osteogenic response. Particle size was negatively related with impeller rate. Increasing the rotation rate of an axial impeller (1.0 mm blade diameter) from 250 rpm to 500 rpm decreased particle diameter from 341.7±17.0 μm to 177.3±13.0 μm. A corresponding experiment with 0.3 mm diameter impeller resulted in a diameter decrease from 173.2±9.4 μm to 86.2±14.2 μm. MSC-seeded GmC were cultured in packed beds, loosely simulating a void-filler environment. All conditions exhibited increased DNA-normalized

calcium deposition over three weeks of culture, though the effect was most pronounced in osteogenic medium.

In a follow-on study, GmC were modified to enhance stiffness-induced osteogenesis. Size and shear modulus (G') were positively related with increasing gelatin and hydroxyapatite content. The diameter of 6.0% gelatin GmC increased from 86.2±14.20 μm to 149.6±6.2 μm in 14.0% GmC. Hydroxyapatite addition increased the diameter of 6.0% GmC from 80.3±7.1 μm to 149.5±4.3 μm with 5.0% HA. Rheometric mechanical characterization revealed increasing gelatin and hydroxyapatite concentration to be related with matrix stiffness. G' of 6.0% gelatin matrix was increased from 34.7±3.7 kPa to 47.5±3.7 kPa in 14.0% gelatin. HA addition increased G' of 6.0% gelatin to 70.8±2.9 kPa in 10.0% HA. Cytocompatibility related with gelatin:HA ratio and all seeding efficiencies exceeded 92%. Viability and DNA were negatively related with calcium content and peaked after one week of culture. DNA-normalized ALP and calcium deposition were upregulated in all conditions, indicating osteogenicity even in the absence of supplements.

Lastly, MSC were pre-seeded onto or simultaneously mixed with GmC in a fibrin matrix to suspend and culture cells in carrier gel. Both seeding methods resulted in osteogenic activity on 6.0% and 14.0% gelatin GmC. Notably, DNA content was essentially maintained over three weeks in culture, which had been a limitation in previous studies, particularly when calcium was present in the GmC. Calcium deposition was markedly increased in osteogenic medium in both GmC types and seeding models, suggesting that a protein carrier gel may allow improved osteogenic development of GmC.

Overall, this research illuminates processing-structure-function relationships in mechanobiologically osteoinductive, non-toxically genipin-crosslinked GmC designed for long-term bone-filling applications. Microcarriers can be used to culture and deliver progenitor cells,

and to potentiate their osteogenic ability. Packed-bed culture and delivery in a protein matrix can create an environment to enhance formation of new bone tissue, and may have utility for treatment of large bone defects.

Chapter 1 Project Aims

Healing of large bone defects remains an important clinical challenge due to limited osseointegration of bone cell-depleted implants. Critically-sized defects can occur from trauma, surgical resection, or avascular necrosis. In severe cases, extensive non-healing bone defects result in non-unions that greatly reduce the quality of life for afflicted patients. Repair of such defects calls for a defect-bridging cellularized therapeutic intervention to replace and regenerate lost bone tissue. Current autologous and allogeneic bone grafts have demonstrated less than ideal osseointegration in addition to limited availability. Accordingly, this project has been constructed in a manner meant to develop an abundant, modularly-injectable, cytocompatible space-filling platform that promotes osteogenesis and/or supports osteogenic enhancements. These objectives were addressed through the design and study of a bone tissue-simulative gelatin-based microspherical module, tailorable through mineral matrix-reinforcement for potential mechanobiological osteoinduction.

The initial step in this research, contained in Chapter 2, was a thorough review of the literature available on microsphere or microcarrier cell culture platforms. These microparticles are typically spherical and ranging between average diameters of 1 and 1,000 microns. The resulting literature review covers many of the much more traditional applications for microcarriers in cell expansion, as well as a more recently developed variety designed for tissue implantation or static in-vitro culture of progenitor cells.

Chapter 3 is comprised of the development and refinement of a method for producing the cell-instructive, space- or bone-void- filling microspheres. Generally speaking, gelatin has a few

very relevant properties. Gelatin, itself, is known to be highly cytocompatible and widely, commercially available, making it a useful replacement for bone matrix products. Also, it is essentially disorganized collagen, which is a key component of bone tissue. This makes it more simulative of the bone tissue microenvironment, compositionally. Literature suggests that such an environment can be osteoconductive, if not osteoinductive. Gelatin, when crosslinked with suitable chemistry, can be tailored to mechanical stiffnesses which engender mechanical stimulation of attached cells into an osteogenic differentiative lineage. These properties combined with the injectable size and shape of microcarriers generated in the work of this chapter were, based on information discovered in Chapter 2, to likely promote more uniform volumetric bone tissue regeneration. In particular, specific cell-matrix interactions were harnessed to independently promote osteogenesis on discrete microcarriers.

The work of Chapter 4 involves experimentation with methods of further improving on the novel, osteogenically-stimulative micro-modular matrix developed for Chapter 3. The scientific premise of this project is that mechanobiological cell-matrix interactions can effectively guide progenitor cell differentiation and function independently of exogenously-supplied factors post-potential-implantation. These micro-modular substrates were mechanically tailored through the modulation of gelatin, hydroxyapatite, and post-emulsification mineralization composition. As in the previous chapter, these cell-presenting microcarriers were then combined into consolidated, deliverable osteogenic modules.

The goal of Chapter 5 was to embed microcarriers within a fibrin matrix along with cells to simulate an implant environment and study the retention of osteogenic activity. Essentially, the most osteogenically-beneficial types of GmC tested from earlier chapters were reused in this chapter. Seeding methods were assessed for any potential osteogenic impact.

The approach of this work was to use the common, bone tissue-simulative materials of stiff gelatin-based microcarriers (GmC) to culture human bone marrow-derived stem cells (MSC) and guide their differentiation within and without a tissue-simulative environment. It probes the capacity for osteogenic differentiation of MSC on GmC through key indicators of bone-formation, validated through the following Aims:

1.1 Aim 1: Fabricate GmC that support osteogenic differentiation of MSC.

Analyze GmC size, mechanical properties, and biological impact on surface-cultured MSC. Results establish MSC carrying capacity, matrix stiffness, and a baseline osteogenic effect for generated GmC.

1.2 Aim 2: Promote the osteogenic potential of GmC using specific biomaterial modification schemes.

Improve the osteogenicity of GmC modules through gelatin modulation, hydroxyapatite embedment, or solution-based mineralization strategies. Results build on those of the previous aim, assessing the influence of these modifications.

1.3 Aim 3: Evaluate the osteogenic potential of MSC-GmC modules in tissue implant-mimic carrier gel culture.

Culture and assess MSC osteogenic phenotype on GmC within a fibrin-based carrier gel. Key endpoints include biological asssay of fibrin gel-bound MSC.

Chapter 2 Background

A variety of materials-based approaches to accelerate the regeneration of damaged bone have been developed to meet the important clinical need for improved bone fillers. This comprehensive review covers the materials and technologies used in modular microcarrier-based methods for delivery of progenitor cells in orthopaedic repair applications. It provides an overview of the field and the rationale for using microcarriers combined with osteoprogenitor cells for bone regeneration in particular. The general concepts and methods used in microcarrier-based cell culture and delivery are described, and methods for fabricating and characterizing microcarriers designed for specific indications are presented. A comprehensive review of the current literature on the use of microcarriers in bone regeneration is provided, with emphasis on key developments in the field and their impact. The studies reviewed are organized according to the broad classes of materials that are used for fabricating microcarriers, including polysaccharides, proteins and peptides, ceramics, and synthetic polymers. In addition, composite microcarriers that incorporate multiple material types or that are mineralized biomimetically are included. In each case, the fabrication, processing, characterization, and resulting function of the microcarriers is described, with an emphasis on their ability to support osteogenic differentiation of progenitor cells in vitro, and their effectiveness in healing bone defects in vivo. In addition, a summary of the current state of the field is provided, as are future perspectives on how microcarrier technologies may be enhanced to create improved cell-based therapies for bone regeneration.

2.1 Microcarriers in orthopaedic regenerative medicine

The need for new materials and methods to accelerate and improve bone healing outcomes has stimulated a broad field of research aimed at potentiating bone regeneration (Chen et. al., 2013; Kim et.al., 2005). Although many bone fractures heal adequately without intervention, there is an unacceptably large number of cases each year in which bone heals sub-optimally, or in some cases fails to heal, which can lead to serious morbidity and chronic non-union (Hsu et.al., 1999; Roberts et. al. 2012; de Grado et. al., 2018). In these cases, more advanced therapeutic approaches are needed, and there has been a strong emphasis on developing new, more potent bone fillers and engineered bone constructs that can regenerate bone even in challenging situations (Hsu et.al., 1999). The development of engineered bone has shown promise in creating bulk tissue constructs that can rapidly fill a defect and support surrounding tissue (Kim et.al., 2005). However, these approaches are hampered by the need for invasive surgery, a lack of new bone ingrowth, and potential compliance mismatch with surrounding tissues (Hsu et.al., 1999; Ethirajan et. al., 2008).

The drawbacks of monolithic, macroscale engineered constructs have motivated the search for alternative strategies to treating large bone defects. In particular, there have been increasing efforts to develop modular approaches, in which discrete biomaterial or engineered tissue units are combined to create bone fillers that can be handled as slurries or pastes (Ethirajan et. al., 2008; Malda et. al., 2006; Barrias et. al., 2005; Declerq et. al., 2005) The concept behind such semisolid systems is that these fillers can have transient fluidic properties sufficient for conformably filling irregularly-shaped cavities, while also allowing immobilization in the defect and providing support of the surrounding tissues as regeneration occurs. These bone-replacement materials are generally designed to be osteogenic in nature, such that they engender biomimetic mineralization of calcium phosphate minerals or allow the subsistence of cells that are capable of fulfilling this role. In

addition, such modular systems can be designed for minimally invasive delivery, which has the potential to reduce residual pain, adverse scarring, and the risk of infection.

The field of orthopaedic repair has progressed as new biological approaches to tissue regeneration have been developed and proven effective. Over the past two decades, the subfield of orthobiologics has evolved to encompass a wide range of biological and bioactive materials that promote healing of musculoskeletal tissues (Calcei et. al., 2019). In addition to autografts and allografts, therapies involving growth factor delivery (Roberts et. al., 2012; Fernandez et. al., 2018; Winkler et. al., 2018), marrow- (Roberts et. al., 2012; Calcei et. al., 2019) and plasma-concentrates (Roberts et. al., 2012; Fernandez et. al., 2018; Calcei et. al., 2019), and transplantation of progenitor cells (Calcei et. al., 2019) are being developed and tested in the clinic. These approaches require specialized biomaterials designs and chemistries to promote the desired bioactivity and resulting biological responses. In particular, the delivery of cells presents a challenge in ensuring the viability, maintenance, and stimulation of differentiated function that is required for an effective cell-based therapy. In response to these needs, a variety of cell-based approaches to orthobiologic bone repair have been developed, using a wide range of materials (Verrier et. al., 2016). In addition, a diverse set of cell types, sources, and formulations have been applied to potentiate the regeneration of bone.

The development of microcarriers for cell delivery combines the discrete modular approach to tissue engineering with the bioactive strategies of orthobiologics. The use of such engineered particulate materials is a promising strategy to create functional bone fillers. While there has been considerable effort to develop therapies based on macroscale particles with diameters in the millimeter range (Verrier et. al., 2016; Chao et. al. 2015), there has been less emphasis on establishing microscale approaches. Engineered microcarriers have the advantage that they can be

designed to be conducive to cell attachment, to promote cell differentiation, and to degrade at a controlled rate. Their shape and size can be tailored to accommodate a range of cell densities and to form injectable microcarrier populations for downstream injectability. The composition and properties of such a carrier material can also be tailored to facilitate delivery, distribution, and immobilization of the microcarrier phase. These features make microcarrier-based delivery systems attractive for bone regeneration applications.

2.2 Microcarriers as vehicles for cell culture and delivery

Cellular therapies typically require large numbers of cells and the production of this biomass can be a barrier to creating an effective therapy. The high surface area to volume ratio afforded by the use of microcarrier-based cell culture, relative to standard two-dimensional culture in flasks or dishes, makes it attractive for generating large cell populations. A large surface area allows proliferation and expansion of cells adhered to the microcarrier surface. In some applications, biochemicals secreted by the adhered cells are harvested for therapeutic or other uses (Chen et. al., 2013; Blüml et. al., 2007). In other applications, the cells themselves are harvested by enzymatically releasing them from the microcarrier surface (Hsu et. al., 1999). In addition, the use of suspension culture techniques, typically in stirred bioreactors, allows efficient delivery of nutrients and controlled diffusion gradients. Such culture systems have been used for over 50 years for a variety of cell types of commercial interest in the biotechnology industry (Blüml et. al., 2007). However, microcarriers have not been as extensively used in the field of tissue engineering, despite their advantages in sustaining high volume cell growth.

Mesenchymal stromal cells (MSC) are adult progenitor cells that have been used widely in regenerative medicine. They can be harvested from a variety of tissues, including bone marrow

and fat, and therefore offer a relatively accessible cell source for tissue engineering applications (Chen et. al., 2013; Calcei et. al., 2019). There is a broad literature on the isolation, expansion, characterization, and use of MSC for therapeutic purposes, though their exact mechanisms of action remain the subject of investigation. It is clear that these cells can secrete substances that potentiate regeneration through paracrine mechanisms (Winkler et. al., 2018; Sart et. al., 2015), and it has also been shown that they can have immunomodulatory effects (Tseng et. al., 2012; Goncharenko et. al., 2017). The range of their differentiation capacity is still a subject of debate; however, it is generally accepted that MSC can act as progenitors for bone, cartilage, and adipose tissues (Chen et. al., 2013; Sart et. al., 2013). In particular, it is well established that MSC form mineralized tissues when exposed to the appropriate environment, both in vitro and in vivo (Verrier et. al., 2016; Sart et. al., 2013). Therefore, MSC are a valuable cell source in bone regeneration applications, particularly in situations where native progenitor cells are depleted and/or cannot be mobilized to the site of injury. In these instances, transplantation of MSC offers a way to enhance bone tissue repair. However, there is a need for improved methods to culture, differentiate, and deliver MSC for therapeutic purposes.

The combination of MSC and microcarrier culture is a promising way to culture, differentiate, and deliver potent progenitor cells in large numbers. Careful selection and design of the materials used to fabricate the microcarrier substrate offers a mechanism for controlling cell proliferation and differentiation. Furthermore, the modular microcarrier format allows delivery of the cultured cells while still attached to a supportive and potentially bioactive substrate. The implanted cells and microcarriers can be designed to degrade at a controlled rate post-transplantation, thereby releasing the attached cells and allowing new tissue to replace the bone filling implant. Advances in biomaterials science have made it possible to control the properties

of the microcarrier such that the desired biological functions are promoted over time. Therefore, microcarrier-mediated MSC delivery offers the possibility to tailor the spatial and temporal behavior of advanced bone graft materials.

The treatment of large and challenging bone defects using this strategy is particularly promising because these indications require a volumetric bone filler that has osteogenic properties. The microcarrier format allows large numbers of cells to be grown and differentiated under controlled conditions. It is likely that regeneration of larger defects will require the transplantation of billions and perhaps trillions of cells, and use of microcarriers in suspension culture and bioreactor systems facilitates scale-up and production of well-characterized batches for such therapeutic use. Furthermore, microcarrier-bound cells can be delivered directly to bone defects while leaving their cell-matrix contacts intact. The microcarrier matrix can therefore be designed to promote osteogenic differentiation, and this stimulus can be maintained both prior to and after cell transplantation. Importantly, the packed bed geometry of microcarrier populations facilitates diffusion and perfusion to supply nutrients to the cells post-transplantation, and therefore may perform better than other approaches in ischemic situations.

The following sections of this review provide a description of the materials and strategies that have been used to create microcarriers for cell-based regeneration of bone. It focuses on approaches designed for MSC and osteoblast culture and delivery, with an emphasis on the materials used to create microcarriers and their function in directing osteogenic processes. These materials are used alone and in combination to mimic key aspects of bone composition and function, while also providing a supportive and instructive substrate for living cells. In addition, this paper covers the fabrication and processing of microcarriers, and how they are cultured and delivered for bone regeneration applications. An impressive variety of approaches to modular

microcarrier-enabled bone regeneration have been developed. However, these technologies have yet to have an impact in the clinic. This review is aimed at describing the current state of knowledge in this still growing field by summarizing the approach and main findings of the studies that have been done to date, and the impact that these findings may have on future studies and translation of microcarrier-based bone regeneration technologies to the clinic.

2.3 Microcarrier Fabrication, Processing, and Characterization

Many microcarrier types are produced by simple emulsification, which offers the advantages of bulk processing and relatively high throughput. In general, batch emulsification involves mixing two immiscible liquids to create a dispersion containing a separated colloidal phase within a bulk continuous phase. The mixing rate and properties of the colloidal and bulk phases can be varied to control the size and size distribution of the resulting particles, and emulsification has proven well-suited to creating polymer and polysaccharide particles on the nano- and micro-meter scale. Water-in-oil emulsion techniques are often used to suspend a polymer solution within a processing oil, creating a spherical discrete phase within the larger continuous, nonpolar phase. This discrete phase can be easily settled out of suspension and is often extracted with the aid of secondary interface-stabilizing surfactants.

Microfluidic flow-focusing droplet generation is a modified version of bulk emulsification aimed at tight control of particle size. In these microfluidic systems, an aqueous polymer solution and typically a nonpolar oil or other fluid are co-extruded in a specific geometrical arrangement to produce consistently-sized droplets (Goncharenko et. al., 2017). The size of these droplets can be altered through inputs of the junction geometry for the intersecting fluids and the flow rates of each fluid. However, these systems are limited in the viscosity of the polymer solutions that can be used, and microcarriers are necessarily created one at a time, which can prolong production

times. One variation of the microfluidic flow-focusing technique uses a gas stream in the place of an oil phase. Such methods have been found particularly useful in the formation of ceramic particles (Barrias et. al., 2005; Ribeiro et. al., 2006; Barrias et. al., 2004; Barrias et. al., 2005; Lourenço et. al., 2017; Oliveira et. al., 2008; Mateus et. al., 2008). Once particles have been formed and crosslinked, they are washed, dried, and sintered at elevated temperature.

Coacervation-based production methods for microcarriers are typically similar in general set-up to batch emulsification techniques, as displayed in Figure 2.1. The term, coacervation, is often used in reference to complex coacervation processes involving the mixture of two distinct solutions of a cationic macromolecular species and an anionic macromolecular species. This generally induces conglomeration and precipitation of a concentrated colloidal phase. Simple coacervation, which is more common to the process of microcarrier fabrication, refers to the phase separation of a macromolecular solution from a more dilute continuous phase to produce a relatively concentrated particulate colloidal phase. This process is often triggered by a change in temperature or pH, and has been used to create microcarriers for cell culture. Coacervate particles, like water-in-oil emulsified particles, can be collected by centrifugation and subsequently processed to stabilize and modify their morphology (Shen et. al., 2013).

Post-fabrication processing of microcarriers often includes crosslinking of the matrix to impart stability, reduce swelling, and resist dissolution. A variety of chemical, thermal and photonic crosslinking methods can be applied to microcarriers. For osteogenic applications, covalent crosslinking using glutaraldehyde or other aldehydes is often used to chemically bind primary amine groups between macromolecules (Declerq et. al., 2005). Carbodiimide-based crosslinking of amines using 1-ethyl-3-(dimethylaminopropyl) carbodiimide (EDC) and N-hydroxysuccinimide (NHS) is also a commonly used stabilization method (Perez et. al., 2014). In

specific instances, other crosslinkers may be of use, for example the use of divalent cations to stabilize alginate-based materials (Lourenço et. al., 2017). Similarly, formed and stabilized microcarriers can be characterized using a variety of standard techniques. The size and morphology of microcarriers can be measured using optical microscopy-based imaging software or laser diffractometry-based dimensional estimation equipment (Kim et. al., 2005; Hsu et. al., 1999; Wu et. al., 2004). The composition of microcarriers can be determined using X-ray diffraction or Fourier transform infrared analysis (Kim et. al., 2005; Ethirajan et. al., 2008; Boanini et. al., 2011).

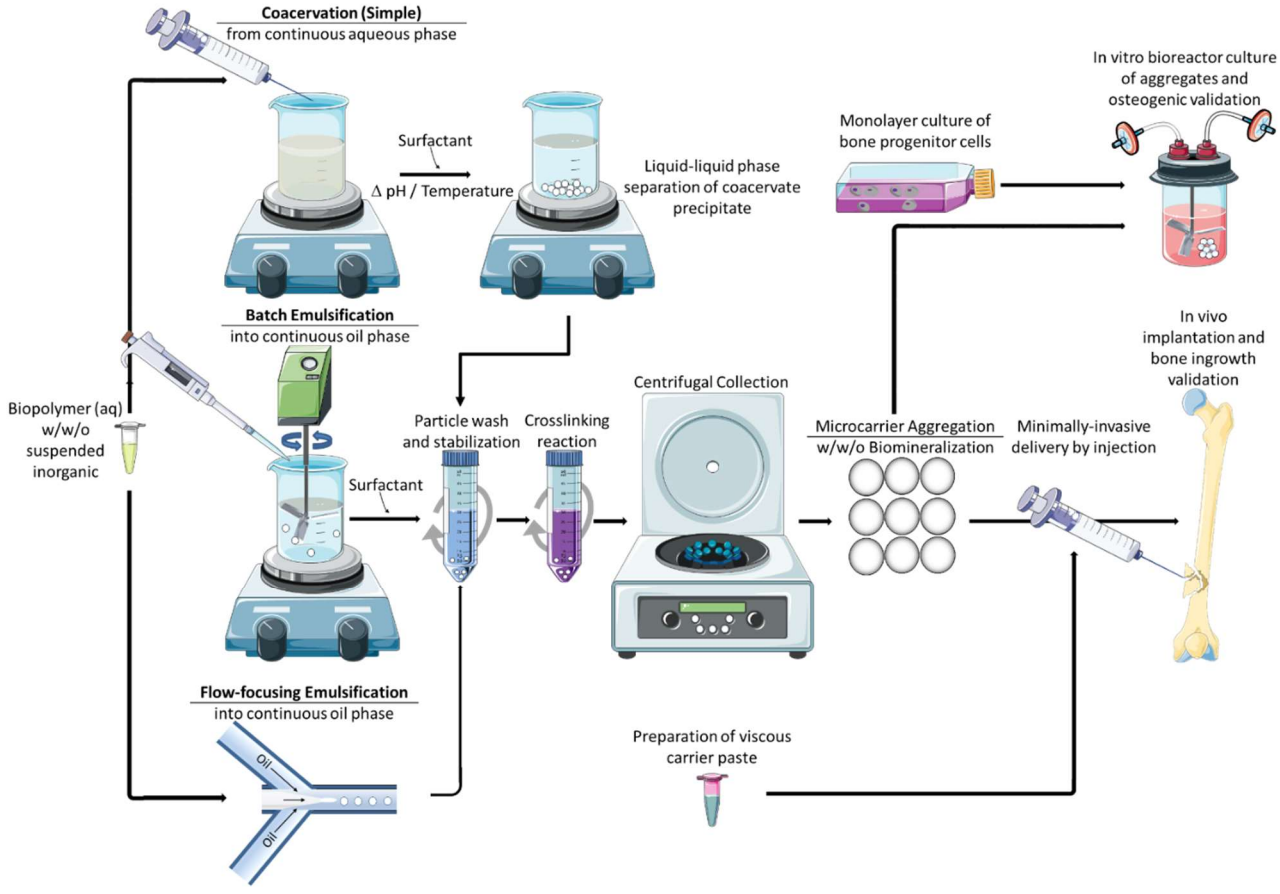

Figure 2.1: Schematic showing general microcarrier fabrication, processing, and application in bone tissue regeneration. Image contains altered elements from smart.servier.com.

Biomineralization is another common post-processing technique for microcarriers intended for bone regeneration applications (Park et. al., 2014; Maeda et. al., 2004; Shi et. al., 2011; Du et. al., 2013; Yu et. al., 2009). Calcium mineral can be incorporated directly into the matrix of microcarriers to better simulate the composition of native bone (Kim et. al., 2005; Hsu et. al., 1999; Wu et. al., 2004). In addition, incubation of microcarriers in high calcium concentration solution like SBF or Ringer's solution can be used to induce the deposition of a mineral phase (Park et. al., 2014; Maeda et. al., 2004; Shi et. al., 2011; Du et. al., 2013; Yu et. al., 2009). Control of the composition and thermodynamics of these techniques allows the tailoring of the mineral phase of microcarriers to promote desired functionality. Calcium phosphate mineral is often used because of its chemical similarity to carbonated apatite, a calcium-deficient form of hydroxyapatite that makes up as much as 65 wt% of adult bone (Braun et. al., 2003). Tricalcium phosphate is often added to microcarrier matrices (Perez et. al., 2011; Perez et. al., 2013; Park et. al., 2011), and this mineral phase can be transformed into hydroxyapatite through preferential dissolution of less stable calcium phosphate minerals and their recrystallization into more stable forms, in a process governed by the Ostwald-Lussac rule of stages (Mann et. al., 2001). Calcium carbonate-based minerals can be used in a similar manner, and under controlled conditions can be transformed into calcium phosphate mineral phases that resemble those in biological hard tissue (Maeda et. al., 204; Wang et. al., 2016). Furthermore, the inclusion of specific protein and polysaccharide materials in combination with such mineral phases is often applied to mimicking the physiological environment of bone (Kim et. al., 2005; Hsu et. al., 1999; Ethirajan et. al., 2008; Wu et. al., 2004; 42).

2.4 Microcarrier Materials, Characteristics, and Function

2.4.1 Polysaccharide-composite microcarriers

Polysaccharide materials are generally abundant and well characterized, and they have been used extensively to produce microcarriers. Commercially available products such as the cellulose-based Cytopore (Blüml et. al., 2007) and dextran-based Cytodex lines (Overstreet et. al., 2003) are polysaccharide microcarriers with varying size, composition, and porosity. Although Cytopore beads are generally more suited to the culture of Chinese hamster ovary (CHO) epithelial cells, baby hamster kidney fibroblasts (BHK-21), HeLa cervix cancer epithelial cells, and Vero kidney epithelial cells, the collagen-coated Cytodex line has been used in a number of bone progenitor cell studies (Kamiyah et. al., 1995). Cytodex beads made in the 150-250 μm range have been used in several studies to expand and osteogenically stimulate osteoblasts and osteoblast precursor cells for greater alkaline phosphatase (ALP) activity and mineral deposition (Howard et. al., 1983; Shima et. al. 1988; Sautier et. al., 1992; Goh et. al., 2013).

Chitosan is a common polysaccharide biomaterial that has been tested as a base constituent for the construction of osteogenic microcarriers, like those pictured in Figure 2.2. Porous microspheres of chitosan doped with up to 30% hydroxyapatite have been successfully prepared and characterized (Granja et. al., 2004). A relationship was established between the percentage of added hydroxyapatite and the microcarrier size. Pure chitosan microcarriers had diameters of 220-250 μm, which increased with hydroxyapatite addition to a diameter of 400-530 μm at 30% hydroxyapatite. This positive trend in size was accompanied by a negative trend in water sorption, which dropped from as much as 400% in pure chitosan to below 100% with mineral addition. Chitosan microcarriers have also been created using either coacervate precipitation or emulsion crosslinking, followed by immersion in simulated body fluid to create a coating of carbonated hydroxyapatite (Shen et. al., 2013). The biological effects of these chitosan-based modules (350-710 μm diameter) were evaluated using MC3T3-E1 pre-osteoblast cells. Cell proliferation was

found to be markedly higher on the coacervate-precipitated carriers, relative to emulsion-crosslinked carriers, potentially due to the rougher surface topography of the former. Mineral coating further enhanced proliferation. Interestingly, mineral coating increased ALP activity of emulsion-crosslinked carriers, but did not have the same effect on coacervate-precipitated carriers, though the latter generally exhibited higher ALP activity. Collagen deposition increased after mineral coating in both microcarrier types, though uncoated coacervate-precipitated microcarriers showed more deposition than emulsion-crosslinked counterparts. These studies suggest that both surface chemistry and roughness, as well as the presence of a mineral phase can be used to enhance the osteogenic capacity of microcarriers.

Pullulan is a natural polysaccharide polymer that has been used widely in the food and pharmaceutical industries and is being investigated for medical applications (Singh et. al., 2017). This material has been used to create porous microcarriers (150 μm average diameter), which were then seeded with SaOS-2 osteosarcoma cells and cultured in either static or dynamic suspension culture conditions (Aydogdu et. al., 2016). Pure pullulan microcarriers were compared to those with a mineral surface coating or coated with silk fibroin, as well to silica glass control microcarriers. Cell viability after seeding was generally below 50% for the pullulan-based carriers, and was only slightly higher on glass controls. Pure and silk-fibroin-coated microcarriers showed upregulation of ALP activity in both static and dynamic culture, while mineralized carriers showed the lowest activity, possibly due to the inhibitory effect that increased calcium ions may have on the ALP enzyme. Dynamic culture did not produce marked changes in ALP activity in pullulan-based carriers. However, there was a strong increase in ALP activity on glass microcarriers in dynamic culture, relative to static controls. This study suggested that pullulan-based carriers can

support osteogenic differentiation, though response to dynamic culture was highest on very stiff silica substrates.

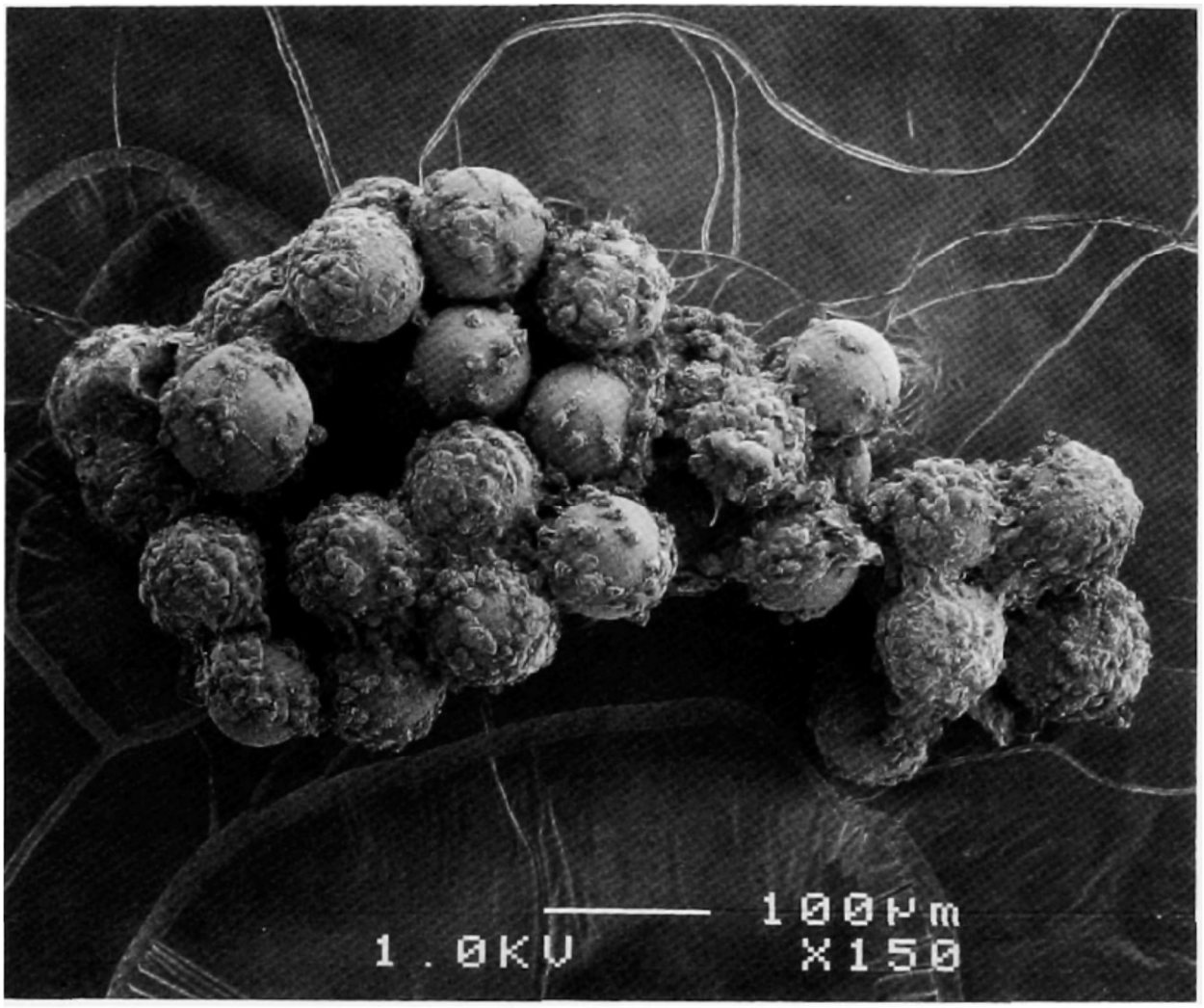

Figure 2.2: Scanning electron micrograph of rat MSC 14 days after attachment to Cytodex 3 microcarriers. Image reproduced from Qiu et al., 1998.

2.4.2 Protein- and peptide-composite microcarriers

Microcarriers created for use in osteogenic applications are very often composed of a collagen-derived base material, like in Figure 2.3, supplemented with calcium-based compounds to further enhance functionality. These two components roughly mimic the composition of the native bone extracellular matrix, which is essentially a mineralized matrix of collagen (Braun et.

al., 2003). Gelatin is a mixture of peptides derived from the hydrolysis of collagen, and is therefore often used as a microcarrier base material. Collagen and collagen peptides have the advantage that cells can recognize, bind to, and degrade these materials, giving them enhanced biological functionality relative to most synthetic materials. These proteins and similar protein-based materials can be extracted from animal tissues using a variety of techniques, which impart specific physical and biological properties on the resulting matrix. Similarly, there are a variety of forms of calcium phosphate compounds that have been used to augment protein-based microcarriers. The selection of base material and filler can be leveraged to control cell function, including for osteoconductive, osteoinductive, and osteogenic purposes.

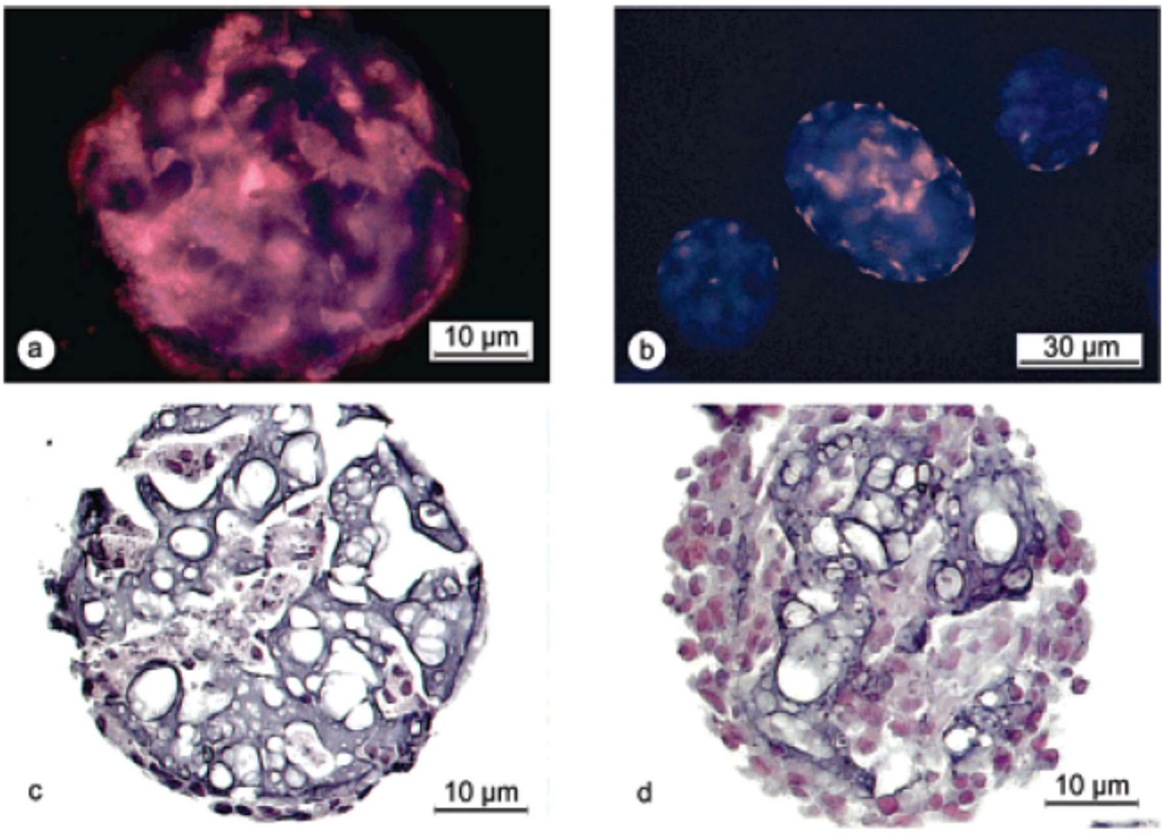

Figure 2.3: Cultispher-S gelatin microcarriers seeded with osteogenic cells. Panels (a) and (b) are stained with propidium iodide to show cell viability at day 14. Panel (c) shows hematoxylin & eosin staining at day 14. Panel (d) shows Masson's Trichrome staining at day 28 of culture. Reprinted (adapted) with permission from Declerq et al., 2005.

Gelatin-based microcarriers are available commercially. Cultispher-S microcarriers are composed of highly crosslinked porcine gelatin (Declerq et. al., 2005; Sart et. al., 2013), and are designed with high porosity for cell loading. It was found that rat MSC exhibited markedly higher levels of the osteogenic markers osteocalcin and alkaline phosphatase when cultured on Cultispher-S microcarriers, compared to conventional tissue culture polystyrene (Yang et. al., 2007). When tested in vivo, it was shown that MSC cultured on Cultispher-S carriers resulted in improved trabecular bone formation relative to cell-free microcarriers in long bone defects (Yang et. al., 2007), and similar effects were observed upon application to periodontal defects (Yang et. al., 2010). Earlier studies also investigated microcarriers composed principally of collagen Type I (Cellagen^{TM}) for the expansion of human osteoblasts. It was demonstrated that osteoblasts cultured on collagen microcarriers in spinner flask culture displayed a higher proliferative capacity over a 15-day period, when compared to cells cultured on tissue culture polystyrene. Spinner culture on collagen microsphere substrates was also shown to dramatically upregulate osteocalcin levels relative to monolayer cultures (Overstreet et. al., 2003).

In experimental systems, gelatin-based microcarriers have been augmented with various forms of calcium phosphate mineral. Gelatin mixed with tricalcium phosphate (TCP) was used to create microcarriers by emulsification in olive oil (Perez et. al., 2014), followed by crosslinking using 1-ethyl-3-(dimethylaminopropyl) carbodiimide (EDC), N-hydroxysuccinimide (NHS) chemistry. Subsequently, the microcarriers were incubated in Ringer's solution for seven days to convert TCP to calcium-deficient hydroxyapatite via hydrolysis, as in a preliminary exploratory study (Perez et. al., 2011). The resulting microcarriers (100-300 μm diameter) were seeded with SaOS-2 osteosarcoma cells and were used in static and dynamic suspension culture studies, with

Cytodex-3 microcarriers serving as controls. In static conditions, cells attached to the gelatin-HA microcarriers but no statistical increase in cell number was observed over three days of culture, while cell number on Cytodex-3 microcarriers increased approximately 4-fold over the same time period. In contrast, under dynamic culture conditions, cell proliferation was clearly enhanced on gelatin-HA microcarriers, compared to Cytodex controls. This study illustrates that interactions between the cell substrate and the culture conditions that can lead to differences in cell behavior, and in particular highlights the benefit of using gelatin-based microcarriers in dynamic suspension culture.

Other studies have examined the mode of incorporation of calcium phosphate minerals into gelatin-based materials. Microcarriers formed of apatite and gelatin were fabricated through a sol-gel process by mixing gelatin with calcium hydroxide and subsequent reaction with phosphoric acid (Kim et. al., 2005). The resulting apatite-gelatin microspheres (112 μm average diameter) were crosslinked using EDC chemistry. The sol-based emulsification method was found to impart a finer, nanoscale distribution of the calcium orthophosphate apatite crystal phase within the continuous gelatin phase, when compared to microcarriers made by direct mixing of pre-formed apatite powder into gelatin solution. Culture of MG-63 human osteosarcoma cells on the sol-formed microcarriers showed that they supported cell proliferation and osteogenic function. In a related study, apatite mineral was formed inside glutaraldehyde-crosslinked gelatin nanoparticles (230-250 nm diameter) created using a "miniemulsion" technique (Ethirajan et. al., 2008). This method of biomimetic mineralization promoted the constrained formation of a single crystalline hydroxyapatite phase throughout the gelatin spheres. These gelatin-CaP particles were too small to support the culture of mammalian cells, though the same technique could potentially be used for larger particles. These studies are important because they demonstrate control of the micro-

and nano-scale structure of mineral in gelatin materials, which can be tailored to mimic native bone mineral.

Table 1: Characteristics and applications of osteogenic microcarriers

Microcarrier bulk materials	Diameter (μm)	Bone progenitor cells	Target (*in vitro*/*in vivo*)
Dextran (Cytodex-1,2,3) and gelatin (Cytodex-2,3)	150–250	Osteoblasts, osteoblast precursor cells, MC3T3-E1 cells, fetal rat calvarial cells, rat bone MSC	*In vitro* static and dynamic (high aspect ratio vessel) culture
Chitosan and hydroxyapatite	220–710	MC3T3-E1 cells	*In vitro* static culture
Pullulan and silk–fibroin	100–215	Human osteosarcoma SaOS-2 cells	*In vitro* static and dynamic (orbital shaker) culture
Gelatin (Cultispher-S, etc.) and α-tricalcium phosphate, hydroxyapatite, or silk–fibroin	20–652.3	UMR-106 rat osteosarcoma cells, rat bone MSC, rat ear MSC, SaOS-2 cells, human osteosarcoma MG-63 cells, mouse bone MSC, MC3T3-E1 cells	*In vitro* static, poly(lactide-*co*-ε-caprolactone) scaffold, and dynamic (spinner flask) culture; *in vivo* rat subcutaneous site, long-bone defect, and periodontal defect
Type I collagen (Cellagen®, etc.) and hydroxyapatite, α-tricalcium phosphate, calcium-deficient hydroxyapatite, apatite	30–1038	Human and rat osteoblasts, SaOS-2 cells, rat bone MSC, human MSC	*In vitro* dynamic (spinner flask) and static culture; *in vivo* rat calvarial defect and rabbit femoral defect
Calcium silicate	241	MC3T3-E1 cells	*In vitro* static culture
45S5 Bioglass and polylactic acid or poly(lactic-*co*-caprolactone)	100–432	Rat bone MSC, MC3T3-E1 cells	*In vitro* dynamic (rotating-wall or high aspect ratio vessel) and static culture
Phosphate-based ($0.4P_2O_5$: 0.16CaO : 0.175–0.2Na_2O : 0.24MgO : 0–0.025Ti) glass	100–200	Autologous bone marrow concentrate cells	*In vivo* sheep knee bone defect
Calcium titanium phosphate and alginate	50–796	Rat bone MSC, MG-63 cells	*In vitro* static and dynamic (spinner flask) culture
Hydroxyapatite and alginate, α-tricalcium phosphate, or β-tricalcium phosphate	100–749	MG-63 cells, goat MSC, MC3T3-E1 cells, human osteoblastic cells, human bone and adipose MSC	*In vitro* static culture; *in vivo* mouse subcutaneous site, mouse calvarial defect, mouse mandibular defect, rabbit calvarial defect
α-Tricalcium phosphate and alginate	100–500	MC3T3-E1 cells	*In vitro* static culture
Polystyrene and type I collagen	125–212	Human placental multipotent cells, human embryonic stem cell-derived MSC, bone MSC, mouse MSC (C3H10T1/2)	*In vitro* static culture
Polylactic acid	150–250	MG-63 cells	*In vitro* static culture
Poly(lactide-*co*-glycolide) and hydroxyapatite, calcium carbonate, or polyphosphate	50–860	Mouse osteoblast-like OCT-1 cells, SaOS-2 cells, rat osteoblasts, human MSC	*In vitro* static and dynamic (high aspect ratio vessel) culture; *in vivo* mouse subcutaneous site and rat calvarial defect

Gelatin-based microcarriers have also been used in other formats aimed at regenerating bone. Addition of gelatin microspheres (20-100 μm diameter range) to MSC cultures in attachment-inhibiting cultureware demonstrated that aggregates of cells and microspheres formed over time (Hayashi et. al., 2011). The presence of microspheres in the aggregates resulted in higher cell viability and production of alkaline phosphatase, a marker of osteogenic differentiation. It was proposed that the inclusion of gelatin particles increased the porosity of the aggregates, and therefore enhanced nutrient and oxygen delivery. In a separate study, direct precipitation of a mixed solution of gelatin and calcium phosphate was used to fabricate small (<10 μm diameter), spherical, and highly porous particles that were conducive to attachment, viability, and proliferation of human osteoblast-like G-292 cells (Chao et. al., 2015). Implantation of composites of these microspheres and cells in a critical size rat calvarial defect model resulted in strongly improved bone regeneration at four and eight weeks, relative to clinically-used fibrin glue and a commercially available bone filler material (Osteoset® calcium sulfate mini-beads). In another study, gelatin microspheres (50-100 μm diameter) were incorporated into injectable co-N-isopropylacrylamide macromer materials designed for in-situ gelling (Vo et. al., 2016). The gelatin phase acted as a substrate for cell attachment and as an enzymatically-degradable porogen. Testing in a rat critical size cranial defect model revealed a greater level of mineralization and bony bridging in microsphere-containing samples, relative to controls. These studies highlight the potential improvement in bone regeneration achieved when combining osteogenic cells and a rationally designed carrier material, relative to current clinical options.

Other forms of collagen peptides and preparations have also been combined with calcium mineral to form microcarriers. Hydroxyapatite particles dispersed in reconstituted fibrous collagen Type I were prepared by emulsification in olive oil and crosslinked with glutaraldehyde (Hsu et.

al., 1999). Increased stirring speed during emulsification resulted in a decrease in average microcarrier diameter, which ranged from 220-1040 μm. A further decrease in microcarrier diameter could be achieved by the addition of a surfactant during emulsification, down to a range of 75-300 μm average diameter. Primary rat osteoblast cells proliferated and increased their production of alkaline phosphatase when cultured on these microcarriers. In a follow-on study, the ultrastructure of the matrix in similar microcarriers was examined (Wu et. al., 2004). The hydroxyapatite was distributed evenly in the matrix and did not hinder collagen fibril formation. Primary rat osteoblasts cultured on these microcarriers under osteogenic conditions proliferated and maintained metabolic activity, and also mineralized the underlying collagen-HA matrix. In a third study, similar microcarriers were made to have bone-mimetic composition of 35:65 wt% collagen:hydroxyapatite at an average diameter of 500 μm (Hsu et. al., 2005). The collagen-HA microcarriers were compressed into discs and were press-fit into a critical size cranial defect in the rat, without the addition of exogenous cells. After 16 weeks if implantation, the collagen-HA microcarriers were completely resorbed and showed good bone ingrowth, whereas pure hydroxyapatite control implants were not completely resorbed.

Collagen microcarriers incorporating tricalcium phosphate (TCP) and calcium phosphate cements are of interest because of their similarity to bone matrix and ability to support osteoblast function.39 Microcarriers made from CPC with a range of particle sizes became more spherical and cell-adhesive when collagen was added to the matrix (Perez et. al., 2013). It was shown that nanoscale calcium phosphate cement particles (2.4 nm average diameter) had the effect of increasing ALP activity when using Saos-2 osteosarcoma cells, whereas cell proliferation decreased on microcarriers relative to on silica glass controls. In a follow-on study, similarly-formulated composite collagen and calcium-deficient hydroxyapatite microcarriers were

implanted in femoral defects in a rabbit model (Cuzmar et. al., 2015). Compared to injectable calcium phosphate cement, both with and without the addition of collagen, the microcarriers produced a ten-fold increase in bone ingrowth at 3 months. These results again emphasize that the geometry and composition of microcarriers can be used to tailor their function in bone regeneration applications.

Sol-gel preparation can also be used to create apatite-loaded collagen microcarriers, in a process analogous to that developed for gelatin (Kim et. al., 2005). Pure collagen and collagen-apatite microcarriers (166 μm average diameter) were made using peptides derived from collagen sponge material using emulsification and subsequent crosslinking with EDC-NHS chemistry (Kim et. al., 2007). Apatite was then precipitated within the collagen microcarrier matrix as homogeneously-dispersed nanocrystals, to a loading of approximately 30 wt%. Pure collagen microcarriers were somewhat smaller (120 μm average diameter), again reflecting a relationship between mineral loading and particle size. Rat bone marrow-derived MSC cultured on these collagen-apatite microcarriers proliferated more rapidly compared to those on pure collagen microcarriers. In addition, MSC grown on collagen-apatite microcarriers expressed higher levels of the osteogenic marker ALP, relative to MSC cultured on pure collagen microcarriers or on standard tissue culture plates. These findings reinforce the use of a defined mineral phase in enhancing the function of peptide- and protein-based microcarriers.

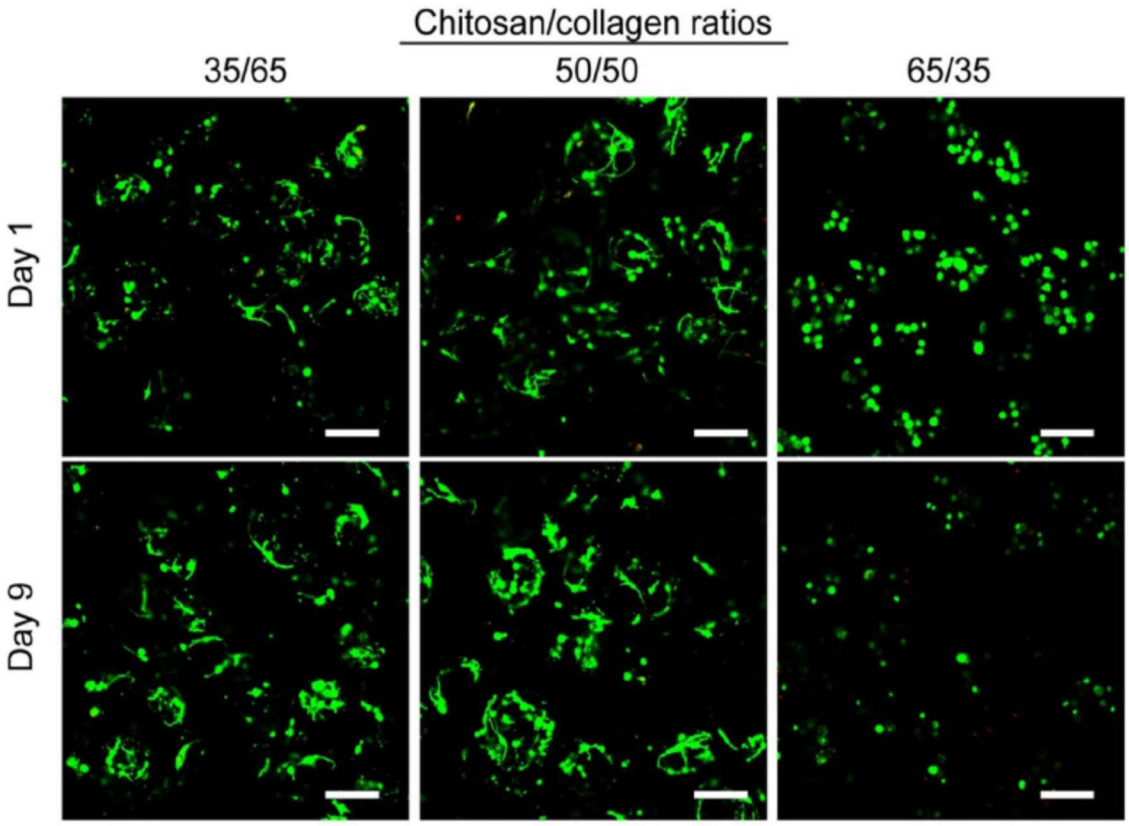

Figure 2.4: Viability staining of MSC embedded in modular microbeads with varying chitosan/collagen ratios at days 1 and 9 in culture (scale bar represents 200 μm). Cytoplasm of living cells is stained green and the nucleus of dead cells is stained red. Images reproduced with permission from S. Karger AG, Basel, Wang et al., 2013.

Protein-based microcarriers designed to fully envelop progenitor cells for delivery in bone regeneration applications have also been developed. Composites of collagen Type I and the polysaccharide agarose were used to prepare microbeads (30-150 μm diameter range) by emulsification, with human MSC embedded directly within the microbead matrix (Lund et. al., 2008). 3D microcarrier culture resulted in increased bone sialoprotein production and calcium deposition, relative to 2D controls. Similar microbeads (90-290 μm diameter range) were also fabricated using a collagen-chitosan matrix with embedded human MSC, as shown in Figure 2.4 (Wang et. al., 2013). High cell viability was supported in these microcarriers and osteogenic

capacity was demonstrated. Populations of microbeads could be concentrated into a paste for delivery through a standard 25G needle without loss of cell viability. Implantation of collagen-chitosan microbeads containing bone marrow mononuclear cells supplemented with purified MSC in an ectopic site in the rat resulted in markedly enhanced bone formation, relative to controls (Wise et. al., 2016). An extension of this work involved augmenting the collagen-chitosan matrix with exogenous hydroxyapatite, and examining bone regeneration in an orthotopic, critical size cranial defect model in the mouse (Annamalai et. al., 2019). This study showed the value of pre-differentiating MSC prior to implantation, and showed that such microbeads could be used to conformally fill and heal a critical size defect.

Silk fibroin has been investigated in a variety of regenerative medicine applications (Goncharenko et. al., 2017; Luetchford et. al., 2020; Aydogdu et. al., 2016), including for the production of osteogenic microcarriers. Gelatin-fibroin microcarriers were prepared at a 30:70 wt% gelatin:fibroin composition, both with and without mineralization using calcium phosphate (Goncharenko et. al., 2017). MSC attached and spread on these microcarriers and proliferated more robustly on gelatin-fibroin substrates than on Cytodex-3 controls, but it was observed that mineralization greatly decreased cell proliferation. In contrast, ALP activity was strongly upregulated on gelatin-fibroin microcarriers that had been mineralized with calcium phosphate. The effect of composition on the function of gelatin-fibroin was further examined using microcarriers (300-400 μm diameter range) (Luetchford et. al., 2020). The seeding efficiency and subsequent proliferation of rat MSC seeded on these microcarriers decreased with increasing silk fibroin content. However, a 75:25 wt% fibroin:gelatin composition was found to be the most osteogenic in terms of osteopontin expression, relative to control Cultispher-S microcarriers. These

studies suggest that mineralization of non-collagenous matrices is also beneficial in achieving osteogenic differentiation of progenitor cells.

2.4.3 Ceramic and ceramic-composite microcarriers

Bioactive glasses are a class of calcium sodium phosphosilicate ceramics that have been used widely in bone healing applications (de Grado et. al., 2018; Winkler et. al., 2018; Baino et. al., 2018). Their use as microcarriers typically involves pre-coating or otherwise incorporating a calcium phosphate mineral phase. Optimization of the microcarrier coating procedure has shown that extended sequential exposure to Tris-HCL followed by tissue culture medium results in a more functional coating, with a transition over time from amorphous calcium phosphate to carbonated hydroxyapatite, and a resulting positive effect on the osteogenic differentiation of MSC (Ducheyne et. al., 1997). It has also been suggested that carbonated hydroxyapatite coatings preferentially adsorb fibronectin and other cell-binding proteins, which may enhance biological function (Malda et. al., 2006; Hong et. al., 2009). Microspheres (100-150 μm diameter) created using bioactive glass have been studied for orthopaedic use as solid microparticles, hollow microspheres, and as part of polymer composite microspheres that were coated with mineral through submersion in simulated body fluid (Qiu et. al., 2000; Qiu et. al., 2001). Cell culture studies showed that bone marrow stromal cells attached to the microcarriers and produced extracellular matrix that could be mineralized. This process also produced larger cell-microcarrier aggregates. Similarly mineralized bioactive glass microshells were shown to support osteogenic differentiation of rat MSC, as indicated by alkaline phosphatase, collagen type I, and osteopontin expression (Qiu et. al., 1998). Mineral deposition by rat MSC was also demonstrated on such microspheres using scanning electron microscopy (Verrier et. al., 2016; Qiu et. al., 2002). Composite microspheres of bioactive glass and poly(lactic-co-caprolactone) incubated in simulated body fluid (SBF) for one week

exhibited complete CaP mineral coverage along with inducing significantly higher ALP activity than purely poly(lactic-co-caprolactone) microspheres on day 14 and 21 of culture in osteogenic media (Yu et. al., 2009). Other work on phosphate-based bioactive glass microspheres has suggested that the release of ions is important to their stimulation of bone regeneration, as well as the need to allow for appropriate degradation rates to support collagen deposition and matrix remodeling (Winkler et. al., 2018; Baino et. al., 2018; McLaren et. al., 2019).

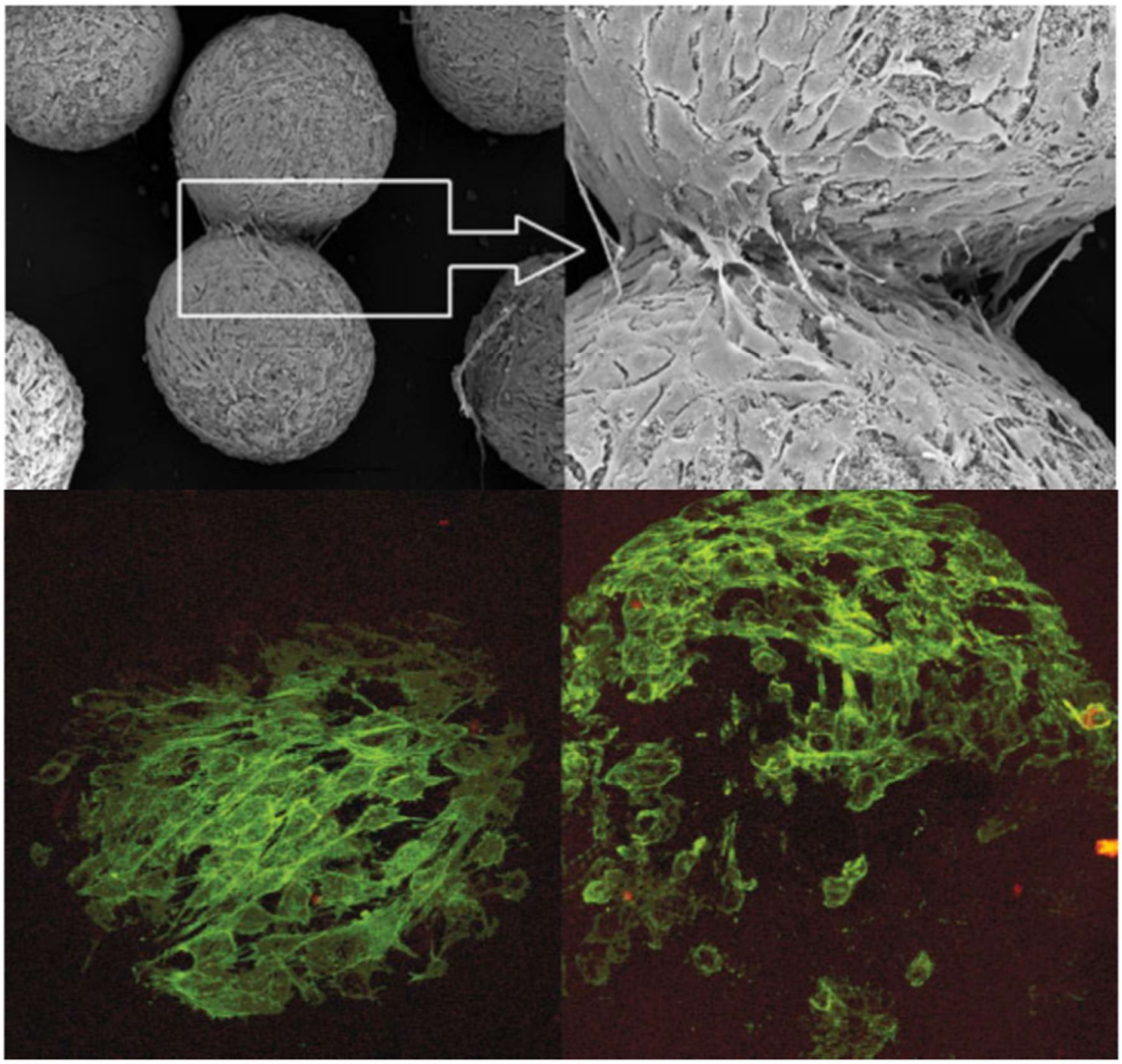

Figure 2.5: Upper panels: scanning electron micrographs (left: x110; right: x1000) of osteogenic cells on hydroxyapatite microcarriers after day 3 of culture. Lower panels: confocal laser scanning micrographs of osteogenic cells on hydroxyapatite microcarriers after day 3 of culture. Lower

panels: confocal laser scanning micrographs of osteogenic cells on hydroxyapatite microcarriers (x100) on day 5 of culture. Reprinted from Mateus et al., 2008 with permission from Elsevier.

Calcium titanium phosphate (CTP) microcarriers are a material variation on bioactive glasses (Barrias et. al., 2005; Ribeiro et. al., 2006; Barrias et. al., 2004; Barrias et. al., 2006). Particles of CTP (600 μm average diameter) were compared to polystyrene microcarriers (200 μm average diameter) in terms of the support and differentiation of rat MSC (Barrias et. al., 2005). Attachment efficiency of MSC to CTP microspheres was lower than that on corresponding polystyrene microcarriers, though the cells proliferated over two weeks in culture on both substrates. However, ALP and osteocalcin secretion was shown to be higher on CTP microcarriers, relative to polystyrene controls. Another formulation of composite titanium phosphate glass microcarriers (50-100 μm diameter range) has also been compared to similarly-sized silica glass microspheres (Lakhkar et. al., 2015; Navarro et. al., 2005). These microcarriers supported the proliferation of MG-63 osteosarcoma cells in static and spinner flask culture over one week. In a similar study using human MSC, it was observed that CTP microcarriers potentiated BMP expression, relative to silica glass, and in particular that osteopontin was highly upregulated over time on CTP microcarriers. These studies suggest that the chemical structure of calcium titanium phosphate microcarriers is conducive to the osteogenic differentiation of bone progenitor cells.

Hydroxyapatite is a ceramic of particular interest in orthopaedic regeneration applications because it closely mimics the mineral phase of native bone (Kim et. al., 2005; Winkler et. al., 2018; Braun et. al., 2003). This mineral has been incorporated as an additive in microcarriers based on a variety of materials, and has also been used as the primary constituent in microparticles designed for cell delivery. Hydroxyapatite microspheres (400-550 μm diameter range) were shown to support the adhesion, proliferation, and osteoblastic lineage of human MG-63 osteosarcoma cells,

as captured in Figure 2.5 (Barrias et. al., 2004; Mateus et. al., 2008). The effect of the density and porosity of hydroxyapatite particles was examined using microcarriers (200-700 μm diameter range) designed for the delivery of goat MSC (Fischer et. al., 2003). Larger, microporous, MSC-seeded carriers resulted in no visible bone formation when implanted subcutaneously in athymic mice, and produced only a vascularized fibrous tissue. Smaller, dense microcarriers exhibited higher cell attachment efficiency, and resulted in trablecular-like bone formation in a subcutaneous site. The effect of surface topography on cell seeding was examined using spherical, hollow hydroxyapatite microcarriers (360 μm average diameter) seeded with murine osteoblasts (Lee et. al., 2008). These microcarriers supported cell attachment and proliferation both on the outer concave and inner convex surfaces. These findings emphasize the importance of microcarrier morphology and topography on the response of seeded progenitor cells.

Tricalcium phosphate (TCP) is a ceramic with similar composition to hydroxyapatite, but which typically has a lower Ca:P ratio than native hydroxyapatite. TCP can be converted to hydroxyapatite by sintering and chemical processing (Perez et. al., 2014; Park et. al., 2014; Perez et. al., 2011; Perez et. al., 2013; Park et. al., 2011; Cuzmar et. al., 2015), and the latter is generally found to be more osteoconductive (Kong et. al., 2008). Microcarriers (100-250 μm diameter range) have been formed out of composites of HA and TCP and were seeded with bone marrow-derived MSC (Mankani et. al., 2006). Implantation of MSC-seeded HA-TCP microcarriers into both calvarial and mandibular defects in the mouse resulted in significant new bone formation by six weeks. In contrast, unseeded HA-TCP microparticles implanted into similar defect sites resulted in poor bone formation even at very long time points. Perforated HA-TCP microcarriers (370 μm average diameter) were also prepared and used as a culture substrate for human adipose-derived MSC (Park et. al., 2010; Park et. al., 2013). Calcium deposition increased on these microcarriers

over time in response to osteogenic stimulation in the culture medium, although the response was not as strong as from cells grown on tissue culture plastic. Implantation of unseeded versions of these HA-TCP microcarriers in rabbit calvarial defects resulted in the production of mature bone within the microcarrier cavities and lamellar osteons over six weeks. These observations suggest that in these composite microcarriers the HA component nucleates mineralization, while the degradation of the TCP phase provides space for new tissue formation.

Ceramic materials have also been augmented with other components to enhance the bone regeneration capability of microcarriers. Strontium-doped hydroxyapatite microspheres (520 μm average diameter) were combined with an injectable, in-situ crosslinkable RGD-alginate carrier gel to treat critical size femoral defects in the rat (Lourenço et. al., 2017). Micro-computed tomography and histological analysis indicated more robust bone formation in strontium-augmented implants, relative to strontium-free controls. Microcarriers augmented with strontium also degraded more quickly, leaving less residual material in the implant site. The result was increased collagen deposition and new bone formation in the interstitial space between microcarriers. Composite TCP-alginate microcarriers (100-500 μm diameter range) were fabricated and increasing TCP content was related with an increase in diameter (Park et. al., 2014). These carriers were subsequently incubated in SBF and their pore size could be modulated through control of the freezing temperature during lyophilization, with increasing freezing temperature resulting in larger pores. Using MC3T3-E1 pre-osteoblast cells, it was shown that cell proliferation and ALP activity under osteogenic conditions were similar on TCP-alginate microcarriers, relative to tissue culture plastic controls, suggesting that such microcarriers support the osteoblastic differentiation of progenitor cells.

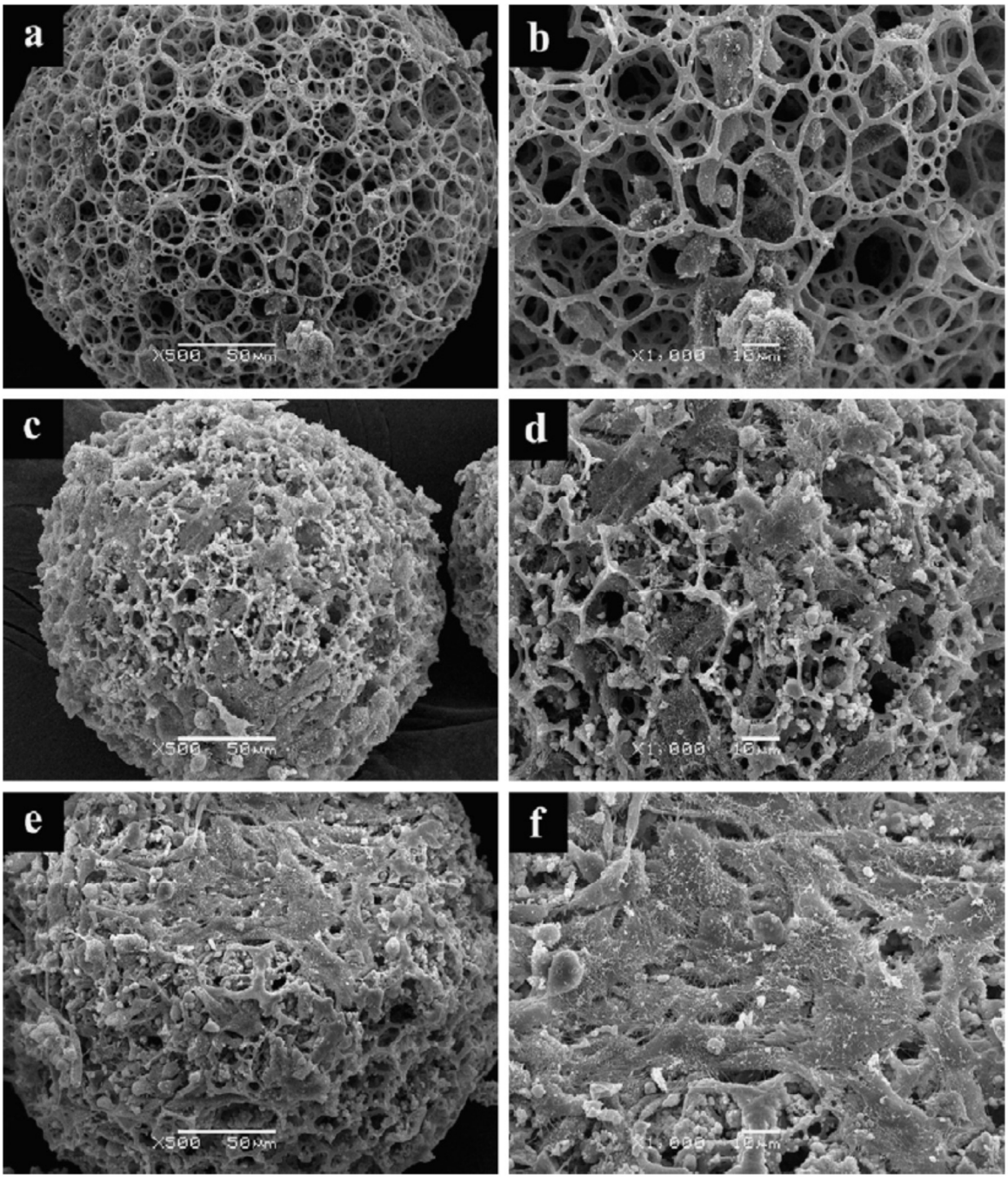

Figure 2.6: Scanning electron micrographs of MG-63 cells on day 3 of culture on (a, b) PLA microcarriers, (c, d) 8-day mineralized PLA microspheres, and (e, f) 17-day mineralized PLA microspheres. Reprinted from Shi et al., 2011 with permission from Elsevier.

2.4.4 Synthetic Polymer-composite Microcarriers

Polystyrene is widely used in tissue cultureware because it can be plasma treated to promote cell attachment (Guruvenket et. al., 2004). This polymer can also be used to fabricate spherical microparticles, which have found broad utility in the biotechnology field as microcarriers (Zühlke et. al., 1994; Röder et. al., 1994). Uncoated and collagen-coated SoloHill® polystyrene microcarriers (125-210 μm diameter range) were seeded with human MSC derived from bone marrow, placenta, or embryonic stem cells (Tseng et. al., 2012). Similarly, untreated or collagen-coated polystyrene tissue culture plates served as controls. It was observed that MSC cultured on collagen-coated microcarriers exhibited markedly higher ALP activity, collagen secretion, and calcium deposition compared to culture plate controls, even in the absence of osteogenic stimulation by growth factors. Both disruption of cytoskeletal actin using latrunculin B and inhibition of actomyosin contraction using blebbistatin reduced the osteogenic response, suggesting that in this system the microcarriers induced osteogenesis in MSC through enhancing cytoskeletal tension.

Polylactic acid (PLA) has been used widely for regenerative medicine applications, including for orthopaedic repair, as in Figure 2.6 (Maeda et. al., 2004; Shi et. al., 2011; Du et. al., 2009). Microspheres of PLA used for bone regeneration generally incorporate a ceramic phase to enhance osteogenic properties. The addition of calcium phosphate mineral can also mediate the production of acidic degradation products of PLA, and can act as a template for further biomineralization. Hollow spheres (500-1000 μm diameter range) were fabricated from a composite of PLA and calcium carbonate ($CaCO_3$) via emulsion (Maeda et. al., 2004). Subsequent immersion in SBF for one week resulted in production of a carbonated hydroxyapatite layer, as demonstrated by x-ray diffraction analysis. Similar porous PLA microspheres (110-250 μm diameter) were produced and treated in sodium hydroxide solution to hydrolyze surface functional

groups (Shi et. al., 2011; Du et. al., 2013). Subsequent mineralization studies in SBF showed that pre-hydrolized microcarriers mineralized to a greater degree than untreated controls, and that the degree of mineralization increase with time after day 5. Seeding of human osteoblast-like MG-63 cells on mineralized microcarriers showed high cell viability (>80%) over five days of culture.

Composite poly(lactide-co-glycolide) (PLGA) microcarriers made with 50 wt% hydroxyapatite exhibited increased attachment efficiency of mouse OCT-1 osteoblast-like cells with increasing sodium hydroxide treatment (Shen et. al., 2010). Cells proliferated over time in culture and alkaline-treated microcarriers were shown to be more osteogenic than untreated controls. PLGA microcarriers have also been used in dynamic culture systems for SaOS-2 human osteosarcoma cells (Botchwey et. al., 2001). While rotating dynamic culture decreased the proliferation rate, it also increased ALP activity in this cell line. Surface-mineralization of PLGA microcarriers also increased the attachment efficiency of rat osteoblast cells, relative to untreated controls (Kang et. al., 2008). Similarly, surface mineralization was shown to increase bone regeneration by these cell-seeded PLGA microcarriers when implanted into subcutaneous sites in athymic mice for 6 weeks. PLGA-based microcarriers have additionally been shown to generate nearly complete bone restoration in rat critical-size calvarial defects after 12 weeks of implantation (Wang et. al., 2016).

2.5 Summary and future perspectives

A wide variety of microcarriers have been developed with the target of augmenting bone regeneration. The studies reviewed in this paper are characterized by the rational combination of materials and chemistries to achieve desired physical and biological functions. Polysaccharides, proteins, peptides, ceramics, and polymers all have applied in this way. Composites of these materials are often used in an effort to harness and combine the desired properties of the individual

components to create a more functional matrix. In some cases, these materials directly mimic the composition of biological bone tissue. In other cases, they are designed to promote cell attachment and function for the purpose of potentiating the biological response. Direct addition of calcium phosphate compounds or promotion of a biomineralization is a key strategy in creating many of these microcarrier types, since this mineral phase is a major component of bone tissue and has been demonstrated to have osteogenic effects on progenitor cells. Overall, there has been a remarkable diversity in the approaches taken to creating microcarriers for orthopaedic applications, and to designing their composition for enhanced biological function.

The use of cell-based approaches to orthopaedic tissue regeneration is more complex than purely materials-based approaches. However, only cells can produce new bone and therefore if appropriate cell types are not available at the site of injury, they must either be recruited endogenously or delivered exogenously. In large and ischemic bone defects, recruitment of progenitor cells is impaired, and cell delivery has the potential to greatly augment the healing process. Microcarrier-based strategies to cell therapy have the advantage that cells are delivered on a substrate that can be designed to direct their differentiation and function. In addition, the microcarrier material acts as a space-filling extracellular matrix that can have biological and mechanical function. Importantly, populations of microcarriers can often be delivered as a moldable paste or putty, and therefore can conformally fill defects. In most cases, these microcarrier-based approaches do not provide load-bearing mechanical stability. However, cell-seeded biomaterial microcarriers offer new and potentially improved options to fill bone defects that may be superior to current approaches in healing challenging cases.

The literature reviewed in this paper emphasizes the materials used to create microcarriers, and how the properties of the materials affect cell function. Materials chemistry is an important

component of cell-matrix interactions, since cells bind directly to the microcarrier substrate and receive both physical and biological signals via that binding. Similarly, the topography of the substrate can be an important determinant of cell function, particularly in the case of progenitor cells such as MSC. Surface roughness, geometry, and porosity all have been demonstrated to affect cell differentiation, and these features can be designed into microcarriers in a variety of ways. Similarly, mechanical stiffness of materials is known to be a strong determinant of progenitor cell fate, particularly in orthopaedic applications. In addition, microcarrier materials can be designed to be more or less resistant to degradation in the physiological environment, which enables control over the dynamics of resorption and replacement of microcarriers by new biological tissue. Taken together, there are a wide range of options of materials design parameters that can be employed to make microcarriers optimally functional and effective in bone regeneration applications.

While remarkable progress has been made in the design, fabrication, characterization, and application of microcarriers for orthopaedic applications, there are exciting opportunities for further improvement of these technologies. New materials and composites are being developed that may facilitate tailoring of the cell-instructive properties of microcarriers. In particular, a better understanding and tighter control over material mechanical properties may allow more targeted cell differentiation. Materials can also be designed to change their properties dynamically over time or upon application of a specific stimulus, so that integration into the host is enhanced. Immobilization and release of bioactive factors is an area that has also been extensively studied in regenerative medicine, but has not been applied widely for microcarrier-based applications. Growth factors, function-specific ligands, gene delivery vectors, and a variety of other stimuli can be incorporated into and presented by the microcarrier matrix. Genetic modification of cells to be better suited for microcarrier delivery, and to be more effective upon delivery, is another exciting

avenue that has not been extensively pursued in the field of microcarrier technology. Finally, there is a growing recognition that control of the biological response, and in particular the inflammatory and immunological response, is a key to achieving functional tissue regeneration. There remains great potential in using rationally-designed microcarriers for the delivery and directed differentiation of progenitor cells, with the goal of rapidly and effectively regenerating bone tissue.

Chapter 3 Fabrication and Characterization of Osteogenic Function of Progenitor Cell-Laden Microcarriers

Biomaterial-based bone regeneration strategies often include a cellular component to accelerate healing. Modular approaches have the potential for minimally-invasive delivery and the ability to conformally fill complex defects. In this study, spherical gelatin microparticles were fabricated via water-in-oil emulsification and were subsequently crosslinked with genipin. Microparticle diameter depended on impeller geometry, and increased stirring rates consistently produced smaller particles with narrower size distributions. Increasing the concentration of gelatin resulted in larger particles with a broader size distribution. Viscoelastic characterization showed that increased gelatin concentration produced stiffer matrices, though the mechanical properties at lower gelatin concentration were more stable across strain rate. Microparticles of 6.0 % wt/vol gelatin were then applied as microcarriers for packed-bed culture of human mesenchymal stromal cells (MSC) at seeding densities of 5.0×10^3, 2.5×10^4, or 5.0×10^4 cells/cm^2 of surface area, in either control or osteogenic medium. Cell viability was uniformly high (>90%) across seeding densities over 22 days in culture. MSC number stayed approximately constant in the 5.0×10^3 and 2.5×10^4 cells/cm^2 samples, while it dropped over time at 5.0×10^4 cells/cm^2. Alkaline phosphatase activity was significantly upregulated in osteogenic conditions relative to controls at day 15, and absolute calcium deposition was strongly induced by days 15 and 22. However, calcium deposition per cell was highest in the lowest cell density, suggesting an inhibitory effect of high cell numbers. These results show that genipin-crosslinked gelatin microcarriers can be reproducibly fabricated

and used as microcarriers for progenitor cells, which may have utility in treating large and complex bone defects.

3.1 Introduction

Trauma and disease-induced bone fractures can be severely debilitating, in particular when the structure of the local microenvironment and/or cell populations are disrupted. Inhibition of bone regeneration by injury or disease can result in significant clinical morbidity, including delayed bone healing and non-unions (Roberts et. al., 2012; Fernandez et. al., 2018). The field of biomaterials science has addressed these issues through the development of a variety of promising approaches to improving bone healing outcomes. Many of these approaches apply the conventional tissue engineering paradigm of combining osteogenic cells with a supportive biomaterial scaffold, in some cases in conjunction with controlled factor release, to guide and potentiate bone regeneration (Verrier et. al., 2016; Perez et. al., 2018). Mesenchymal stromal cells (MSCs) are often used in these applications because of their demonstrated involvement in the regeneration of bone (Lin et. al., 2019; Sobacchi et. al., 2018), as well as their putative paracrine and immunomodulatory effects (Pajarinen et. al., 2019; Barrias et. al., 2005). Cell-based approaches are particularly promising because only cells can create new bone, and in situations where regenerative cells are absent from the wound site they must either be recruited or provided exogenously (Paren et. al., 2019; Rao et. al., 2013).

There is increasing interest in the development of biomaterials-based modular tissue engineering systems, in which discrete units of material and/or engineered tissues are delivered to achieve a specific function. Modular approaches allow minimally-invasive delivery, and even complex defects can be conformally filled (Chen et. al., 2013; Kim et. al., 2005). The modular strategy also allows different types of tissue constructs to be combined to form complex and

multiphasic engineered tissues (Verrier et. al., 2016; Rao et. al., 2015). To date, the main approaches for creating therapeutic bone fillers have used larger particulates, often auto- or allograft, with dimensions on the order of millimeters (Chao et. al., 2015; Petruskevicius et. al., 2002). However, the potential of micron-range colloidal particulates to enhance cellular development and tissue-specific function is now being investigated more widely (Nweke et. al., 2020). Particles in this size range are commonly called microcarriers, and are designed to maximize their capacity for attachment of cell populations, and for use as a cell culture and delivery method. Through careful biomaterial selection and fabrication, microcarriers can be created with tailored combinations of bioactivity, rigidity, and degradability.

In general, the microcarrier format offers a number of advantages over other cell culture and delivery approaches. A variety of microcarrier types are used routinely in the biotechnology industry (Chen et. al., 2020; Ornelas-Gonzalez et. al., 2021), and there is a well-developed body of science on process control, aseptic processing, and quality assurance. Microcarriers provide a very high surface area to volume ratio and therefore allow large cell populations to be supported in relatively small volumes: it is remarkable to consider that 10 ml of a concentrated paste of 150 μm-diameter microcarriers could support almost 250 million cells. Microcarriers can also be cultured in suspension, which greatly simplifies their maintenance, harvesting and potential use for cell transplantation. Importantly, cells cultured on microcarriers can be collected without the need for trypsinization and removal from their substrate, and intact populations of microcarriers can therefore be used for cell delivery, for example, as a cell-containing tissue filler. Such use maintains the very important cell-matrix and cell–cell contacts that are critical to tissue survival, engraftment, and development post-transplantation. In addition, cell delivery in a packed-bed

geometry of concentrated microcarriers promotes diffusion-based and/or microvasculature-enabled perfusion of nutrients to and from the transplanted cells in ischemic environments.

Microcarriers for bone regeneration commonly use biomaterials with established biological relevance (Saltz et. al., 2016, Shadjou et. al., 2015), including collagen, gelatin, calcium phosphates, apatites, bioactive glasses, and calcium carbonates (Ghomi et. al., 2021, Ballouze et. al., 2021). Typically, microspheres of such cytocompatible materials are generated through the batch emulsification or pinched flow droplet formation of an aqueous polymer solution phase into a surrounding nonpolar phase (Nweke et. al., 2020). Batch-emulsification provides the benefit of rapid microparticle production, but at the cost of greater size polydispersity. Particle size and size distribution can be modulated to some degree by varying the viscosity of the continuous phase, the rate of emulsification, and the impeller geometry, as well as by the addition of surfactants and post-production filtration (Hsu et. al., 1999; Bliatsiou et. al., 2018). In contrast, microfluidic or flow-focusing techniques are capable of generating particles with a narrow size distribution; however, the rate of production is comparatively low (Goncharenko et. al., 2017; Barrias et. al., 2005).

Gelatin and other collagen-derived materials have been used extensively as base materials for microcarriers due to their broad availability, ease of processing, and generally excellent cytocompatibility. There is a rich literature on the use of collagen and gelatin microparticles as cell carriers, and several commercial products are available, including collagen Cellagen (Overstreet et. al., 2003), gelatin Cultispher®-S (Sart et. al., 2013; Yang et. al., 2007), and porous gelatin-coated dextran Cytodex®-3 microcarriers. The fabrication of collagen (Hsu et. al., 1999; Perez et. al., 2014) and gelatin (Lau TT, Wang C, & Wang DA, 2010; Lau TT, Wang C, Peng SW, Su K, & Wang DA, 2010; Lau et. al., 2012; Solorio et. al., 2010; Turner et. al., 2017; Annamalai

et. al., 2018) microparticles has been demonstrated using bulk emulsification (Vo et. al., 2016; Kim et. al., 2007), microfluidics (Luetchford et. al., 2020), coacervation (Shen et. al., 2013), and sol–gel synthesis (Kim et. al., 2005). In some cases these microcarriers are augmented with other macromolecules such as chitosan (Annamalai et. al., 2019) or silk fibroin (Goncharenko et. al., 2017; Luetchford et. al., 2020), or with a mineral phase such as tricalcium phosphate (Chao et. al., 2015; Perez et. al., 2014), calcium-deficient hydroxyapatite (Perez et. al., 2011; Cuzmar et. al., 2015), or hydroxyapatite (Kim et. al., 2007; Hsu et. al., 2005).

Collagen and collagen-peptides foster the attachment and reorganization by many cell types, including a variety of progenitor cells known to be involved in bone formation. Additionally, these materials are autocatalytically, thermally, or chemically-crosslinkable at room temperature and in physiological conditions (Perez et. al., 2014). The mechanical properties of collagen-based materials can be further controlled through the addition or reduction of reinforcing agents. Such physical changes can in turn alter the osteogenic capacity of the substrate, as evidenced by changes in key phenotype markers, including alkaline phosphatase, osteocalcin, and calcium deposition. Gelatin in particular has found use in a number of bone defect filler applications, as a result of this material's low cost, ease of handling, and general cytocompatibility (Chao et. al., 2015; Hsu et. al., 1999; Overstreet et. al., 2003; Sart et. al., 2013; Yang et. al., 2007; Dosta et. al., 2020; Hayashi et. al., 2011). Gelatin is available as a highly purified product, and consists of collagen polypeptides that are soluble in hot water. When cooled below 25°C, the peptides form a hydrogel, which can be crosslinked to produce a stable matrix. These materials retain the cell-binding sites of native collagen, and therefore are excellent cell culture substrates.

In the current study, gelatin microparticles were fabricated through an oil-in-water emulsification method, with a focus on achieving a high production rate and a narrow population

size distribution. The effect of impeller geometry, stirring rate, and gelatin concentration on the size and size distribution of gelatin microparticles was assessed. Formed microparticles were subsequently crosslinked with genipin, a small molecule that imparts markedly less residual cytotoxicity to protein- and peptide-based matrices, relative to commonly used aldehyde crosslinkers (Yang et. al., 2018). The viscoelastic mechanical properties of the crosslinked gelatin matrices were assessed using shear rheometry. MSC were seeded onto select genipin-crosslinked gelatin microparticle formulations to create cell microcarriers consisting of osteoprogenitor cells attached to a peptide matrix. These microcarriers were cultured in a packed-bed geometry to loosely mimic how such particles can be delivered in bone defect-filling applications. The viability, proliferation, and differentiated state of the MSC were assessed over a period of 3 weeks in both control and osteogenic culture. Few previous studies have focused on the use if genipin-crosslinked gelatin microcarriers for osteogenesis, and most have been limited to shorter culture times (Lau TT, Wang C, & Wang DA, 2010; Lau TT, Wang C, Peng SW, Su K, & Wang DA, 2010; Lau et. al., 2012). The goal of the current study was to characterize the fabrication of genipin-crosslinked gelatin microcarriers and their capacity for support of bone cell maintenance, growth and differentiation, with an emphasis on the ability to promote osteogenic differentiation of human progenitor cells.

3.2 Materials and Methods

3.2.1 Materials

Type A (acid-treated porcine skin) 225 bloom strength gelatin was procured from Sigma Aldrich (St. Louis, MO). A 100 cSt polydimethylsiloxane (PDMS) product was procured from Clearco Products (Bensalem, PA). Pluronic® L101, a nonionic, difunctional, block copolymer

surfactant, was procured from BASF Corporation (Vandalia, IL). Genipin, a naturally-derived crosslinking agent, was procured from Wako Chemicals (Richmond, VA).

3.2.2 Generation of gelatin microcarriers

A water-in-oil emulsification process, illustrated schematically in Figure 3.1, was used to generate gelatin microscale droplets. Aliquots of 5.0 ml of the desired gelatin concentration (6.0%, 10.0%, or 14.0% [wt/vol] gelatin in PBS at pH 7.4) were equilibrated within a 37°C water bath before dropwise addition to a stirred 50 ml PDMS oil bath held at 40°C on a heated plate. The resultant emulsion was stirred at set rates of 250, 380, or 500 rpm with custom impellers. These impeller designs are shown in Figure 3.2 as: a radial-blade impeller with a 7 mm by 12.47 mm cross-section 35 mm-long blade and two dual-blade axial impellers with cylindrical blade diameters of 0.33 or 1.0 mm. While the radial-blade impeller has been used in previous studies, the axial impellers have been custom designed for the generation of microparticles used as microcarriers in this current study. After 5 min of stirring at 40°C, using one of these three impellers, the resulting emulsion was transferred to a 4°C ice bath and stirring was continued for an additional 30 min to allow microdroplet solidification. The resulting suspension of solid gelatin microparticles was mixed with PBS at 23°C containing 0.01% (vol/vol) Pluronic L101 surfactant and centrifuged at 300 × G for 5 min to collect the gelatin microparticles and separate them from the PDMS phase (Annamalai et. al., 2018). Remaining surfactant solution was extracted from collected microparticles by re-suspension and washing in PBS for further processing.

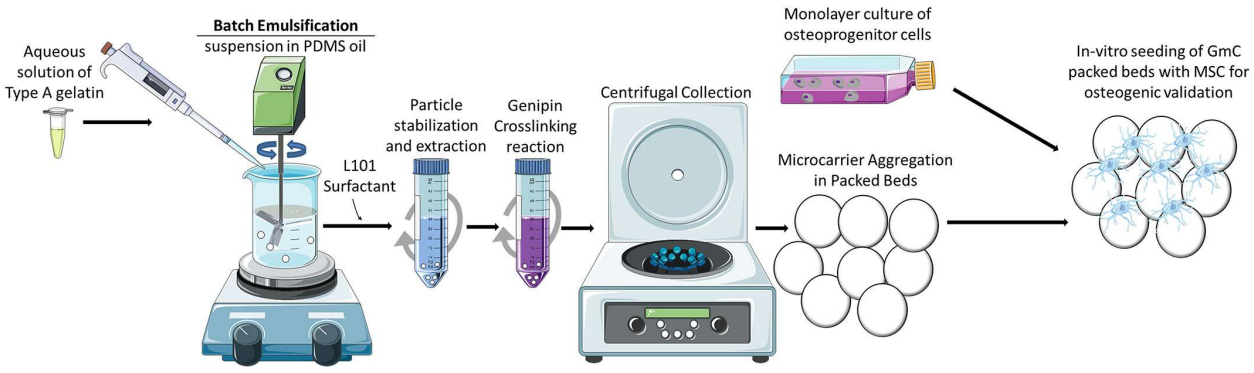

Figure 3.1: Schematic showing gelatin microcarrier production by water-in-oil emulsification and subsequent seeding with cells. Microcarriers in this study were composed of type A gelatin crosslinked with genipin.

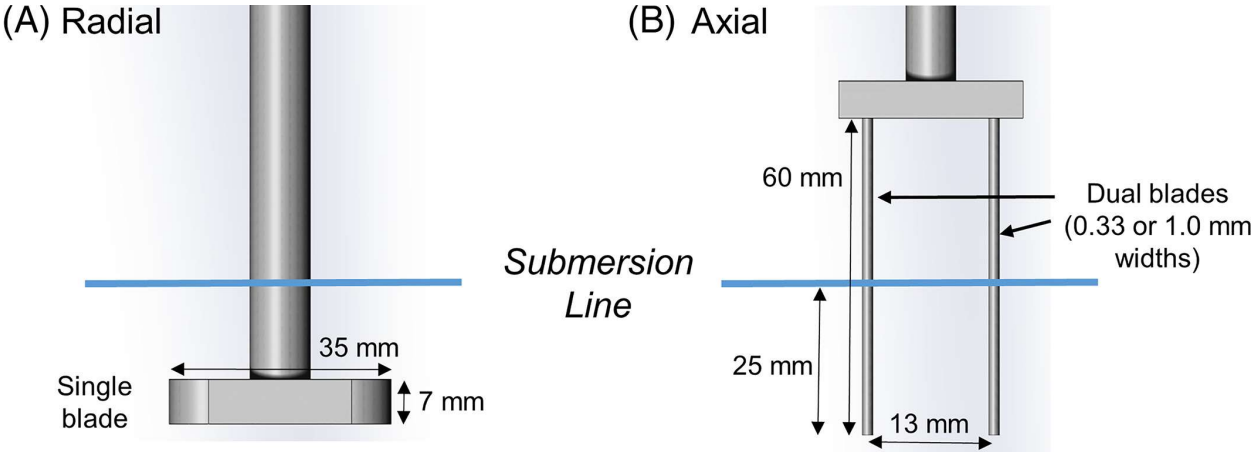

Figure 3.2: Comparative schematics of (A) radial-bladed impeller and (B) dual axial-bladed impellers. The axial-bladed impeller geometries used in this study differed only in blade cross-sectional dimensions, either 0.33 mm (Axial-0.3) or 1.0 mm (Axial-1.0).

3.2.3 Genipin crosslinking of gelatin microcarriers

Gelatin microparticles were admixed to 1.0% (wt/vol) genipin in PBS solution under continuous rotational suspension to allow crosslinking to occur. Degree of crosslinking was time-dependent and a mixing duration of 48 h at 23°C was used to allow total saturation of reactive amine groups (Solorio et. al., 2010). Genipin creates crosslinks by catalyzing reactions between lysine residues on amine moieties of the gelatin molecule. Hydrogels crosslinked in this manner have been determined to reach a maximum degree of crosslinking of approximately 90%, which imparts a mild red autofluorescence the gelatin material (Turner et. al., 2017, Hwang et. al., 2011).

The gelatin used in this study had a melting temperature of approximately 32°C, such that crosslinking could be carried out at room temperature without fusion of particles. Crosslinked gelatin microcarriers (GmC) were washed successively in ethanol and deionized (DI) water to extract residual genipin. All microcarriers were subjected to 10 min of ethanol-submersion sterilization and UV sterilization (Sylvania UV-C 255 nm germicidal T8 30W lamp) before use.

3.2.4 Particle size analysis

General examination and characterization of the morphology of gelatin microparticles was accomplished using light microscopy. GmC micrographs were captured with an inverted phase contrast microscope and analyzed using NIS Elements viewer software (Nikon). Automated particle size measurement was performed using laser diffraction analysis (Malvern Mastersizer 2000S, Westborough, MA). Samples of microcarrier dispersions were suspended in DI water within the sample reservoir agitated at 1750 rpm. The count median diameter for GmC was measured until the recorded laser obscuration exceeded 5%. Using Mie light scattering theory, a gelatin refractive index of 1.52, and water's refractive index of 1.33, the particle analyzer calculated a distribution of spherical particle diameters by scanning 30,000 snapshots over a 30 s time-span. Data generated from automated particle analysis were used to graph particle size distributions and calculate population statistics. Histograms presented in this work use bins in which the bin labels represent the maximum size of the lower bin, which is also the minimum size of the next larger bin.

3.2.5 Mechanical characterization of gelatin materials

Rheological analysis was used to determine the impact of gelatin concentration on material mechanical properties. Gelatin hydrogels were characterized using a rotational rheometer (AR-G2,

TA Instruments, Newcastle DE) with a Peltier temperature-controlled stage and 8 mm parallel plate measurement head. Measurements were taken at 25°C on 10 mm diameter discoid samples of 6.0%, 10.0%, or 14.0% (wt/vol) gelatin at a pre-load of 0.5 N with a gap height of 3 mm. A 0.1–10 radian/second (rad/s) oscillating frequency sweep test was conducted at a constant oscillating strain of 0.1% to identify the linear viscoelastic region (LVER). A 0.1%–10% oscillating strain sweep test was then administered at a constant oscillating frequency of 1 rad/s to establish a modulus-strain relationship for the specified concentrations of gelatin hydrogels. Finally, a 20 s time sweep test was administered at a constant oscillating frequency of 1 rad/s and constant oscillating strain of 0.1%.

3.2.6 Cell culture

Human bone marrow-derived mesenchymal stem cells (MSC, RoosterBio, Frederick MD) were expanded to passage 7 in defined growth medium (RoosterNourish™, RoosterBio, Frederick MD). Control medium (CTRL) consisted of Dulbecco's Modified Eagle's Medium (DMEM) supplemented with 10% (vol/vol) fetal bovine serum (FBS) and 1% (vol/vol) penicillin–streptomycin. Osteogenic (OST) medium was prepared by adjusting CTRL medium to final concentrations of 0.2 mM L-ascorbic acid 2-phosphate, 10 mM β-glycerophosphate, and 100 nM dexamethasone. All cell culture was performed in a standard incubator at 37 °C in a 5% CO2. Upon reaching 70%–80% confluence in T-175 polystyrene culture flasks, MSC were trypsinized and suspended in medium for seeding of GMC at cell densities of 5000 MSC/cm^2 (5 K/cm^2), 25,000 MSC/cm^2 (25 K/cm^2), or 50,000 MSC/cm^2 (50 K/cm^2). GmC used in cell culture experiments were generated using an Axial-1.0 impeller at 500 rpm, resulting in an average GmC diameter of 177.3 μm. GmC were cultured in packed beds in a conical tube to loosely simulate

how microcarriers would be assembled if used as a bone void-filling material. Nutrient medium was changed every 3–4 days over the span of a three-week culture period.

3.2.7 Cell viability, number, ALP activity, and calcium deposition

On day 1 after seeding, and subsequently on day 8, day 15, and day 22 of culture, MSC were assayed for DNA content, ALP activity, and calcium deposition. These assays were used to characterize the number, proliferation rate, and differentiated state of the MSC. Additionally, vital staining was performed on days 8, 15, and 22 to determine the viability, general shape, and distribution of MSC in microcarrier culture.

Packed-beds of MSC-loaded microcarriers were transferred to 24-well plates for visual inspection and were incubated with 0.1% (vol/vol) calcein AM and 0.1% (vol/vol) ethidium homodimer in DMEM for 45 min prior to rinsing and suspension in PBS. Both fluorescence and bright-field imaging on an inverted microscope were used to assess cell viability and morphology. Live cells were captured in the green fluorescence channel while the red channel of the same field of view was imaged to capture any dead cells and microcarrier autofluorescence. Corresponding bright-field images of these fields captured all cells and microcarriers.

The quantity of cellular DNA in samples was assayed as a measure of relative cell numbers, which were used to normalize ALP activity and calcium deposition, using the commercially available Quanti-iT™ PicoGreen double-stranded DNA assay kit (Invitrogen, Grand Island, NY) as described previously.36 Briefly, total DNA was isolated from packed-bed culture samples through solubilization in 0.1% (wt/vol) sodium dodecyl sulfate 10 mM Tris–HCL solution (0.1%SDS TBS) adjusted to a pH of 7.5. Samples were subsequently centrifuged at 10,000 × G for 10 min before aspiration of supernatants for further use in quantifying DNA content by PicoGreen assay using the manufacturer's protocol and reagents. Briefly, lysate samples, alongside reference

samples of Lambda-DNA standards, were admixed with 0.5% (vol/vol) PicoGreen 1 mM ethylenediaminetetraacetic acid (EDTA) TBS for 5 min of reaction time. Fluorescence signal from each reacted sample, pipetted into a 96-well plate, was read with an excitation wavelength of 485 nm at an emission wavelength of 528 nm.

ALP activity was quantified as described previously36 by first lysing MSC in 0.1% SDS TBS, centrifuging at 10,000 × G for 10 min, and then collecting the respective supernatants. Sample supernatants were each admixed with 1.5 M 2-amino-2-methylpropanol-buffered 5 mM p-nitrophenyl phosphate substrate solution in a 96-well plate for 30 min of reaction on shaker plate. This reaction was stopped with the addition of 3.0 N NaOH to all sample wells. Sample absorbance was measured at 405 nm.

Calcium deposition was measured using an orthocresolphthalein complex one (OCPC) method described in earlier studies (Babur et. al., 2015; Saito et. al., 2013). Briefly, sample sediments from 10,000 × G centrifugation were digested in 1.0 N acetic acid overnight on a 37°C shaker plate. These were each then admixed with a 5:5:2:88 volume ratio blend of 14.8 M ethanolamine-boric acid buffer (pH 11), 1 mg/ml OCPC solution, 50 mg/ml 8-hydroxyquinoline in 95% ethanol solution, and deionized water in a 96-well plate for 10 min of reaction on shaker plate. Sample absorbance was then measured at 575 nm.

3.2.8 Statistical analysis

Microcarrier sizes, mechanical data, ALP activities, calcium levels, and DNA yields are all reported as numerical mean ± SD with n=3. For these data sets, groups were compared and analyzed by ANOVA and t-test. A resulting F-value of greater than F-critical and a p-value of less than 0.05 between groups were considered statistically significant.

3.3 Results and Discussion

3.3.1 Gelatin microparticle morphology and size

The effect of impeller geometry and rotation speed on the morphology, average size, and size distribution of gelatin microparticles was assessed both through optical imaging and automated particle size analysis. All formulations of batch-emulsified gelatin microparticles exhibited highly spheroidal geometries with regular borders and visually smooth surfaces. The diameter of microcarriers is functionally significant since it determines the surface area available for cell attachment on each particle. The size distribution of a population of microcarriers is important because it determines the achievable packing density of microparticles (Man et. al., 2005; Baule et. al., 2014), as the well as the overall surface area available for cell attachment.

Figure 3.3 shows the effect of impeller geometry on microparticle size using a rotational speed of 500 rpm, using a 6.0% wt/vol gelatin matrix. Panels A–C show images of the produced microparticles and the corresponding size histograms. Microparticles generated by the radial impeller, displayed a relatively monodisperse size distribution dominated by very small gelatin particles (6.7 ± 0.3 μm). This impeller geometry was used in previous studies (Solorio et. al., 2010; Turner et. al., 2018; Annamalai et. al., 2019) to create very small (6–21 μm diameter) microspheres designed for growth factor delivery. However, microcarriers designed as platforms for cell culture and delivery require sufficient surface area to support cell attachment, differentiation, and growth. Therefore, we experimented with other impeller geometries to create microcarriers of appropriate size and size distribution.

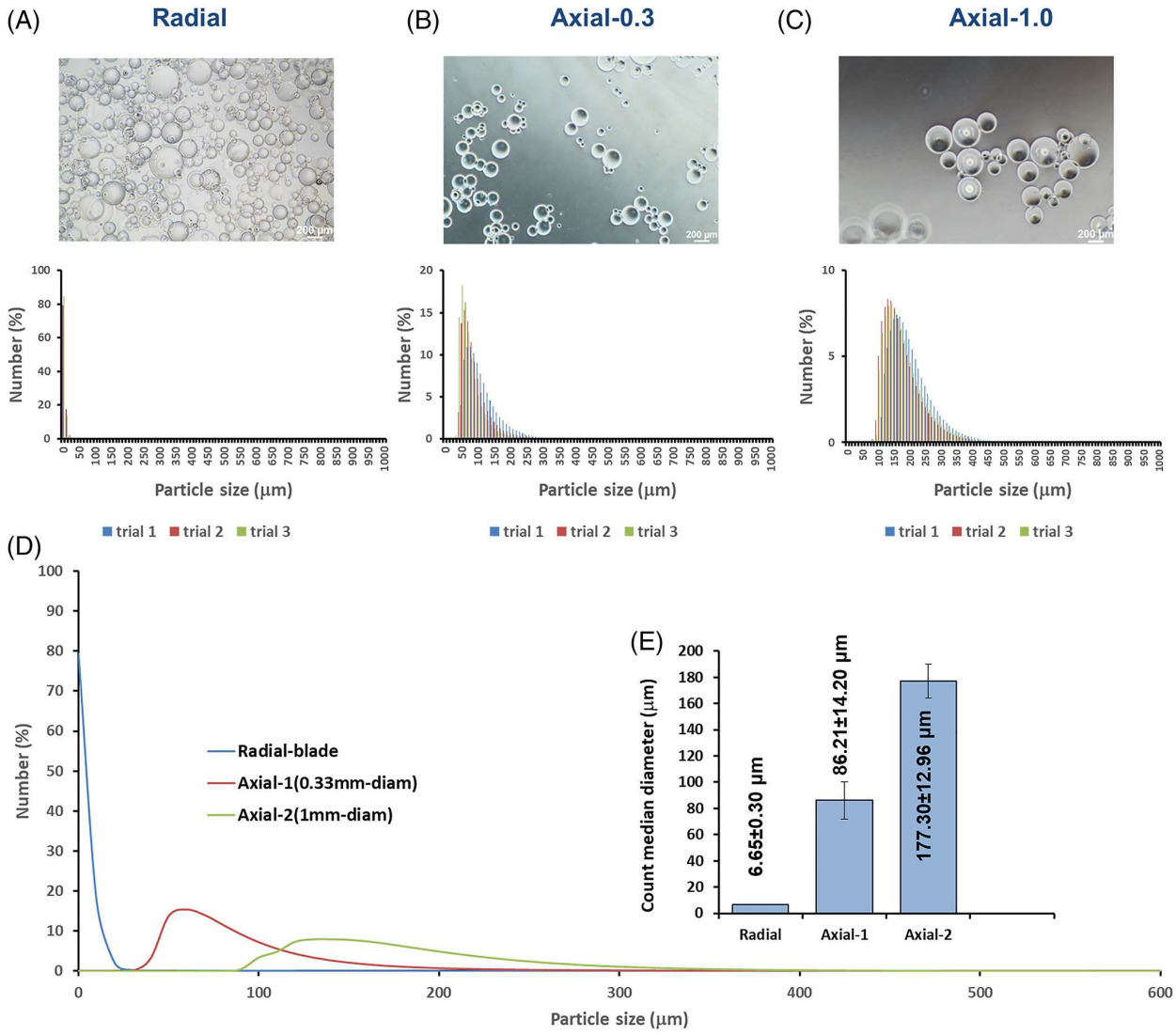

Figure 3.3: Effect of impeller geometry on microparticle size using a stirring rate of 500 rpm. Upper panels show brightfield optical microscopy and batch-to-batch size distribution of microparticles formed by (A) radial-blade, (B) 0.33 mm diameter axial-blade, and (C) 1.0 mm diameter axial-blade impeller geometries. Aggregate data are presented as (D) representative size distributions, and (E) median ± SD for each impeller geometry.

Axial impellers were introduced in the interest of confining critical shear forces to a minimized range of rotational radii, and hence values. This confinement was, in turn, intended to confine the size range of generated GmC. The two axial impeller geometries that were investigated differed in the diameter of the impeller blade: the Axial-0.3 configuration used 0.33 mm diameter

blades, while the Axial-1.0 version used 1.0 mm diameter blades. Axial blade impellers produced larger particles at the same rotation speed, relative to the radial impeller. The Axial-0.3 impeller created GmC with median diameters of 86.2 ± 14.2 μm, while the Axial-1.0 configuration produced microcarriers with median diameters of 177.3 ± 13.0 μm. Batch to batch reproducibility was very high for all impeller types (Figures S1 and S2). The error bars in Figures 3.3-3.5, and 3.6 represent the variation in average particle size between batches at the same fabrication conditions, further showing the repeatability between batches. The histograms in panel (d) of Figures 3.3-3.6 show the variation of particle size within a given batch, since they show the entire population size distribution. A comparison across all impeller geometries (Figure 3.3D) shows the distinct population size distribution produced by each impeller type at a single rotational speed. Microparticle populations produced by the radial configuration were generally too small for use as cellular microcarriers, and therefore subsequent experiments were performed with axial-blade impellers.

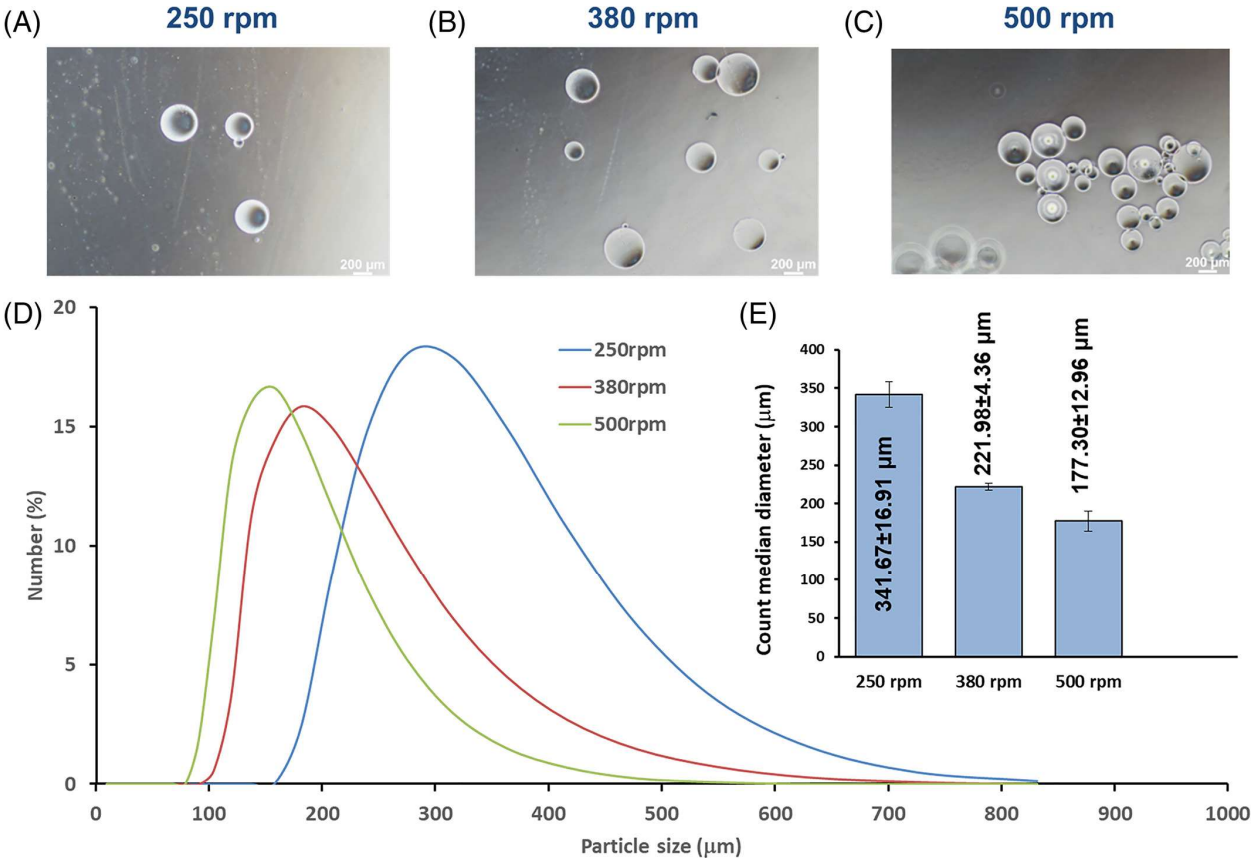

Figure 3.4: Effect of stirring rate on gelatin microparticle size using the Axial-1.0 impeller geometry. Upper panels show brightfield optical microscopy of microparticles formed at (A) 250 rpm, (B) 380 rpm, and (C) 500 rpm stirring rates. Aggregate data are presented as d) representative size distributions, and e) median ± SD for each stirring rate.

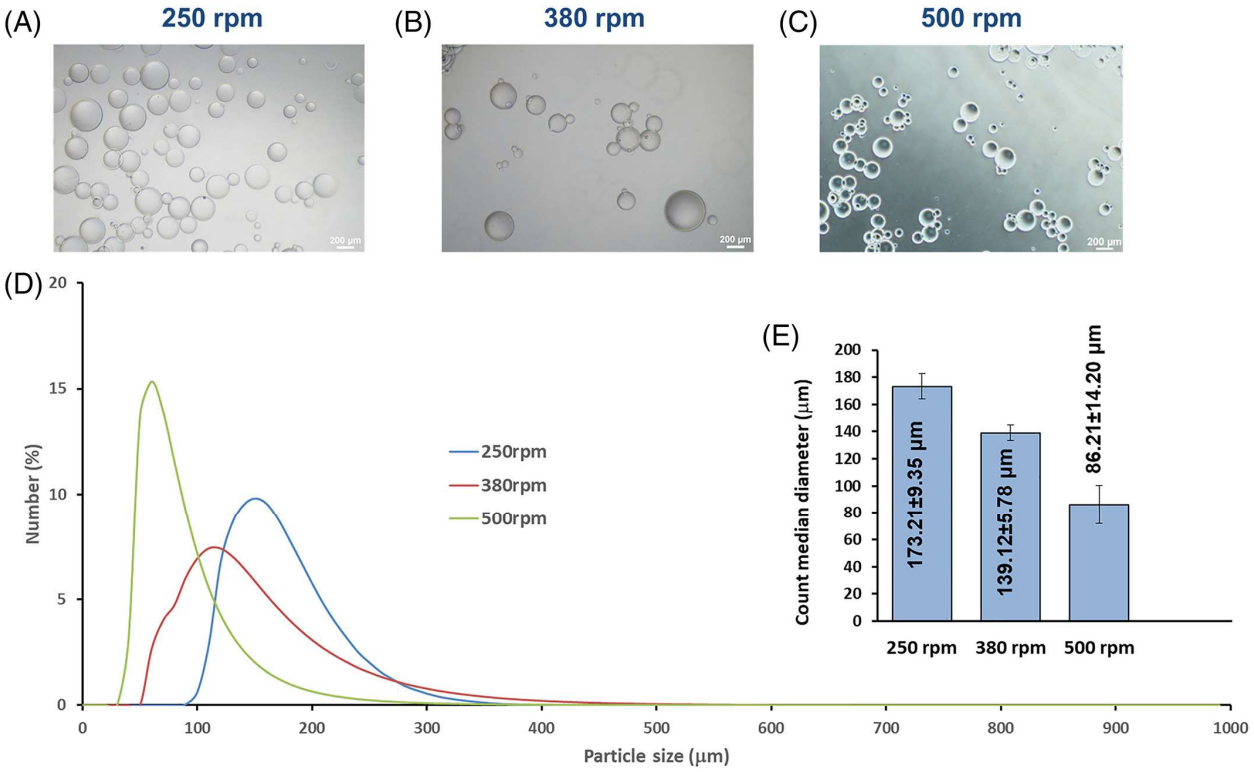

Figure 3.5: Effect of stirring rate on gelatin microparticle size using the Axial-0.3 impeller geometry. Upper panels show brightfield optical microscopy of microparticles formed at (A) 250 rpm, (B) 380 rpm, and (C) 500 rpm stirring rates. Aggregate data are presented as (D) representative size distributions, and (E) median ± SD for each stirring rate.

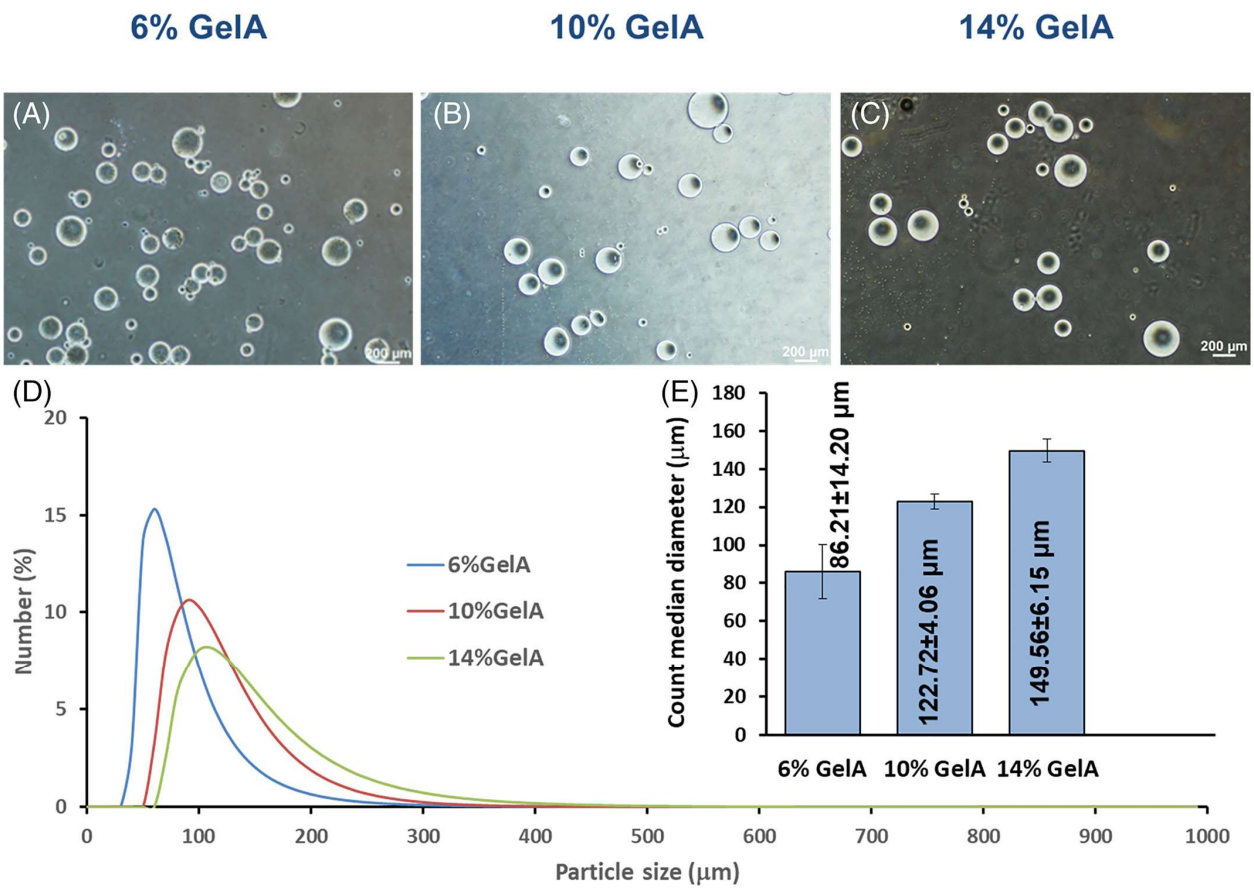

Figure 3.6: Effect of gelatin concentration on gelatin microparticle size using the Axial-0.3 impeller at 500 rpm. Upper panels show brightfield optical microscopy of microparticles formed at (A) 6.0% wt/vol, (B) 10.0% wt/vol, and (C) 14.0% wt/vol gelatin. Aggregate data are presented as (D) representative size distributions, and (E) median ± SD for each gelatin concentration.

The effect of impeller rotation speed was further examined using the axial blade configuration, again using a 6.0% wt/vol gelatin matrix. Increasing rotation speed of the Axial-1.0 impeller from 250 to 380 to 500 rpm produced microparticles with count median diameters of 341.7 ± 16.9 µm, 222.0 ± 4.4 µm, and 177.3 ± 13.0 µm, respectively, as shown in Figure 3.4. The population size polydispersity decreased moderately with increasing impeller rate, as shown by the histograms of particle size (Fig. 3.4D) and aggregate sizing data (Fig. 3.4E). A similar study using the Axial-0.3 impeller resulted in median microparticle diameters of 173.2 ± 9.4 µm, 139.1 ± 5.8 µm, and 86.2 ± 14.2 µm, at 250, 380, and 500 rpm, as shown in Figure 3.5. The size distribution became narrower at the highest impeller rate and this impeller configuration resulted

reproducible microcarrier batches in the general size range of 100–200 μm in diameter, which has been shown to be supportive of osteogenic activity of progenitor cells (Shapoff et. al., 1980; Leiblein et. al., 1980). Importantly, this size of microparticles is able to support attachment of multiple cells (50–100 per microcarrier, depending on size) and can also be injected through a needle as small as 21 gauge (inner diameter ~ 500 μm without damage.

Figure 3.6 shows the effects of gelatin concentration on the size of gelatin microparticles created using the Axial-0.3 impeller at a stirring speed of 500 rpm. The microparticles produced were similar in visual appearance (Fig. 3.6A–C), with a smooth and spherical morphology. Increasing the concentration of gelatin base material from 6.0% to 10.0% and 14.0% (wt/vol) resulted in decreased polydispersity of the microparticle population, as shown by the histogram of the particle size distribution (Fig. 3.6D). Increasing gelatin concentration also resulted in a clear increasing trend in median particle size, with median diameters of 86.2 ± 14.2, 122.7 ± 4.1 μm, and 149.6 ± 6.2 μm, respectively, as shown in the aggregate population data (Fig. 3.6E).

In general, microparticle size exhibited a positive relationship with the quantity of dissolved solids and a negative relationship with the rate of stirring during emulsification. Additionally, these results suggested a negative relationship between the dissolved solids quantity and the population size polydispersity of the generated microparticle batch. These relationships provide flexibility when designing microcarriers for particular applications. In other studies, surfactants have been employed during emulsification in efforts to achieve greater control over size distribution, though their effect has generally not been strong and there can be concern about the effect on cell viability and function (Hsu et. al., 1999, Kim et. al., 2007, Shen et. al., 2013). In the present study, microparticles were made without surfactants in the range of approximately 10–350 μm in diameter, depending on the impeller geometry, stirring rate, and matrix composition. It

should be noted that gelatin concentrations as low as 2.0% (wt/vol) could be used to fabricate microparticles (data not shown); however, at low concentrations the resulting particles were irregular, non-spherical, and generally more fragile. Stable, spherical particles are preferred in cell delivery applications since their flow and packing properties are more predictable.

3.3.2 Mechanical properties of gelatin materials

A range of mechanobiology studies have identified a link between cell culture substrate stiffness and the differentiation capacity of progenitor cells (Handorf et. al., 2015; Vining et. al., 2017; Butcher et. al., 2009; Cox et. al., 2011). Gelatin is markedly less stiff than the natural collagen-hydroxyapatite composite of bone, but has been used widely as a cytocompatible and stable substrate for the culture of many cell types. Importantly, surfaces of stiffness well below that of the ceramic compounds in native bone have been shown to provide osteogenic enhancement to progenitor cells (Ruiz et. al., 2008).

In the present study, the mechanical properties of gelatin at defined concentrations suitable for microparticle preparation were assessed using oscillatory shear rheometry, as shown in Figure 3.7. Hydrogels prepared with of 6.0%, 10.0%, and 14.0% (wt/vol) gelatin were found to have shear storage moduli (G') of 34.7 ± 3.7 kPa, 45.8 ± 1.8 kPa, and 47.5 ± 3.7 kPa, respectively (Fig. 3.7A). The corresponding loss moduli (G") were 1.0 ± 0.2 kPa, 1.2 ± 0.1 kPa, and 2.0 ± 0.3 kPa, respectively (Fig. 3.7B). The direct positive relationship between gelatin content and shear modulus is presumably a result of greater polymer entanglement and interactions at higher solids content. A strain sweep from 0.1% to 10% at 1 rad/s (Fig. 3.7C) showed that the storage modulus of 6.0% gelatin was markedly less sensitive to strain amplitude that that of the higher concentrations. This lower sensitivity to strain amplitude may result from an increased ratio between chemical and physical crosslinking, as chemical crosslinking is naturally less susceptible

to physical deformation. The shear modulus determined in this study for 6.0% (wt/vol) gelatin was similar to values previously reported to exhibit an osteogenic effect on similarly crosslinked collagenous substrates (Handorf et. al., 2015; Vining et. al., 2017; Butcher et. al., 2009; Cox et. al., 2011; Engler et. al., 2006). We chose the 6.0% gelatin for further study because of its consistent behavior across strain amplitudes, ease of preparation, and relevance to prior work (Solorio et. al., 2010; Turner et. al., 2018; Annamalai et. al., 2019; Lin et. al., 2017).

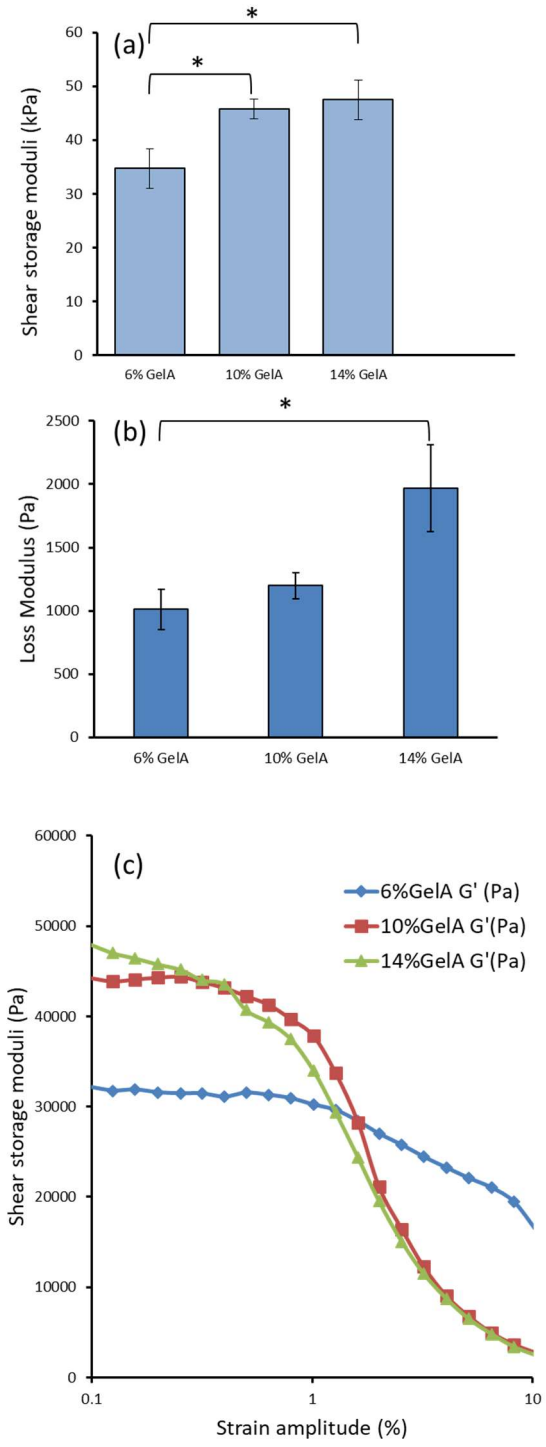

Figure 3.7: Mechanical properties of gelatin formulations determined using shear rheometry. Genipin-crosslinked gelatin materials were analyzed to determine the (A) storage modulus, (B) loss modulus, and (C) effect of strain amplitude for formulations of 6.0, 10.0, and 14.0% wt/vol. Brackets and associated stars indicate statistically significant differences ($p < .05$).

3.3.3 Viability and osteogenic effect of seeding density in GmC culture

Figure 3.8 shows images of formed GmC that were seeded with MSC at nominal cell densities of 5000 cells/cm^2 (5 K/cm^2), 25,000 cells/cm^2 (25 K/cm^2), or 50,000 cells/cm^2 (50 K/cm^2) GMC created using an Axial-1.0 impeller at 500 rpm, resulting in an average diameter of 177.3 μm. GMC were cultured over 3 weeks in either control or osteogenic media. Brightfield images showed highly spherical particles with cells attached to their surfaces (Fig. 3.8A). The genipin-treated microparticles have a blue to purple pigmentation as a side product of the genipin-gelatin crosslinking reaction (Lau TT, Wang C, & Wang DA, 2010; Solorio et. al., 2010; Annamalai et. al., 2019; Nahia-Neves et. al., 2018; Cho et. al., 2006). Viability staining of the cellular component allowed visualization of MSC under fluorescence microscopy. After 2 weeks of culture (Fig. 3.8B), cell viability assay in all sample conditions revealed highly viable cells, as evidenced by abundant green staining of living cells and very little red nuclear staining in dead cells. GmC fluoresce in the red channel due to autofluorescence caused by genipin crosslinking, which facilitated identification of the substrate but had the potential to mask the red signal of dead cells. However, control experiments showed the presence of red-stained dead cell nuclei following ethanol treatment (Figure S3), which could be distinguished from the background gelatin autofluorescence.

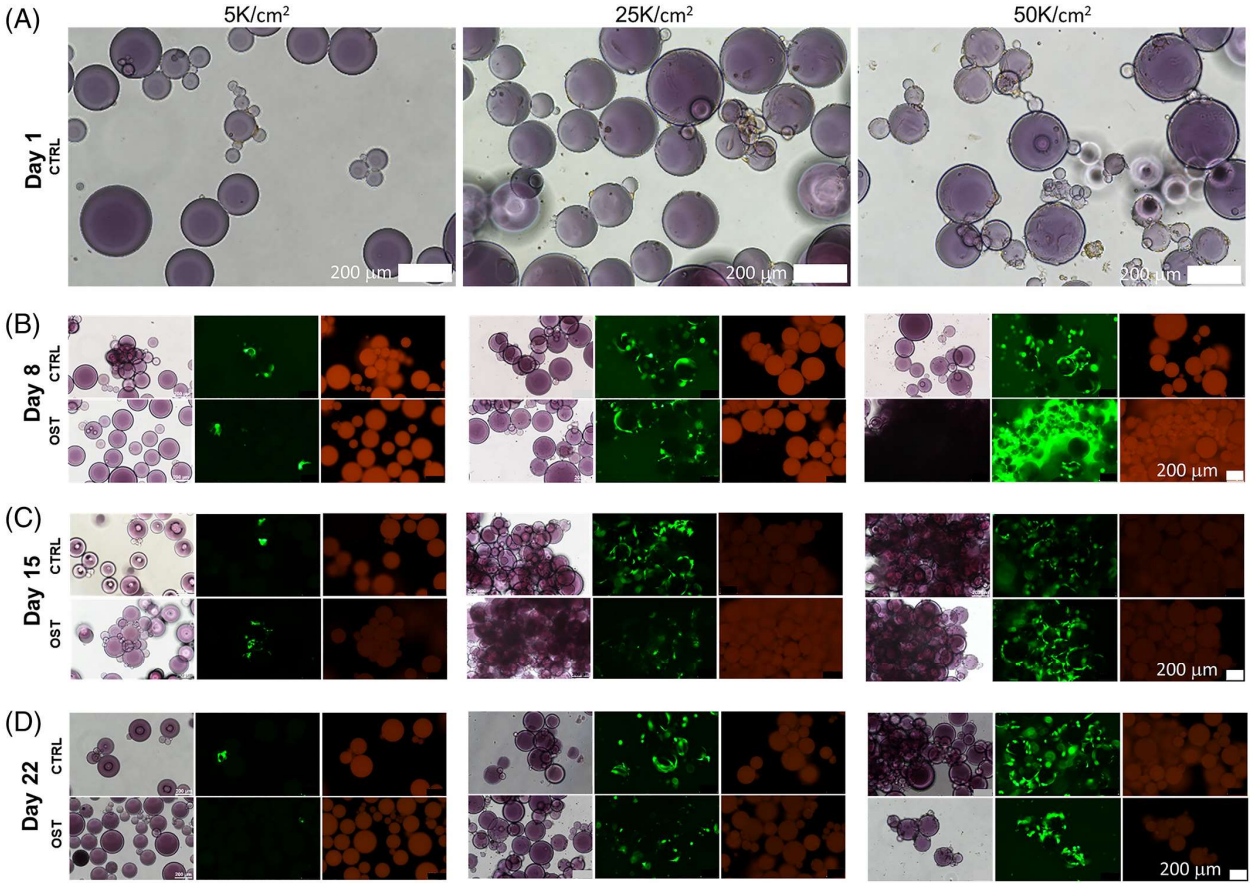

Figure 3.8: Optical microscopy images of MSC-laden gelatin microcarriers seeded at densities of 5000, 25,000, and 50,000 cells/cm^2. Microcarriers were cultured for 3 weeks in packed beds in either control (CTRL) or osteogenic (OST) medium. Brightfield images were taken at (A) day 1 after seeding, and brightfield and fluorescent images were subsequently taken at (B) day 8, (C) day 15, and (D) day 22 after seeding. Vital staining shows the cytoplasm of living cells in green. The genipin-crosslinked gelatin matrix autofluoresces slightly in the red channel, but dead cells can be distinguished by red punctate nuclei. Scale bars represent 200 µm.

Cell viability was high at all cell densities and was maintained for the three-week culture period. The panels in Figure 3.8 show only a single cross-section of the sample, but it was confirmed that cell viability was uniform over the microcarriers. Cell viability was similarly high and uniform on the microcarriers under both control and osteogenic conditions. High cell viability has been observed previously using microcarrier culture (Lau TT, Wang C, & Wang DA, 2010; Wissemann et. al., 1985; Yao et. al., 2013). The gelatin substrate, itself, is highly favorable for cell

attachment, maintenance, and growth (Bello et. al., 2020). In addition to these features contributing to GmC cytocompatibility, the genipin crosslinker is known to be significantly less toxic than more common crosslinkers like glutaraldehyde and 1-ethyl-3-(3-dimethyl aminopropyl) carbodiimide (Perez et. al., 2014). Examination of the green-stained cytoplasm of the cells in Figure 3.8 suggests that MSC were able to attach and spread on the surface of microcarriers and at higher densities formed confluent layers that covered the surface. Previous studies have shown that attachment efficiency of cells to microcarriers is routinely high (Sart et. al., 2013), and in the present study MSC seeding efficiency on 6.0% gelatin microcarriers was >96% (Figure S4). At this seeding efficiency, the average 177 μm diameter microcarrier would be expected to be seeded with approximately 15 cells per microcarrier on day 1 of culture, using a 15 K cell/ml seeding density. The microcarrier format has the advantage that cells are exposed directly to the culture medium over a large surface area, allowing ready diffusion of nutrients, oxygen, and waste products, which in turn promotes high viability. In addition, dead cells will not adhere to the microcarrier surface and therefore will be washed away in the medium. These factors likely contribute to the very high viability of MSC on GmC observed in this study.

Figure 3.9 shows quantification of DNA extracted from packed beds of cultured Microcarriers over time, which provides an indicator of relative cell numbers. At day 1, the assayed cell numbers related in general with the initial seeding density for both CTRL and OST conditions. At the 5 K/cm^2 and 25 K/cm^2 seeding densities, cell number remained relatively constant over the culture period in control medium. At the 50 K/cm^2 density, cell number declined over time in control medium and plateaued at a similar level to the samples with 25 K/cm^2 initial seeding density. In contrast, cell number in osteogenic medium increased by day 8, but then fell back to a level similar to the samples with 25 K/cm^2 initial seeding density at later time points. In general,

there was little cell proliferation observed across the 3 weeks study period. This finding may be due to the use of the packed bed culture geometry, in which the relatively higher regional cell concentration may have inhibited cell proliferation, relative to less concentrated suspension culture. Similar findings have been found in prior work on culturing MSC on scaffolds in static culture, which was shown to enhance osteogenic markers, but decreased cell proliferation (Tsai et. al., 2019). Similar rapid mineralization and matrix deposition was visible in the course of this study. Packed bed samples seeded at 25 and 50 K/cm^2 in CTRL and OST conditions had fused completely by day 15, and this behavior was observed as early as day 8 in 50 K/cm^2 samples. Taken together, these observations suggest a compounded osteogenic effect stemming from both the substrate material and culture method.

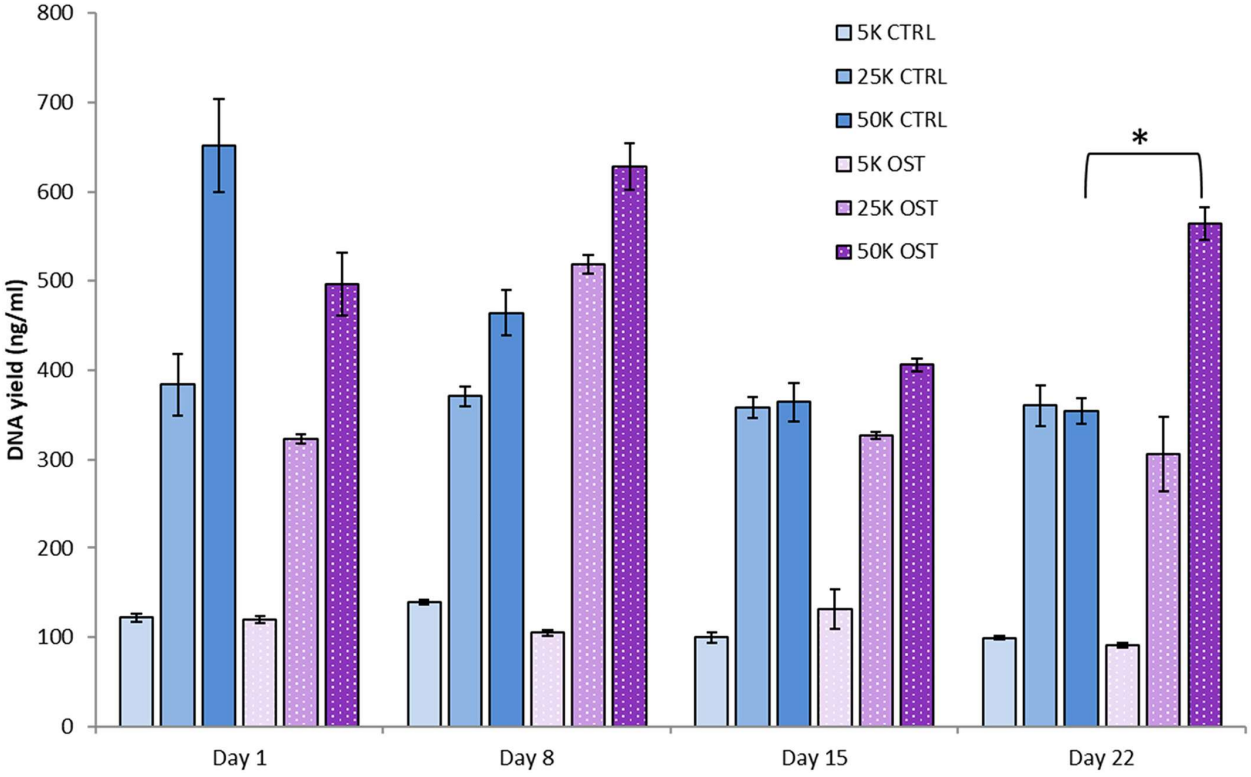

Figure 3.9: DNA content of gelatin microcarrier cultures over 3 weeks in control (CTRL) or osteogenic (OST) medium. Microcarriers were seeded at densities of 5000, 25,000, or 50,000 cells/cm^2 on day 0. Brackets and associated stars indicate statistically significant differences ($p < .05$).

Alkaline phosphatase (ALP) activity is an early marker of osteoblastic function and the process of matrix mineralization (Vimalraj et. al., 2020; Tseng et. al., 2011). Figure 3.10 shows ALP activity of cells cultured on Microcarriers over time in response to control and osteogenic media, both in absolute terms (Fig. 3.10A) as well as normalized to DNA content (Fig. 3.10B). At the lowest cell seeding density (5 K/cm^2), ALP activity did not change significantly over 3 weeks in culture in either control or osteogenic conditions. In contrast, at the higher seeding densities (25 and 50 K/cm^2) ALP activity increased significantly by day 8 and then returned to baseline levels. This effect was especially prominent in osteogenic culture and persisted when the data were normalized for DNA content, which is related to cell number.

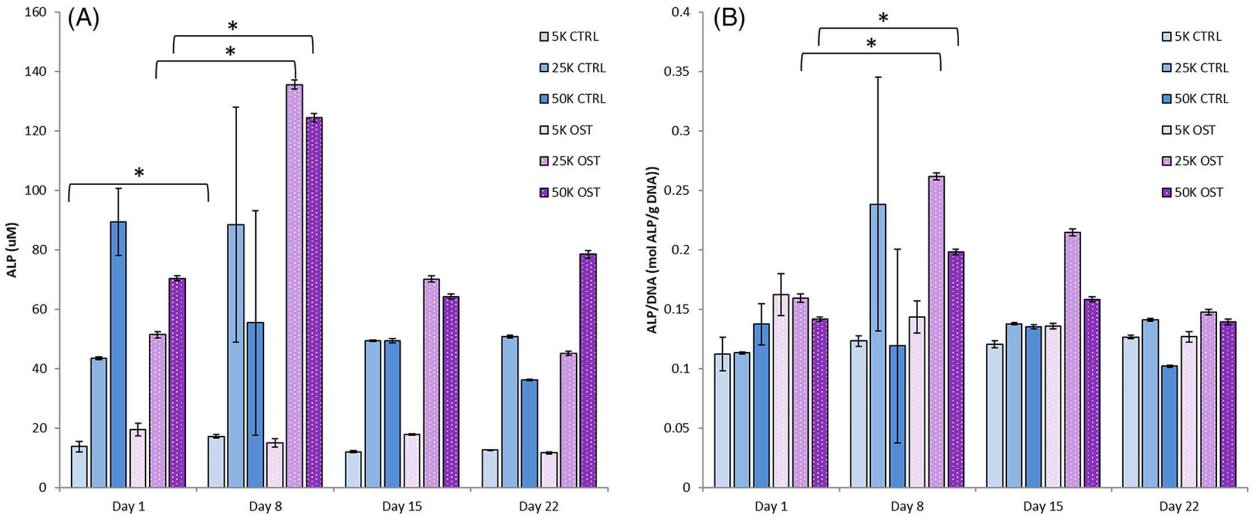

Figure 3.10: Quantification of alkaline phosphatase (ALP) activity of gelatin microcarrier cultures over 3 weeks in control (CTRL) or osteogenic (OST) medium. Microcarriers were seeded at densities of 5000, 25,000, or 50,000 cells/cm^2 on day 0. ALP activity is expressed as (A) absolute amount, and (B) normalized relative to DNA content. Brackets and associated stars indicate statistically significant differences ($p < .05$).

Calcium deposition is a direct indication of matrix mineralization and osteogenesis. Figure 3.11 shows calcium deposition in Microcarriers cultures over time in response to control and

osteogenic media, both in absolute terms (Fig. 3.11A) as well as normalized to DNA content (Fig. 3.11B). Calcium deposition generally increased over time in both control and osteogenic media, though the effect was markedly enhanced in osteogenic conditions. By day 15 and 22 in osteogenic medium, the 25 K/cm^2 cultures had achieved 15.7-fold and 16.9-fold increases in calcium deposition, respectively, relative to day 1. The 50 K/cm^2 cultures in osteogenic medium achieved 17.2-fold and 19.3-fold increases in calcium deposition, respectively, over the same time period. When normalized for DNA content, the general trends of increased calcium deposition over time were still pronounced; however, the effect of cell density became evident. Low seeding density (5 K/cm^2) resulted in higher relative calcium deposition per cell than higher cell densities by days 14 and 21, in both control and osteogenic media. In osteogenic medium, the amount of calcium deposited per cell was inversely related to the initial seeding density, suggesting that higher cell numbers have an inhibitory effect on relative matrix mineralization due to rapid cell reduction.

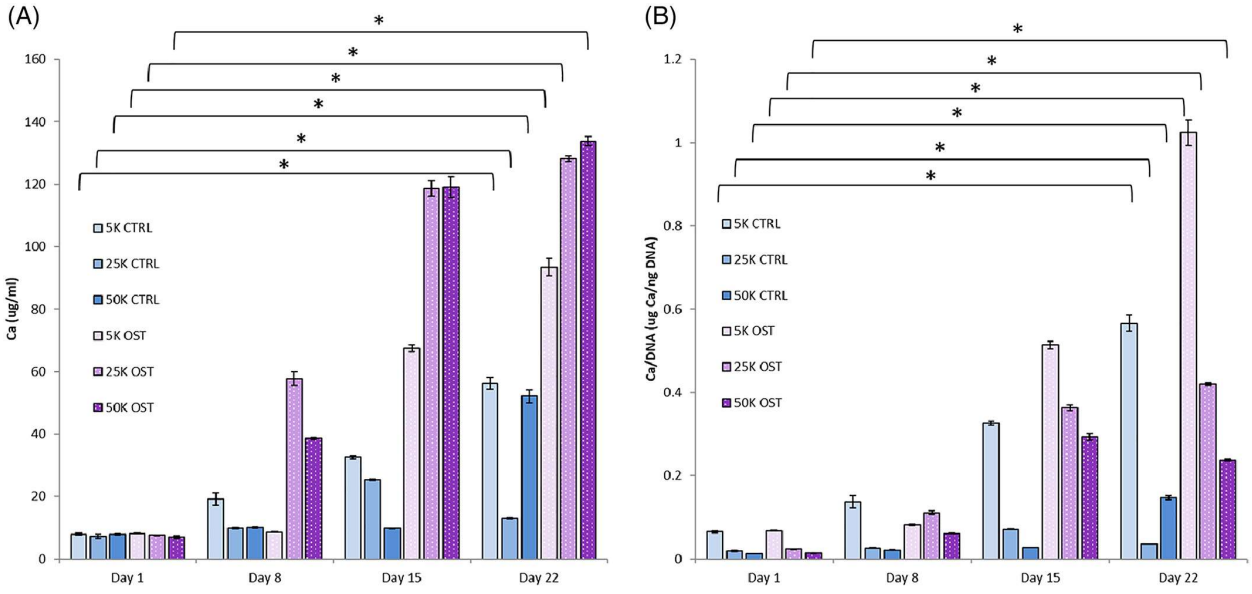

Figure 3.11: Quantification of calcium deposition (Ca) of gelatin microcarrier cultures over 3 weeks in control (CTRL) or osteogenic (OST) medium. Microcarriers were seeded at densities of 5000, 25,000, or 50,000 cells/cm^2 on day 0. Calcium deposition is expressed as (A) absolute amount, and (B) normalized relative to DNA content. Brackets and associated stars indicate statistically significant differences ($p < .05$).

3.4 Conclusions

This study demonstrates that high yields of genipin-crosslinked gelatin microparticles can be reproducibly fabricated using a facile water-in-oil emulsification method. The size and size distribution of microparticle populations can be varied by controlling the impeller geometry, stirring rate, and concentration of gelatin. The mechanical properties of the matrix vary with gelatin concentration, with increasing concentrations resulting in stiffer matrices. Our studies show more specifically that a 6.0% (wt/vol) microparticle used as a microcarrier for adult human MSC maintained high cell viability of attached cells over 3 weeks in culture in both control and osteogenic medium. The progenitor cells undergo osteogenic differentiation over time in culture, as evidenced by increased alkaline phosphatase activity and mineral deposition. The degree of osteogenesis is dependent on the initial seeding density of the microcarriers, with higher densities generally resulting in greater absolute osteogenic function. However, higher cell densities may also inhibit some aspects of matrix mineralization through a negative feedback effect. Taken together, these findings suggest that genipin-crosslinked GmC with a narrow size distribution are easily fabricated without the use of surfactant. The processed GmC support high cell attachment and viability, and are suitable substrates for the osteogenic differentiation of human progenitor cells. Such microcarriers are promising candidates for the culture and delivery of osteoprogenitor cell lines, and may have utility in regenerative medicine approaches to orthopedic tissue repair.

Chapter 4 Effects of Matrix Composition on Gelatin-Hydroxyapatite Microcarrier Osteogenicity to Surface-Cultured Mesenchymal Stem Cells

Bone-tissue regenerative systems typically rely on an osteoprogenitor cell component and biologically-relevant substrate materials. Modular platforms formulated from bone matrix-like biomaterials potentiate the osteogenic culture, direct transplantation with minimal invasiveness, and conformal infill of irregular defects. The work of this study covers the water-in-oil batch emulsification processing of gelatin-apatite microspheres and post hoc genipin crosslinking. Particle size was found to increase with gelatin or hydroxyapatite content Shear rheometric characterization revealed direct positive relationships of matrix modulus to gelatin concentration, hydroxyapatite concentration, and cycles of mineralization. Additionally, hydroxyapatite concentration was found to be indirectly related to hydrogel swelling ratio, adult human mesenchymal stromal cell (MSC) seeding efficiency, viability signal, and DNA yield. Highest cytocompatibility was associated with 0% hydroxyapatite, non-mineralized substrates. Packed bed-cultured microcarriers of 6.0-14.0 % (wt/vol) gelatin, 1.0-10.0 % (wt/vol) hydroxyapatite 6.0% (wt/vol) gelatin, and 0-5 cycle-solution-mineralized 6.0% (wt/vol) gelatin were subsequently seeded with MSC at a seeding density of 1.5×10^4 cells/cm^2 of GmC surface area in control or osteogenic media. Seeding efficiencies of all non-solution surface-mineralized GmC were all above 90%. Generally, both cell viability and DNA yield, indicators of cell number, peaked one week into culture after which both declined for the remaining weeks across all conditions, in an inverse relationship with GmC surface calcium deposition. Upregulation of DNA-normalized alkaline phosphatase activity and calcium deposition across conditions indicated a degree of

osteogenicity in all culture conditions with or without osteogenic supplements, however, these effects were most pronounced on 6.0% (wt/vol) gelatin and 5.0% (wt/vol) hydroxyapatite 6.0% (wt/vol) gelatin GmC. In totality, the findings suggest that gelatin-calcium-phosphate-mineral GmC promote osteogenic cellular development on transferrable, physically-tunable substrates prior to a certain degree of mineralization, through cytocompatibility reduction. Additional research into GmC osteoprogenitor cell retention can advance their utility in better addressing bone defects.

4.1 Introduction

Severe injuries to bone and surrounding tissues can significantly inhibit regeneration, which in some cases can lead to orthopaedic non-unions (Roberts et. al., 2012; de Grado et. al., 2018). Such injuries may require advanced interventions, including the application of cell- and biomaterial-based solutions that combine osteoprogenitor cells (Presen et. al., 2019; Rao et. al., 2013), a supportive scaffold, regenerative biochemical factors (Verrier et. al., 2016; Perez et. al., 2018; Lin et. al., 2019; Sobacchi et. al., 2018), as well as control of paracrine or immunomodulatory signaling (Pajarinen et. al., 2019; Humbert et. al., 2019). Modular scaffold systems are attractive in these applications because of their potential for minimally invasive delivery, maximal defect infill, and the possibility of creating multiphase tissue constructs (Chen et. al., 2013; Kim et. al., 2005; Nweke et. al., 2020; Rao et. al., 2015). In the bone regenerative field, there are a variety of approaches using milliscale auto- or allo-graft bone filler systems (Chao et. al., 2015; Petruskevicius et. al., 2002). However, microscale modules, or microcarriers, provide increased surface area to volume ratios relative to larger particles, which may have advantages in achieving higher cell capacity, material rigidity, and osteogenicity (Nweke et. al., 2020).

A variety of commercial microcarriers currently exist and are used in a range of biomedical applications (Chen et. al., 2020; Ornelas-Gonzalez et. al., 2021). In addition to their usefulness in the expansion of cells in bioreactors with limited vessel volumes, microcarriers can provide culture surfaces for directed differentiation of progenitor cells. An advantage of culturing cells on microcarriers is that it allows bulk cell transplantation without trypsinization, which can disrupt critical cell-matrix and cell-cell contacts. Furthermore, the culture and delivery of cells as populations in packed beds can be beneficial to cell engraftment, and may enable improved availability of nutrients, even in ischemic environments.

Microcarriers used in bone regeneration typically are formed from relatively abundant, biologically-relevant materials, such as collagen Type I, gelatin, calcium phosphates, calcium carbonates, apatites, and bioactive glasses (Saltz et. al., 2016; Shadjou et. al., 2015; Ghomi et. al., 2021; Ballouze et. al., 2021). These microparticles are often formed through emulsification in batch processes or by dropwise pinched flow microfluidic systems (Nweke et. al., 2020). Typically, microcarriers are crosslinked thermally or chemically after fabrication to improve their stability and mechanical properties (Perez et. al., 2014). Collagen-based materials, like extracted collagen peptides and further-processed gelatin, are cytocompatible, commercially available, and easily processed (Hsu et. al., 1999; Dosta et. al., 2020; Sart et. al., 2013; Yang et. al., 2007; Overstreet et. al., 2003; Hayashi et. al., 2011; Chao et. al., 2015). Their mechanical properties can also be augmented by addition of mineral and other components to enhance their osteogenic capacities. Similarly, calcium phosphate-based and bioactive glass microspheres have been coated in hydroxyapatite mineral through sequential submersion in simulated body fluid (SBF) to achieve positive osteogenic effects (Malda et. al., 2006; Ducheyne et. al., 1997; Hong et. al., 2009; Qiu et.

al., 2000; Qiu et. al., 2001; Qiu et. al., 1998; Winkler et. al., 2018; Baino et. al., 2018; McLaren et. al., 2019).

Microcarriers formed directly from a mineral phase have also been used. Tricalcium phosphate (TCP) is a material with similar composition to native hydroxyapatite, which can be induced to transition to hydroxyapatite through thermal or chemical processing (Perez et. al., 2014; Park et. al., 2014; Perez et. al., 2011; Perez et. al., 2013; Park et. al., 2011; Cuzmar et. al., 2015; Mankani et. al., 2006). Composite microspheres of TCP and hydroxyapatite seeded with mesenchymal stromal cells (MSC) have been shown to support in vitro osteogenic differentiation and promote de novo bone growth when implanted in murine calvarial and mandibular defects (Park et. al., 2010; Park et. al., 2013). Hydroxyapatite is a mineral of particular interest because of its similarity to native bone's reinforcing ceramic phase (Kim et. al., 2005; Winkler et. al., 2018; Park et. al., 2013), and it has been suggested to allow cell adhesion and proliferation (Barrias et. al., 2004; Mateus et. al., 2008). Notably, microscale particles of hydroxyapatite seeded with MSC have been found to result in bone formation in subcutaneous murine implants, while larger particles engendered fibrous tissue formation (Fischer et. al., 2003).

The current study evaluates osteogenic microcarriers formed from gelatin through a water-in-oil emulsification process. Microcarriers were crosslinked with genipin, a small molecule with low cytotoxicity relative to commonly used aldehyde crosslinkers (Yang et. al., 2018). While genipin has been used in other microcarrier applications, its effects over longer term culture have not been investigated (Lau TT, Wang C, & Wang DA, 2010; Lau TT, Wang C, Peng SW, Su K, & Wang DA, 2010; Lau et. al., 2012). The effect of addition of hydroxyapatite to the microcarriers was tested by direct admixing of mineral to the matrix during emulsification, or by post-hoc surface mineralization. Formed microcarriers were characterized in terms of size and population size

distribution, and the mechanical properties were determined using shear rheometry. The microcarriers were then used for the culture of MSC in a packed bed configuration to loosely mimic transplantation. Cell viability, proliferation, and phenotype were monitored over three weeks in culture under control and osteogenic conditions. The goal of this work was to carefully characterize the effects of genipin crosslinking and hydroxyapatite addition on MSC viability and phenotype over multi-week culture.

4.2 Materials and Methods

4.2.1 Materials

Type A (acid-treated porcine skin) 225 bloom strength gelatin and hydroxyapatite nanopowder (particle size <200 nm) were procured from Sigma Aldrich (St. Louis, MO, USA). A 100 cSt polydimethylsiloxane (PDMS) product was procured from Clearco Products (Bensalem, PA, USA). Pluronic® L101, a nonionic, difunctional, block copolymer surfactant, was procured from BASF Corporation (Vandalia, IL, USA). Genipin, a naturally-derived crosslinking agent, was procured from Wako Chemicals (Richmond, VA, USA). Calcium Chloride (CaCl2), disodium hydrogen phosphate (Na_2HPO_4), Tris(hydroxymethyl)aminomethane (Tris), and hydrochloric acid (HCl) were purchased from Sigma-Aldrich.

4.2.2 Generation of gelatin and gelatin-hydroxyapatite microcarriers

A water-in-oil emulsification process, illustrated schematically in Figure 4.1, was used to generate gelatin and gelatin-hydroxyapatite microscale droplets. Aliquots of 5.0 mL of the desired gelatin concentration (6.0, 10.0, or 14.0% (wt/vol) gelatin in PBS at pH 7.4) were equilibrated within a 37 °C water bath. Gelatin-hydroxyapatite aliquots were created by admixing the desired

hydroxyapatite concentration (1.0, 5.0, 10.0% (wt/vol) hydroxyapatite in PBS at pH 7.4) to a 5.0 mL 6.0% (wt/vol) aliquot of gelatin solution and following with 10 minutes of sonication. Each gelatin or gelatin-hydroxyapatite mixture was then added dropwise to a stirred 50 mL PDMS oil bath held at 40 °C on a heated plate. The resultant emulsions were stirred at a set rate of 500 rpm. After 5 minutes of stirring at 40 °C, the resulting emulsion was transferred to a 4 °C ice bath and stirring was continued for an additional 30 minutes to allow microdroplet solidification. The resulting suspension of solid gelatin or gelatin-hydroxyapatite microparticles was mixed with PBS at 23 °C containing 0.01% (vol/vol) Pluronic L101 surfactant and centrifuged at 300 × G for 5 minutes to collect the gelatin or gelatin-hydroxyapatite microparticles and separate them from the PDMS phase [34]. Remaining surfactant solution was extracted from collected microparticles by re-suspension and washing in PBS for further processing.

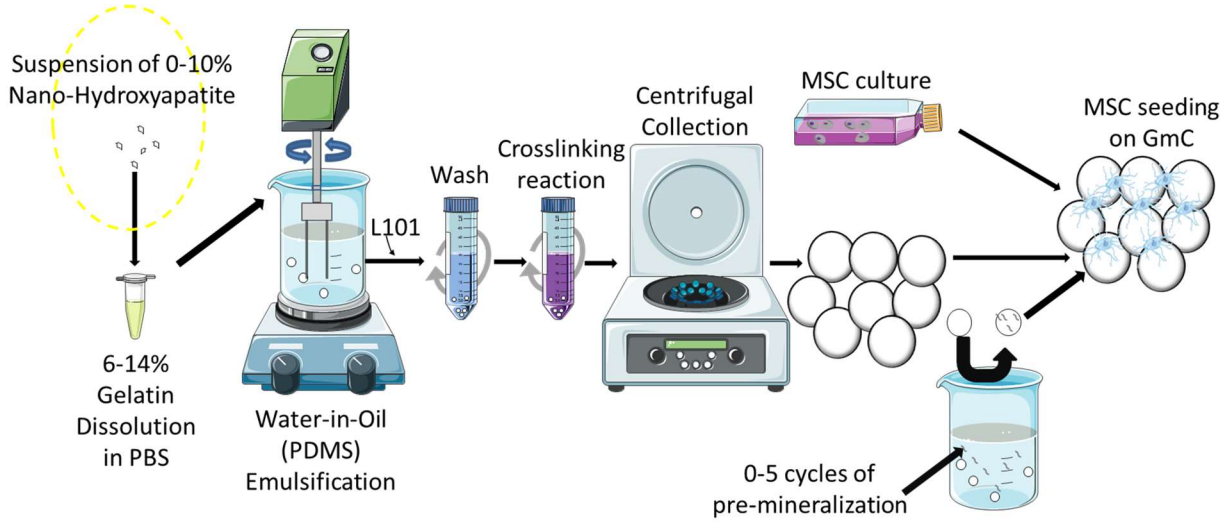

Figure 4.1: Scheme showing gelatin and gelatin-hydroxyapatite microcarrier (GmC) production by water-in-oil emulsification, subsequent loading with cells (MSC).

4.2.3 Genipin crosslinking of gelatin and gelatin-hydroxyapatite microcarriers

Gelatin or gelatin-hydroxyapatite microparticles were admixed to 1.0% (wt/vol) genipin in PBS solution under continuous rotational suspension to allow crosslinking to occur. Degree of

crosslinking was time-dependent and a mixing duration of 48 hours at 23 °C was used to allow total saturation of reactive amine groups (Solorio et. al., 2010). Genipin creates crosslinks by catalyzing reactions between lysine residues on amine moieties of the gelatin molecule. Hydrogels crosslinked in this manner have been determined to reach a maximum degree of crosslinking of approximately 90 %, which imparts a mild red autofluorescence to the gelatin-based material (Hwang et. al., 2011, Turner et. al., 2017). The gelatin used in this study had a melting temperature of approximately 32 °C, such that crosslinking could be carried out at room temperature without fusion of particles. Crosslinked gelatin-based microcarriers (GmC were washed successively in ethanol and deionized (DI) water to extract residual genipin. All microcarriers were subjected to 10 minutes of ethanol-submersion sterilization and UV sterilization (Sylvania UV-C 255 nm germicidal T8 30W lamp) before use.

4.2.4 Solution-supersaturated apatite mineralization of gelatin microcarriers

Alternatively, as companion to direct addition of apatite, GmC composed of 6.0% (wt/vol) gelatin were mineralized through a process of successive exposures to a schedule of supersaturated mineralization solutions. Pre-mineralization, of this type, in advance of cell introduction allows unfettered stiffening of biopolymer constructs. The composition of the aforementioned supersaturation solutions was selected to control the composition of resultant crystal deposits (Sadowska et. al., 2019). GmC were initially immersed in 200 mM $CaCl_2$ solution (pH adjusted to 7.4 with Tris-HCl) for 2 hours under continuous rotational suspension at 37°C. They were next collected and extracted from solution through centrifugation at 300 × G for 5 minutes. These collected GmC were transferred to a 120mM Na_2HPO_4, 30mM $NaHCO_3$ solution for 2 hours under continuous rotational suspension at 37°C. Then, after a second round of centrifugal collection, the treated GmC were rinsed in distilled water and centrifugally collected to end one cycle of

mineralization. Three batches of GmC were passed through 1, 3, or 5 cycles of mineralization, respectively. All were then subjected to ethanol and UV sterilization before further use.

4.2.5 Particle size analysis

General examination and characterization of the morphology of gelatin microparticles was accomplished using light microscopy. GmC micrographs were captured with an inverted phase contrast microscope and analyzed using NIS Elements viewer software (Nikon). Automated particle size measurement was performed using laser diffraction analysis (Malvern Mastersizer 2000S, Westborough, MA). Samples of microcarrier dispersions were suspended in DI water within the sample reservoir agitated at 1750 rpm. The count median diameter for GmC was measured until the recorded laser obscuration exceeded 5%. Using Mie light scattering theory, a gelatin refractive index of 1.52, and water's refractive index of 1.33, the particle analyzer calculated a distribution of spherical particle diameters by scanning 30,000 snapshots over a 30 second time-span. Data generated from automated particle analysis were used to graph particle size distributions and calculate population statistics. Histograms presented in this work use bins in which the bin labels represent the maximum size of the lower bin, which is also the minimum size of the next larger bin.

4.2.6 Mechanical characterization of gelatin and gelatin-hydroxyapatite materials

Rheological analysis was used to determine the impact of gelatin and hydroxyapatite concentration on material mechanical properties. Gelatin, gelatin-hydroxyapatite, and solution-mineralized gelatin hydrogels were characterized using a rotational rheometer (AR-G2, TA Instruments, Newcastle DE) with a Peltier temperature-controlled stage and 8 mm parallel plate measurement head. Measurements were taken at 25 °C on 10 mm diameter discoid samples of 6.0,

10.0, or 14.0% (wt/vol) gelatin at a pre-load of 0.5 N with a gap height of 3 mm. A 0.1-10 radian/second (rad/s) oscillating frequency sweep test was conducted at a constant oscillating strain of 0.1% to identify the linear viscoelastic region (LVER). A 0.1 - 10% oscillating strain sweep test was then administered at a constant oscillating frequency of 1 rad/s to establish a modulus-strain relationship for the specified concentrations of gelatin hydrogels. Finally, a 20 s time sweep test was administered at a constant oscillating frequency of 1 rad/s and constant oscillating strain of 0.1%.

4.2.7 Swelling ratio of gelatin and gelatin-hydroxyapatite materials

Swelling ratios of all gelatin and gelatin-hydroxyapatite hydrogels were determined on 4 mm diameter discoid samples. Samples were biopsy-punched from 3 mm thick gelatin-composite sheets processed in similar fashion to the microcarrier batches of their respective compositions. Each was allowed to swell in PBS over 24 hours and weighed. This measurement was signified as the swollen weight, W_s. Following a subsequent 24 hour lyophilization process, the resultant dried hydrogel samples were weighed. And this measurement was signified as the dry weight, W_d. The following equation was then used to calculate the percentage increase in hydrogel weight from water absorption, signified as the swelling ratio:

$$Swelling\ ratio = \frac{W_s - W_d}{W_d} \times 100\%$$

4.2.8 Cell culture

Human bone marrow-derived mesenchymal stem cells (MSC, RoosterBio, Frederick MD) were expanded to passage 7 in defined growth medium (RoosterNourishTM, RoosterBio,

Frederick MD). Control medium (CTRL) consisted of Dulbecco's Modified Eagle's Medium (DMEM) supplemented with 10% (vol/vol) fetal bovine serum (FBS) and 1% (vol/vol) penicillin-streptomycin. Osteogenic (OST) medium was prepared by adjusting CTRL medium to final concentrations of 0.2 mM L-ascorbic acid 2-phosphate, 10 mM β-glycerophosphate, and 100 nM dexamethasone. All cell culture was performed in a standard incubator at 37 °C in a 5% CO_2. Upon reaching 70–80% confluence in T-175 polystyrene culture flasks, MSC were trypsinized and suspended in medium for seeding onto GmC at a cell density of 15,000 MSC/cm^2 (15K/cm^2) in all cell culture experiments. Nutrient medium was changed every 3-4 days over the span of a three-week culture period.

4.2.9 Cell viability, number, ALP activity, and calcium deposition

On day 1 after seeding of 6.0-14.0% (wt/vol) gelatin or 1.0-10.0% (wt/vol) hydroxyapatite, 6.0% (wt/vol) GmC, and subsequently on day 8, day 15, and day 22 of culture, MSC were assayed for DNA content, ALP activity, and calcium deposition. These assays were used to characterize the number, proliferation rate, and differentiated state of the MSC. Additionally, vital staining was performed on days 8, 15, and 22 to determine the viability, general shape, and distribution of MSC in microcarrier culture. Similarly, on day 1, 7, 14, and 21 of cell culture on 0-5 cycle-mineralized 6.0% (wt/vol) GmC, MSC were assayed for vital staining, DNA content, ALP activity, and calcium deposition.

Packed-beds of MSC-loaded microcarriers were transferred to 24-well plates for visual inspection and were incubated with 0.1% (vol/vol) calcein AM and 0.1% (vol/vol) ethidium homodimer in DMEM for 45 minutes prior to rinsing and suspension in PBS. Both fluorescence and bright-field imaging on an inverted microscope were used to assess cell viability and morphology. Live cells were captured in the green fluorescence channel while the red channel of

the same field of view was imaged to capture any dead cells and microcarrier autofluorescence. Corresponding bright-field images of these fields captured all cells and microcarriers.

The quantity of cellular DNA in samples was assayed as a measure of relative cell numbers, which were used to normalize ALP activity and calcium deposition, using the commercially available Quanti-iT™ PicoGreen double-stranded DNA assay kit kit (Invitrogen, Grand Island, NY) as described previously (Annamalai et. al., 2018). Briefly, total DNA was isolated from packed-bed culture samples through solubilization in 0.1% (wt/vol) sodium dodecyl sulfate 10 mM Tris-HCL solution (0.1%SDS TBS) adjusted to a pH of 7.5. Samples were subsequently centrifuged at 10,000 × G for 10 minutes before aspiration of supernatants for further use in quantifying DNA content by PicoGreen assay using the manufacturer's protocol and reagents. Briefly, lysate samples, alongside reference samples of Lambda-DNA standards, were admixed with 0.5% (vol/vol) PicoGreen 1mM ethylenediaminetetraacetic acid (EDTA) TBS for 5 minutes of reaction time. Fluorescence signal from each reacted sample, pipetted into a 96-well plate, was read with an excitation wavelength of 485 nm at an emission wavelength of 528 nm.

ALP activity was quantified as described previously (Annamalai et. al., 2018) by first lysing MSC in 0.1 % SDS TBS, centrifuging at 10,000 × G for 10 minutes, and then collecting the respective supernatants. Sample supernatants were each admixed with 1.5 M 2-amino-2-methylpropanol-buffered 5 mM p-nitrophenyl phosphate substrate solution in a 96-well plate for 30 minutes of reaction on shaker plate. This reaction was stopped with the addition of 3.0 N NaOH to all sample wells. Sample absorbance was measured at 405 nm.

Calcium deposition was measured using an orthocresolphthalein complex one (OCPC) method described in earlier studies (Babur et. al., 2015; Saito et. al., 2013). Briefly, sample sediments from 10,000 × G centrifugation were digested in 1.0 N acetic acid overnight on a 37°C

shaker plate. These were each then admixed with a 5:5:2:88 volume ratio blend of 14.8 M ethanolamine-boric acid buffer (pH 11), 1 mg/ml OCPC solution, 50 mg/ml 8-hydroxyquinoline in 95% ethanol solution, and deionized water in a 96-well plate for 10 minutes of reaction on shaker plate. Sample absorbance was then measured at 575 nm.

4.2.10 Statistical analysis

Microcarrier sizes, mechanical data, ALP activities, calcium levels, and DNA are all reported as numerical mean ± standard deviation with n=3. For these data sets, groups were compared and analyzed by ANOVA and t-test. A resulting F-value of greater than F-critical and a p-value of less than 0.05 between groups were considered statistically significant.

4.3 Results and Discussion

4.3.1 Characterization of microparticle morphology and cell attachment efficiency

The effect of gelatin and hydroxyapatite content on the average size and size distribution of gelatin microparticles was assessed both through optical imaging and automated particle size analysis. All formulations of batch-emulsified gelatin microparticles exhibited visually smooth-surfaced and spheroidal geometries, as shown in Figure 4.2. Microcarrier diameter is functionally significant to determining available surface area for cell attachment. Size distribution of microcarrier populations is important for the determination of achievable microparticle packing density (Man et. al., 2005; Baule et. al., 2014), which also factors into the total available surface area for cell attachment.

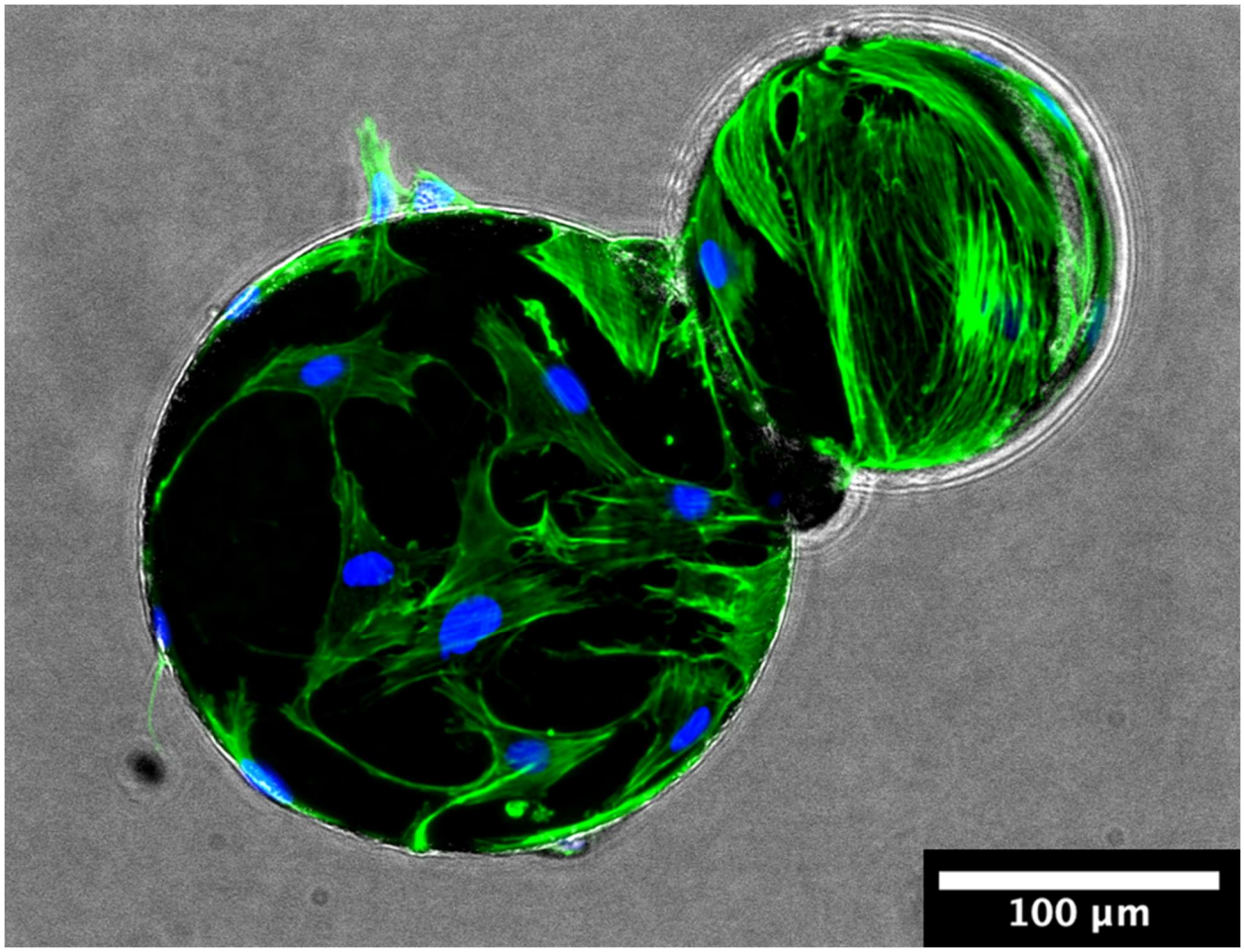

Figure 4.2: Spinning disk confocal microscopy image of MSC-laden 10% hydroxyapatite, 6% gelatin microcarriers (GmC) after one week of culture. MSC were stained with phalloidin for cytoskeletal features and DAPI for nuclei. Scale bar reperesents 100 µm.

Figure 4.3 shows the effect of gelatin and hydroxyapatite content on microparticle size relative to a 6.0 % wt/vol gelatin matrix. Panels A-B show images of the produced microparticles and the representative size distributions for each batch. Batch to batch reproducibility was very high for all GmC types. Importantly, this general size range of microparticle large is enough to support the attachment of multiple cells, small enough to be injected through a 21 gauge (inner diameter ~500 µm) needle without damage, and has been shown to be supportive of osteogenic activity in progenitor cells (Shapoff et. al., 1980; Leiblein et. al., 1980). Figure 4.3A, specifically,

shows the effects of gelatin concentration on the size of gelatin microparticles created at a stirring rate of 500 rpm. Increasing the concentration of gelatin base material from 6.0 % to 10.0 % and 14.0 % (wt/vol) resulted in decreased polydispersity of the microparticle population. Increasing gelatin concentration also resulted in a clear increasing trend in median particle size, with median diameters of 86.2 ± 14.2, 122.7 ± 4.1 μm, and 149.6 ± 6.2 μm, respectively.

Figure 4.3B shows the effects of hydroxyapatite concentration on the size of gelatin microparticles created at a stirring rate of 500 rpm. Increasing the suspended concentration of hydroxyapatite at emulsification from 0.0 % to 1.0 %, 5.0 % and 10.0 % (wt/vol) resulted in a general increasing trend in median particle size, with median diameters of 80.3 ± 7.1, 108.0 ± 2.4 μm, 149.5 ± 4.3 μm, and 134.0 ± 2.2 μm, respectively.

Figure 4.3C shows the average seeding efficiency of MSC on 6.0 %, 10.0 %, and 14.0 % (wt/vol) gelatin GmC to be uniformly high at 96.3 ± 1.1, 95.7 ± 1.7 μm, and 94.1 ± 4.0 μm, respectively. Previous studies have shown that attachment efficiency of cells to gelatin-based microcarriers is typically high (Sart et. al., 2013). Figure 4.3D shows the average seeding efficiency of MSC on 1.0 %, 5.0 % and 10.0 % (wt/vol) hydroxyapatite 6.0 % (wt/vol) gelatin GmC to be uniformly high at 93.4 ± 3.5, 92.2 ± 2.9 μm, and 93.1 ± 0.7 μm, respectively.

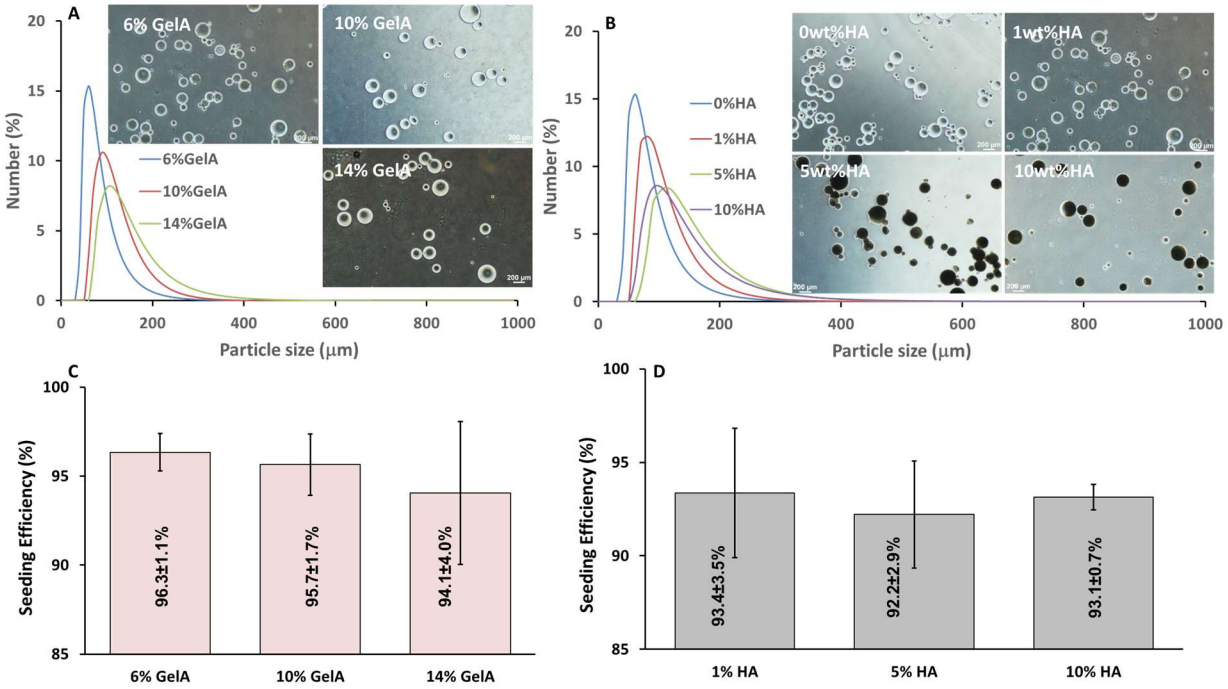

Figure 4.3: (a) Size analysis of 6-14 wt% gelatin GmC, (b) size analysis of 0-10 wt% HA GmC, (c) MSC seeding efficiency on 6-14 wt% gelatin GmC, and (d) MSC seeding efficiency on 0-10 wt% HA GmC. Scale bar represents 400 μm.

In general, microparticle size exhibited a positive relationship with the quantity of dissolved solids and a negative relationship with the rate of stirring during emulsification. Additionally, these results suggested a negative relationship between the dissolved solids quantity and the population size polydispersity of the generated microparticle batch. These relationships provide flexibility when designing microcarriers for particular applications. In other studies, surfactants have been employed during emulsification in efforts to achieve greater control over size distribution, though their effect has generally not been strong and there can be concern about the effect on cell viability and function (Hsu et. al., 1999; Shen et. al., 2013; Kim et. al., 2007). In the present study, microparticles were made without surfactants in the range of approximately 80-150 μm in diameter, depending on the stirring rate and matrix composition. Stable, spherical

particles are preferred in cell delivery applications since their flow and packing properties are more predictable. Additionally, all gelatin-based GmC supported high MSC seeding efficiency.

4.3.2 Mechanical and swelling properties of gelatin and gelatin-hydroxyapatite materials

A range of mechanobiology studies have identified a link between cell culture substrate stiffness and the differentiation capacity of progenitor cells (Handorf et. al., 2015; Vining et. al., 2017; Butcher et. al., 2009; Cox et. al., 2011). Gelatin is markedly less stiff than the natural collagen-hydroxyapatite composite of bone, but has been used widely as a cytocompatible and stable substrate for the culture of many cell types. Importantly, surfaces of stiffness well below that of the ceramic compounds in native bone have been shown to provide osteogenic enhancement to progenitor cells (Ruiz et. al., 2008).

In the present study, the mechanical properties of gelatin-hydroxyapatite and solution-mineralized gelatin, at defined concentrations suitable for microparticle preparation, were assessed using oscillatory shear rheometry, as shown in Figure 4.4. A strain sweep from 0.1-10 % at 1 rad/s (Fig. 4.3A) showed that the storage modulus of gelatin-based hydrogel was less sensitive to strain amplitude at lower concentrations of hydroxyapatite. This lower sensitivity to strain amplitude may result from an increased ratio between chemical and physical crosslinking, as chemical crosslinking is naturally less susceptible to physical deformation. Hydrogels prepared with of 0.0 %, 1.0 %, 5.0 %, and 10.0 % (wt/vol) hydroxyapatite, 6.0 % (wt/vol) gelatin were found to have shear storage moduli (G') of 34.7 ± 3.7 kPa, 53.4 ± 4.4 kPa, 61.6 ± 5.2 kPa, and 70.8 ± 2.9 kPa, respectively (Figs. 4A-B). The direct positive relationship between hydroxyapatite content and shear modulus is presumably a result of higher solids content and structural reinforcement. The corresponding swelling ratios were 817.2 ± 149.3 %, 778.0 ± 2.8 %, 546.7 ± 9.2 %, and 395.2 ± 15.0 %, respectively (Fig. 4.3C). Conversely, the negative relationship between hydroxyapatite

content and hydrogel swelling is likely also due to higher solids content and water displacement. Hydrogels of 6.0 % gelatin subjected to 0, 1, 3, and 5 cycles of solution-mineralization were found to have shear storage moduli (G') of 21.1 ± 0.6 kPa, 21.1 ± 0.6 kPa, 28.2 ± 2.1 kPa, and 63.3 ± 9.6 kPa, respectively (Fig. 4.3D). The shear moduli measured in this study were generally similar to values previously reported to exhibit an osteogenic effect on similarly crosslinked collagenous substrates (Handorf et. al., 2015; Vining et. al., 2017; Butcher et. al., 2009; Cox et. al., 2011; Engler et. al., 2006).

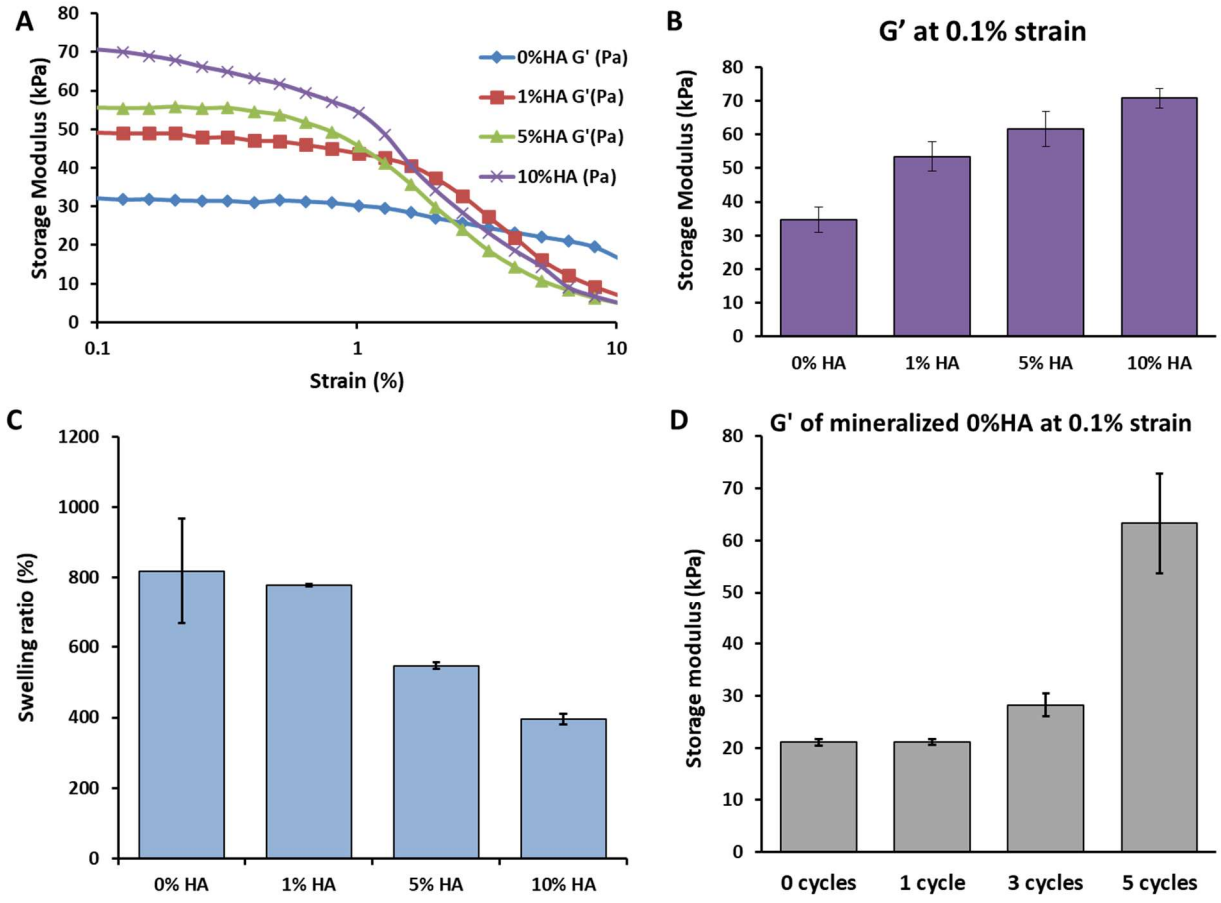

Figure 4.4: Analyses of 0-10 wt% HA genipin-crosslinked gelatin hydrogel (a,b) oscillatory shear rheometry storage moduli over a 0.1-10% strain sweep, (c) swelling ratio, and (d) 0-5 cycle-mineralized 0 wt% HA gelatin hydrogel storage moduli.

4.3.3 Viability and osteogenic effect of matrix properties

Figure 4.5 shows images of MSC cultured on 6.0-14.0% (wt/vol) GmC at a nominal cell density of 15,000 cells/cm^2 (15K/cm^2). MSC were cultured for 3 weeks in either control or osteogenic media. Viability staining of the cellular component allowed visualization of MSC under fluorescence microscopy. After one week of culture, cell viability assessment in all sample conditions revealed highly viable cells, as evidenced by abundant green staining of living cells and very little red nuclear staining in dead cells. GmC fluoresce in the red channel due to autofluorescence caused by genipin crosslinking, which facilitated identification of the substrate but had the potential to mask the red signal of dead cells. However, control experiments showed the presence of red-stained dead cell nuclei following ethanol treatment (data not shown), which could be distinguished from the background gelatin autofluorescence. The degree and intensity of green cytoplasmic staining exhibited a positive relationship with gelatin content.

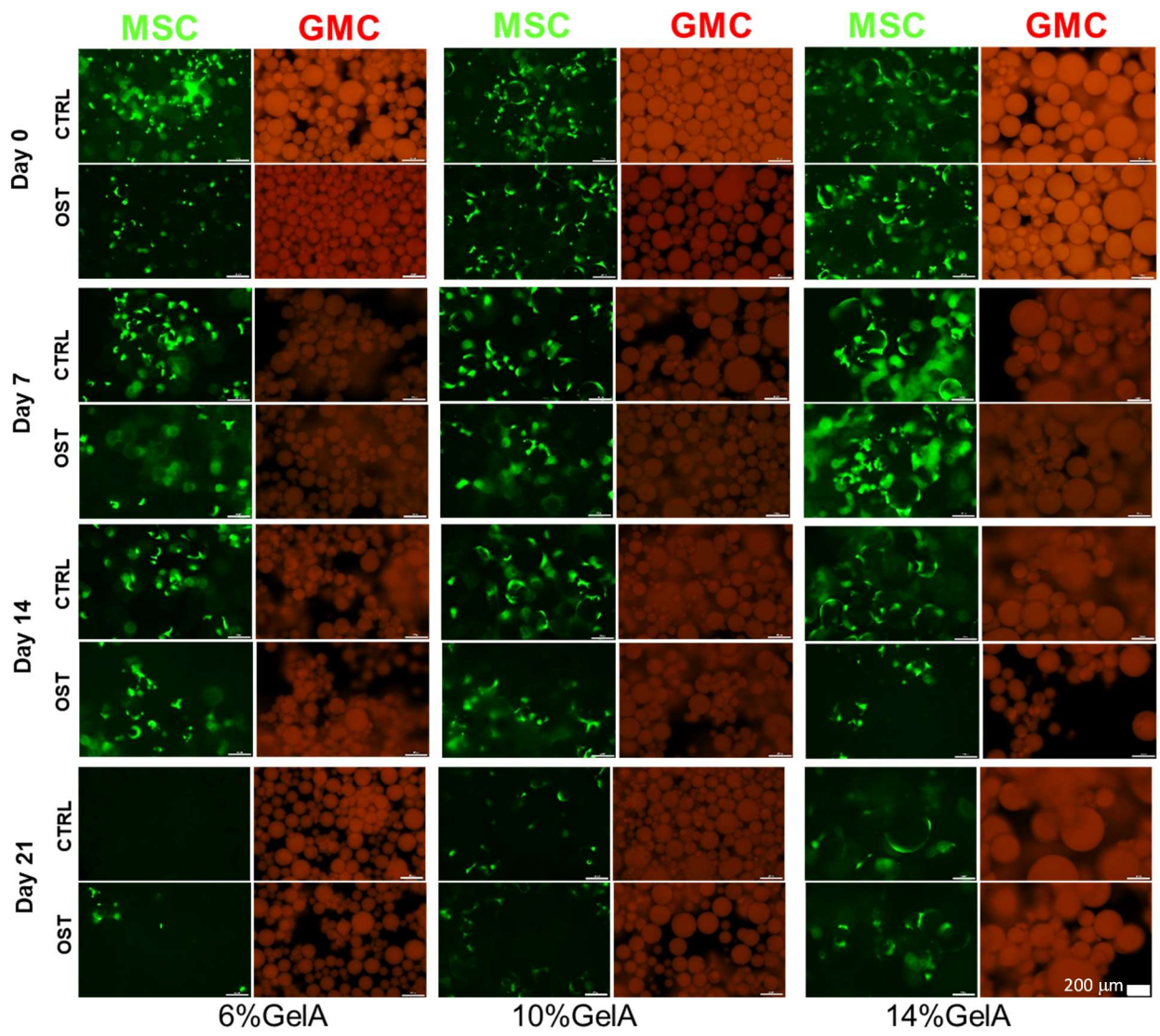

Figure 4.5: Optical microscopy images of MSC-laden 6-14% gelatin microcarriers seeded at a density of 15,000 cells/cm^2. MSC were cultured for three weeks on GmC in either control (CTRL) or osteogenic (OST) media. Fluorescent images were taken on day 0 to day 21 of culture. Vital staining shows the cytoplasm of living cells in green. The genipin-crosslinked gelatin matrix autofluoresces in the red channel. Scale bars represent 200 µm.

Cells in all culture conditions demonstrated a general trend of decreasing green staining over time. This effect was increasingly pronounced as gelatin content decreased, with 6.0% (wt/vol) GmC-cultured MSC DNA quantities diminishing to the lowest levels on the final day of culture. These general relationships between cell staining, gelatin concentration, and time were

reflected in the DNA assay data shown in Figure 4.6. Additionally, high cell viability has been observed previously using collagen-peptide-based microcarrier culture (Lau TT, Wang C, & Wang DA, 2010; Wissemann et. al., 1985; Yao et. al., 2013). The gelatin substrate, itself, is highly favorable for cell attachment, maintenance, and growth (Bello et. al., 2020). In addition to these features contributing to GmC cytocompatibility, the genipin crosslinker is known to be significantly less toxic than more common crosslinkers like glutaraldehyde and 1-ethyl-3-(3-dimethyl aminopropyl) carbodiimide (Yang et. al., 2018).

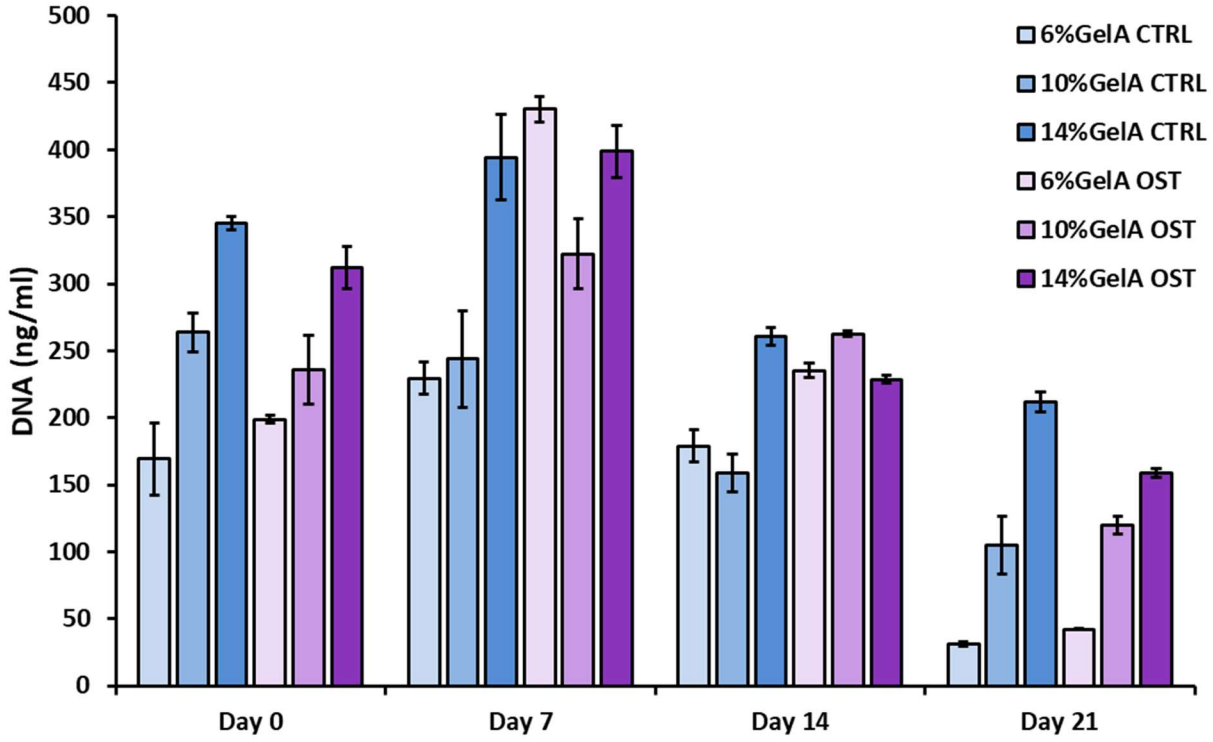

Figure 4.6: DNA growth from MSC seeded at 15K cells per cm^2 and cultured on 6-14wt.% GelA GmC in control and osteogenic media.

Figure 4.7 shows MSC viability staining on 1.0-10.0% (wt/vol) HA, 6.0% (wt/vol) gelatin GmC over 3 weeks of culture in either control or osteogenic media. As in culture experiments on 6.0-14.0% (wt/vol) gelatin GmC, maximum viability staining was observed at one week into

culture for all sample conditions. Hydroxyapatite content did not appear to diminish GmC autofluorescence in the red channel. The degree and intensity of green cytoplasmic staining exhibited a negative relationship with hydroxyapatite content, seeming to indicate lower cytocompatibility of hydroxyapatite to MSC, relative to gelatin. As in gelatin-only GmC culture, there was a general trend of decreasing green staining over time. This was most pronounced on 10.0% (wt/vol) HA, 6.0% (wt/vol) GmC.

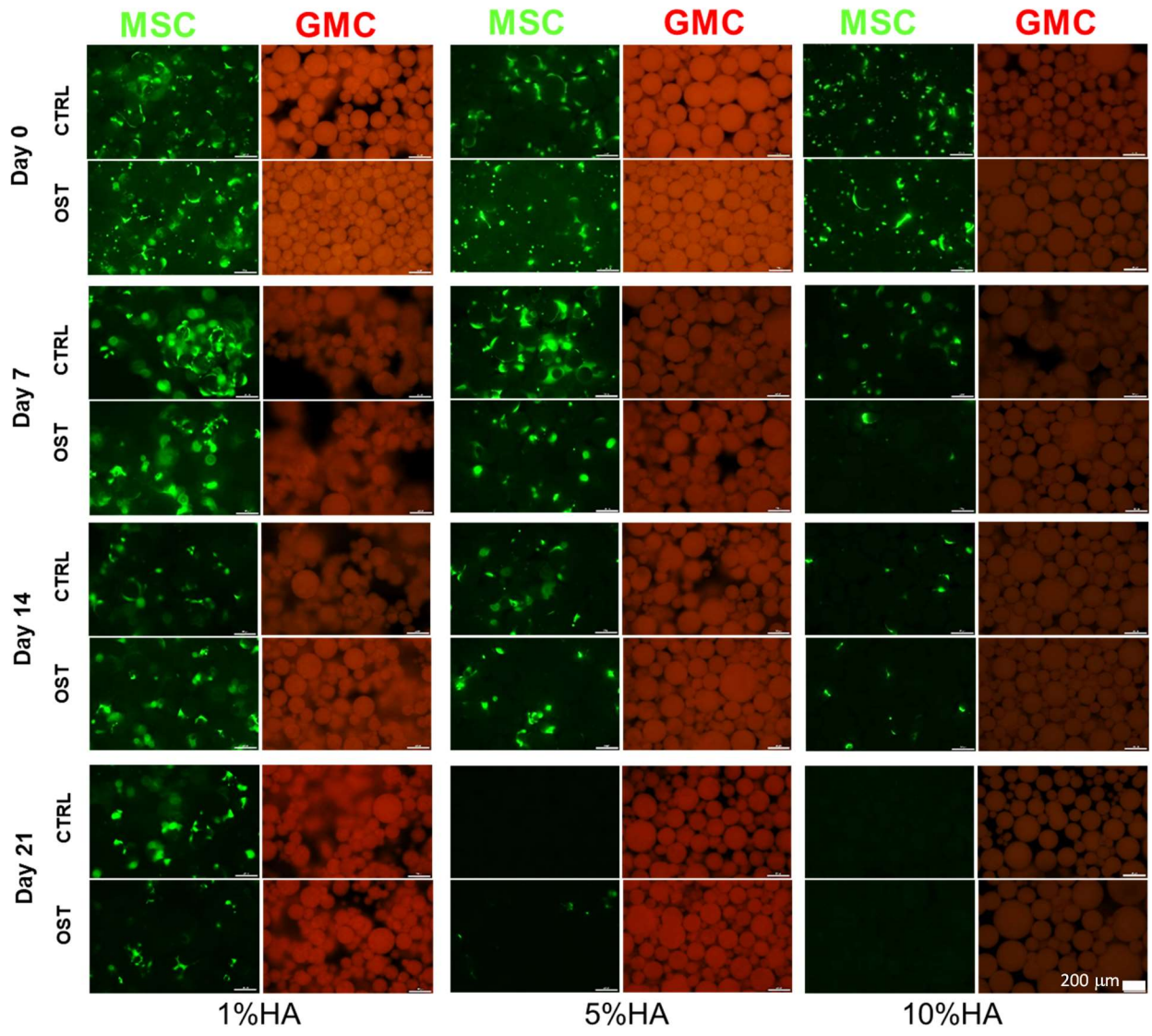

Figure 4.7: Optical microscopy images of MSC-laden 1-10%HA GmC seeded at a density of 15,000 cells/cm^2. MSC were cultured for three weeks on GmC in either control (CTRL) or

osteogenic (OST) medium. Fluorescent images were taken on day 0 to day 21 of culture. Vital staining shows the cytoplasm of living cells in green. The genipin-crosslinked gelatin matrix autofluoresces in the red channel. Scale bars represent 200 μm.

Much like in the gelatin-only GmC culture experiments, general relationships between cell viability staining, hydroxyapatite concentration, and time were reflected in the DNA assay data, which is shown in Figure 4.8. Maximum DNA levels were observed after one week of culture on GmC of lower hydroxyapatite content. These quantities reduced with time in similar fashion to cell viability staining, in a manner increasingly pronounced with increasing hydroxyapatite content in both control and osteogenic media.

Cells proliferated in 1.0% (wt/vol) HA GmC culture for one week of culture only to decrease thereafter. As hydroxyapatite content is increased, proliferation in this type of culture was even further negatively impacted, with DNA quantities decreasing monotonically over the entirety of the experiment in MSC cultured on 10.0% (wt/vol) HA GmC. This may result from the use of packed bed culture geometry, in which a cell concentration relatively higher than in suspension culture, inhibits cell proliferation. Similar findings have been found in prior work where MSC were cultured on scaffolds in static culture, which has been shown to enhance osteogenic markers, while decreasing cell proliferation (Tsai et. al., 2019). In accordance with the findings of this previous study, rapid mineralization and matrix deposition was increasingly observed throughout this study.

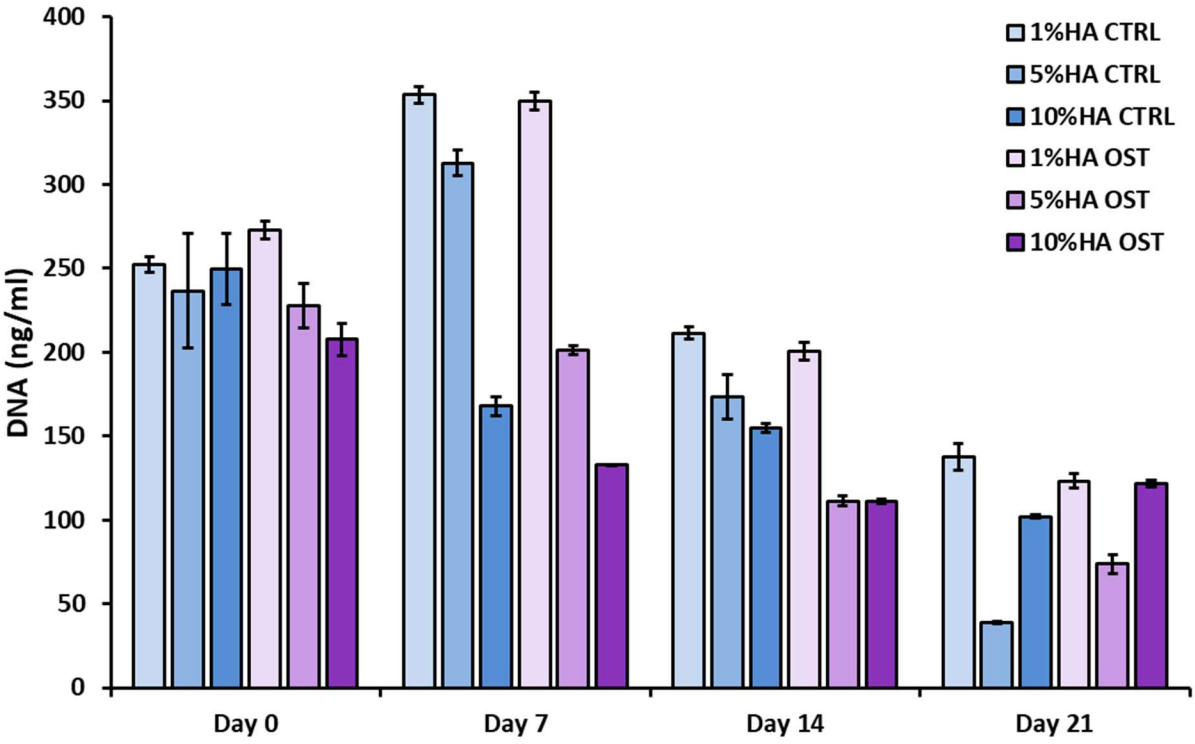

Figure 4.8: DNA growth from MSC seeded at 15K cells per cm^2 and cultured on 1-10wt.%HA GmC in control and osteogenic media.

Figure 4.9 shows Day 1 and Day 21 images of MSC cultured for 3 weeks in either control or osteogenic media on 6.0% (wt/vol) gelatin GmC treated for 0-5 cycles in mineralization solution at a nominal seeding density of 15,000 cells/cm^2 (15K/cm^2). Viable cell area coverage across all conditions and time-points was greatly reduced when compared to culture experiments on gelatin and lab-grade hydroxyapatite-based GmC. Over three weeks of culture, viable cell coverage generally reduced in all mineralized and unmineralized GmC environments, though to a lesser degree in the latter. Similarly, DNA levels remained relatively level in unmineralized GmC culture conditions or diminished in mineralized GmC culture conditions. Essentially, the viable cell data and DNA data reflected a general reduction in cell number in relation to a greater mineral-to-gelatin ratio.

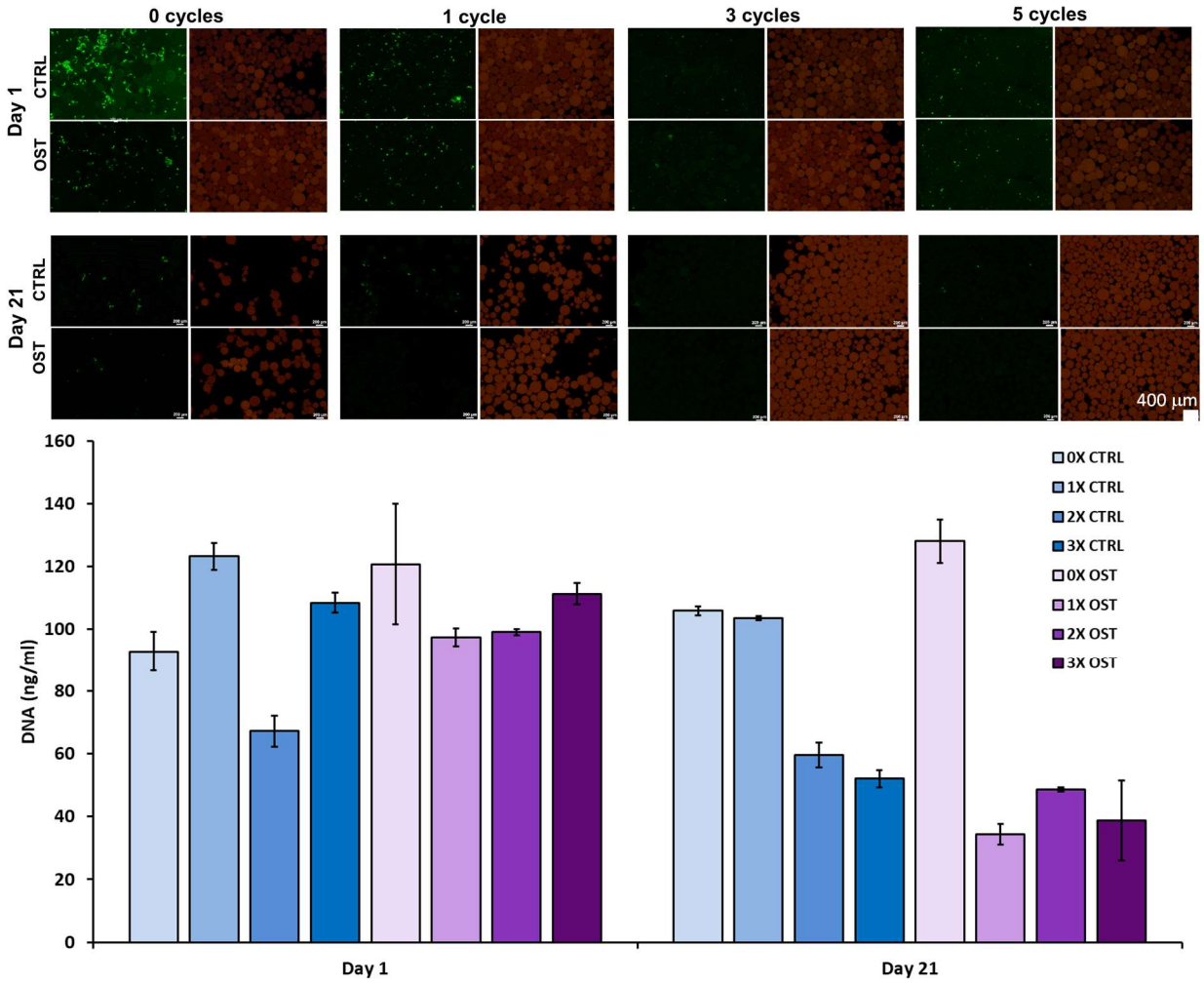

Figure 4.9: Live/Dead staining and DNA levels of MSC cultured on 0-5 cycle supersaturation--mineralized 6%GelA GmC at a seeding density of 15,000 cells/cm^2. MSC were cultured for three weeks on GmC in either control (CTRL) or osteogenic (OST) medium. Fluorescent images were taken on day 0 and day 21 of culture. Vital staining shows the cytoplasm of living cells in green. The genipin-crosslinked gelatin matrix autofluoresces in the red channel. Scale bar represents 400 µm.

Alkaline phosphatase (ALP) activity is an early marker of osteoblastic function and the process of matrix mineralization (Vimalraj et. al., 2020; Tseng et. al., 2011). Figure 4.10A and 4.10B show ALP activity of cells cultured on 6.0-14.0% (wt/vol) gelatin GmC in absolute numbers and in DNA-normalized numbers. While the latter is important for determining osteogenic activity per cell, the former allows ALP to be examined independent of a nonmonotonic DNA level trends.

DNA-normalized ALP quantities increased in all gelatin-only GmC culture conditions, including those without osteogenic supplements. This feature alone is an indicator of osteogenic induction from GmC culture. Additionally, total ALP activity shows a similarly indicative uptick for all osteogenic media cultures on gelatin-only GmC. DNA-normalized and total ALP activities showed a generally inverse order of intensities, with 6.0% (wt/vol) gelatin GmC-cultured MSC exhibiting the greatest uptick. This inversion is largely a function of increased residual DNA levels with greater gelatin content.

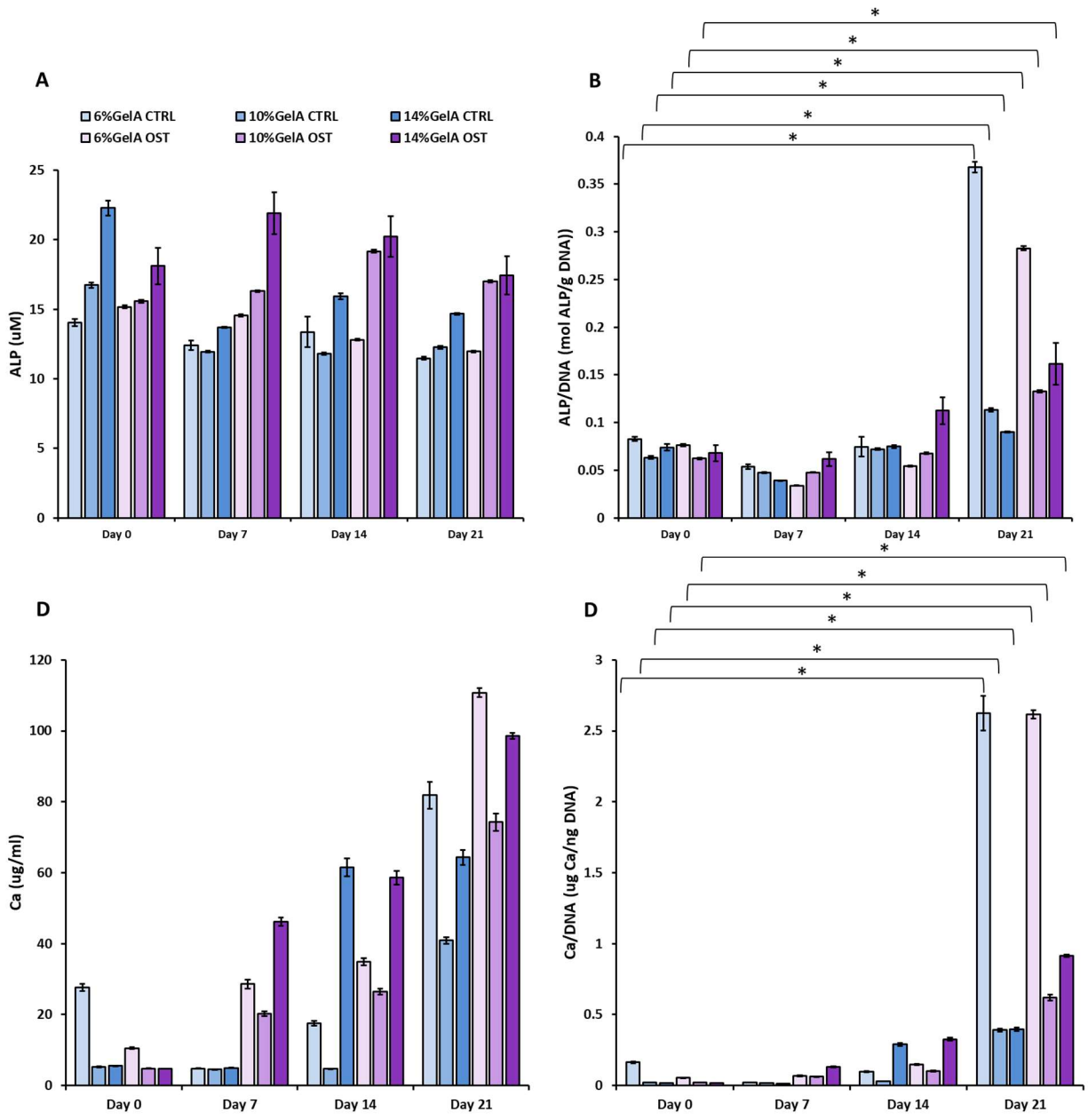

Figure 4.10: ALP and calcium a,c) total and b,d) DNA-normalized levels in the culture of MSC seeded at 15K cells per cm^2 and cultured on 6-14 wt.% GelA GmC in control and osteogenic media.

Calcium deposition is a more direct indicator of osteogenesis, by way of matrix mineralization. Figure 4.10C and 4.10D show total and DNA-normalized calcium deposition in gelatin-only GmC cultures. Both quantities increase in all culture conditions throughout the three-

week culture period, with and without osteogenic supplements. This serves as further evidence of the osteogenic induction provided by the culture condition provided by the full set of gelatin-only GmC tested. MSC cultures on 6.0% (wt/vol) gelatin GmC exhibited the greatest calcium deposition both in total and DNA-normalized terms.

In total ALP activity, shown in Figure 4.11A, the only characteristic peak occurs for 1.0% (wt/vol) hydroxyapatite, 6.0% (wt/vol) gelatin GmC-cultured MSC, but this seems to be partly a function of trends in DNA levels across conditions over time. Summarily, GmC containing lower amounts of hydroxyapatite are more cytocompatible and thus positively affect DNA levels, which is related to cell number. Generally, cell number increase is positively related to DNA levels. In Figure 4.11B, MSC cultured on 1.0-10.0% (wt/vol) hydroxyapatite, 6.0% (wt/vol) gelatin GmC showed DNA-normalized ALP activity to increase over the full culture period in all conditions. The maximum uptick was observed in 5.0% (wt/vol) hydroxyapatite, 6.0% (wt/vol) gelatin GmC in both control (without osteogenic supplements) and osteogenic media.

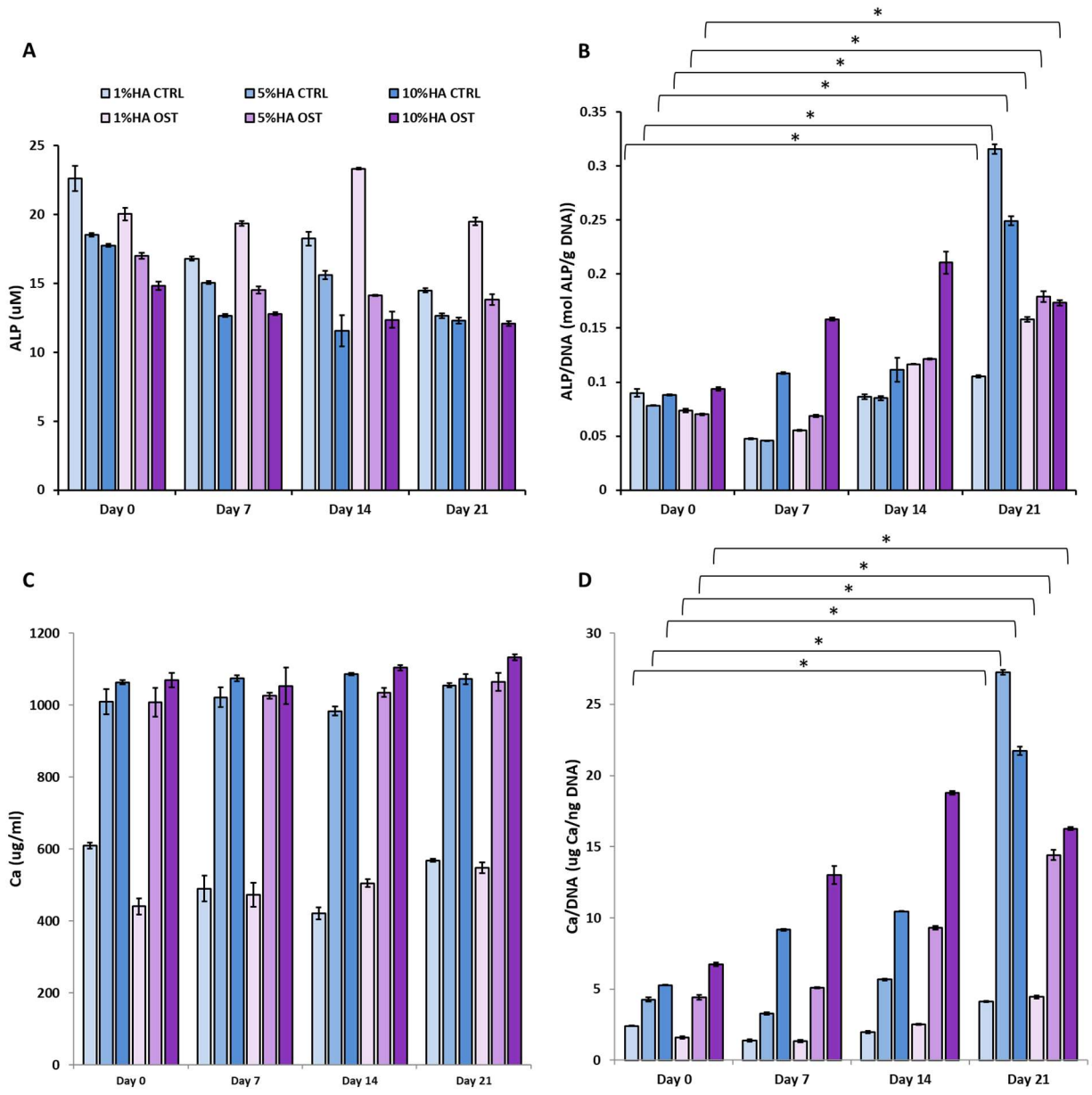

Figure 4.11: ALP and calcium a,c) total and b,d) DNA-normalized levels in the culture of MSC seeded at 15K cells per cm^2 and cultured on 1-10 wt.% HA GmC in control and osteogenic media.

Total calcium deposition (Fig. 4.11C) is less useful than relative numbers for GmC environments in which hydroxyapatite has been introduced to the GmC formulation during its emulsification phase, however it reflects a slight, general increase throughout culture on 5.0% (wt/vol) HA GmC in control and osteogenic media, as well as all other osteogenic media-

conditioned GmC environments. DNA-normalized calcium deposition (Fig. 4.11D) progressively increased throughout culture in a similar pattern to that seen in DNA-normalized ALP activities in all hydroxyapatite-containing GmC culture conditions.

Total ALP activity of cells cultured on 0-3 cycle-solution-mineralized 6.0% (wt/vol) gelatin GmC, seen in Figure 4.12A, were relatively unchanged between the start and end of culture. With the possible exception of 0 cycle-solution-mineralized GmC-cultured MSC in osteogenic medium, all conditions showed relatively small change over time. DNA-normalized ALP activity of cells, shown in Figure 4.12B, showed some increases in 3 and 5 cycle-solution-mineralized GmC control and osteogenically cultured MSC over the three-week culture period. An additional modest increase could be seen in 1 cycle-solution-mineralized GmC-cultured MSC.

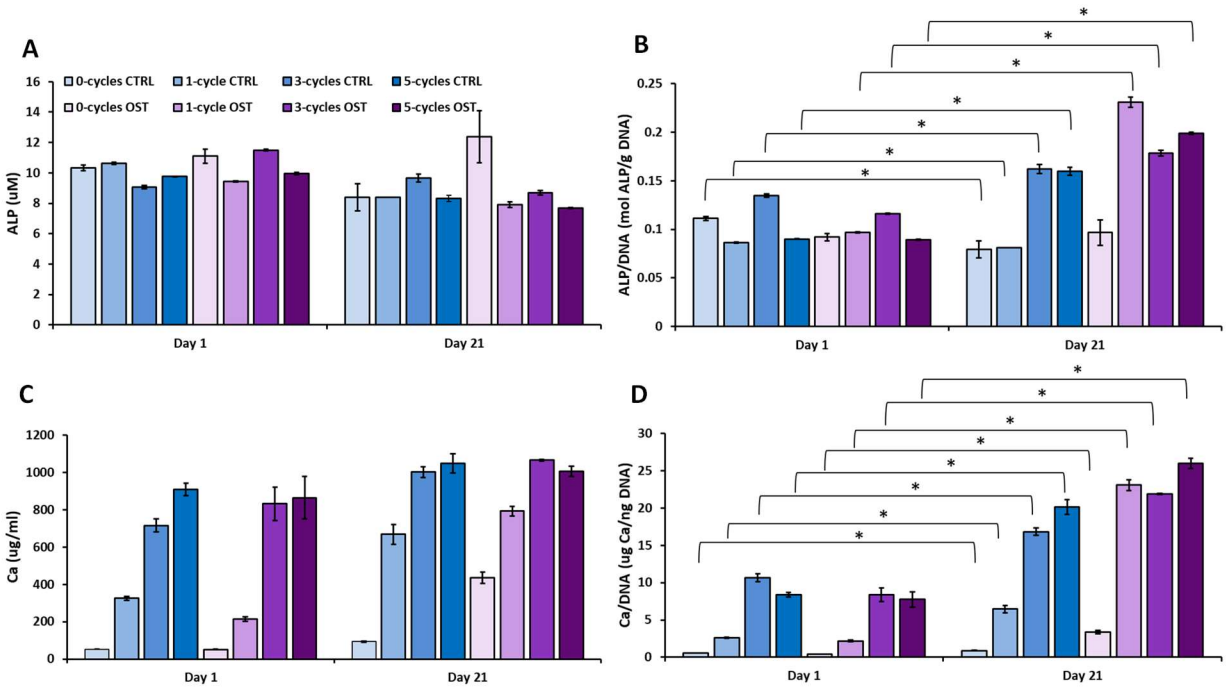

Figure 4.12: Day 1 and Day 21 a) total and b) DNA-normalized ALP activities for MSC cultured on 0, 1, 3, and 5 cycle supersaturated GmC show diminishment after cycles of mineralization. Day 1 and Day 21 c) total and d) DNA-normalized calcium levels for MSC seeded at 15K cells per cm^2 and cultured on 0-5 cycle supersaturation-mineralized 6 wt.% GelA GmC in control and osteogenic media.

Total calcium deposition (Fig. 4.12C) in all culture conditions showed a general increase over time. In addition to this, DNA-normalized calcium deposition (Fig. 4.12D) increased in all culture conditions. These properties, taken together, suggest a modest osteogenic effect from 3 and 5 cycle-solution-mineralized GmC culture over a three-week culture period, with and without osteogenic supplements.

4.4 Conclusions

This study demonstrates that batch-processed microcarrier-size gelatin-calcium-phosphate-based particles can be controlled dimensionally and mechanically with high yield through the use of a facile reproducible water-in-oil emulsification method. Increasing gelatin and hydroxyapatite content generally related with an increase in particle size and shear moduli. Increasing hydroxyapatite content was also found to be inversely related to swelling ratio, adult human MSC seeding efficiency, viable cell area coverage, and associated DNA levels with 0% hydroxyapatite GmC-seeded cells exhibiting the highest cytocompatibility. Some degree of osteogenicity was seen from all GmC-cultured MSC, but those seeded on 6.0% (wt/vol) gelatin and 5.0% (wt/vol) hydroxyapatite, 6.0% (wt/vol) gelatin GmC showed the most pronounced osteogenic effects in terms of DNA-normalized quantities with or without osteogenic supplements.

These studies also showed that gelatin-only and hydroxyapatite-impregnated GmC-cultured MSC populations generally increased viable cell coverage and DNA for one week of culture followed by monotonic decreases in both quantities for the remaining three weeks of culture in both control and osteogenic media. While DNA-normalized and total ALP activity and calcium deposition all indicate osteogenic differentiation, the monotonically decreasing cell number after one week of culture happens in all culture conditions. These declines in cell number all coincide with an increase in surface calcium deposits, which highlights the long-term

deleterious effect of calcium-phosphate-based mineral on cytocompatibility, in spite of tolerability to MSC and other bone progenitor cells at early time-points. This phenomenon is further evidenced by the uniformly reduced viable cell coverage and DNA in culture conditions involving solution-mineralized GmC. The biophysical properties of genipin-crosslinked GmC and their effects in culture discussed thus far allow for batch-processing, controlled module size distribution and substrate stiffness, high cell attachment and viability at early time-points, and robust matrix mineralization from osteogenic induction even in the absence of osteogenic medium supplements. With additional work on improved cell retention, these types of microcarriers can be useful tools for osteoprogenitor cell delivery in bone tissue regeneration.

Chapter 5 Characterization of Osteogenic Progenitor Cell Culture within Gelatin Microcarrier-Embedded Fibrin

5.1 Introduction

Bone tissue disjunction poses a substantial challenge to organized orthopedic regeneration which often call for the introduction of progenitor cell-supporting scaffolds and soluble factors (Roberts et. al., 2012; de Grado et. al., 2018; Presen et. al., 2019; Rao et. al., 2013; Verrier et. al., 2016; Perez et. al., 2018; Lin et. al., 2019; Sobacchi et. al., 2018). These scaffolds may be granulized to minimize invasiveness while maximizing cavity infill with engineered micro- to milli-scale bone tissue/fillers (Chen et. al., 2013; Kim et. al., 2005; Nweke et. al., 2020; Rao et. al., 2015; Chao et. al., 2015; Petruskevicius et. al., 2002). Such microparticles are commonly used for bioreactor cell expansion in a variety of biomedical applications, but the rigidity of these substrates has also been linked with osteogenic directed differentiation (Chen et. al., 2020; Ornelas-Gonzalez et. al., 2021; Nweke et. al., 2020). Surface cell-culturing microparticles, or microcarriers, also negate pre-transplant trypsinization and hence cell-cell-matrix disorganization, potentiating improved engraftment and metabolite transfer.

Orthopedic microcarriers, typically composed of collagen-products and typically calcium-bearing bioceramics, can be generated by batch emulsification or microfluidic droplet flow (Saltz et. al., 2016; Shadjou et. al., 2015; Ghomi et. al., 2021; Ballouze et. al., 2021; Nweke et. al., 2020; Malda et. al., 2006; Ducheyne et. al., 1997; Hong et. al., 2009; Qiu et. al., 2000; Qiu et. al., 2001; Qiu et. al., 1998; Winkler et. al., 2018; Baino et. al., 2018; McLaren et. al., 2019) and crosslinked for stable, yet transiently biodegradable, mechanical support (Perez et. al., 2014). Abundant

collagen derivatives, like gelatin, are both cytocompatible and mechanically tunable through crosslinking or mineral reinforcement (Hsu et. al., 1999; Dosta et. al., 2020; Sart et. al., 2013; Yang et. al., 2007; Overstreet et. al., 2003; Hayashi et. al., 2011; Chao et. al., 2015).

This study looks at the osteogenic impact of batch-emulsified gelatin-based microcarriers on MSC within a tissue-simulative fibrin environment. Genipin, a low cytotoxicity and molar mass compound, was used to crosslink gelatin microparticles following emulsification (Yang et. al., 2018). Few studies had been found to involve genipin-crosslinked gelatin microcarriers in osteogenic culture past seven days post-seeding (Lau TT, Wang C, & Wang DA, 2010; Lau TT, Wang C, Peng SW, Su K, & Wang DA, 2010; Lau et. al., 2012). The impact of a fibrinous hydrogel environment on stationary gelatin microcarrier culture of MSC was assessed in order to simulate the bone microtissue implant environment in an in-vitro setting. Microcarriers used in this experiment were analyzed in terms of size and mechanical performance. This work expands on earlier research into the osteogenicity of packed bed microcarrier MSC culture in an effort to determine the degree to which previously identified osteogenic effects from these gelatin microcarriers is retained within a defect transplant mimic. Cell expansion and phenotype were monitored through 21 days of control and osteogenic media culture.

5.2 Materials and Methods

5.2.1 Materials

Type A (acid-treated porcine skin) 225 bloom strength gelatin was procured from Sigma Aldrich (St. Louis, MO, USA). The 100 cSt polydimethylsiloxane (PDMS) oil was procured from Clearco Products (Bensalem, PA, USA). Pluronic® L101, a nonionic, difunctional, block copolymer surfactant, was procured from BASF Corporation (Vandalia, IL, USA). Genipin, a crosslinking compound of natural origin, was procured from Wako Chemicals (Richmond, VA,

USA). Tris(hydroxymethyl)aminomethane (Tris) and hydrochloric acid (HCl) were purchased from Sigma-Aldrich.

5.2.2 Generation of gelatin microcarriers

A water-in-oil emulsification step, shown detailed in Figure 5.1, was used to generate gelatin-based micron-sized droplets. A 5.0 mL volume of each gelatin concentration of interest, namely 6.0 and 14.0% (wt/vol) gelatin in pH 7.4 PBS was equilibrated in a 37 °C water bath. Each gelatin solution was admixed in dropwise fashion to an impelled 50 mL beaker of PDMS oil held at 40 °C on a hot plate. The resulting emulsions were generated at a set stir rate of 500 rpm. After 5 minutes of stirring at 40 °C, the resulting emulsion was transferred to a 4 °C ice bath and stirring was continued for an additional 30 minutes to allow microdroplet solidification. The resulting suspension of solid gelatin microparticles was mixed with PBS at 23 °C containing 0.01% (vol/vol) Pluronic L101 surfactant and centrifuged at 300 × G for 5 minutes to collect the gelatin microparticles and separate them from the PDMS phase [34]. Remaining surfactant solution was extracted from collected microparticles by re-suspension and washing in PBS for further processing.

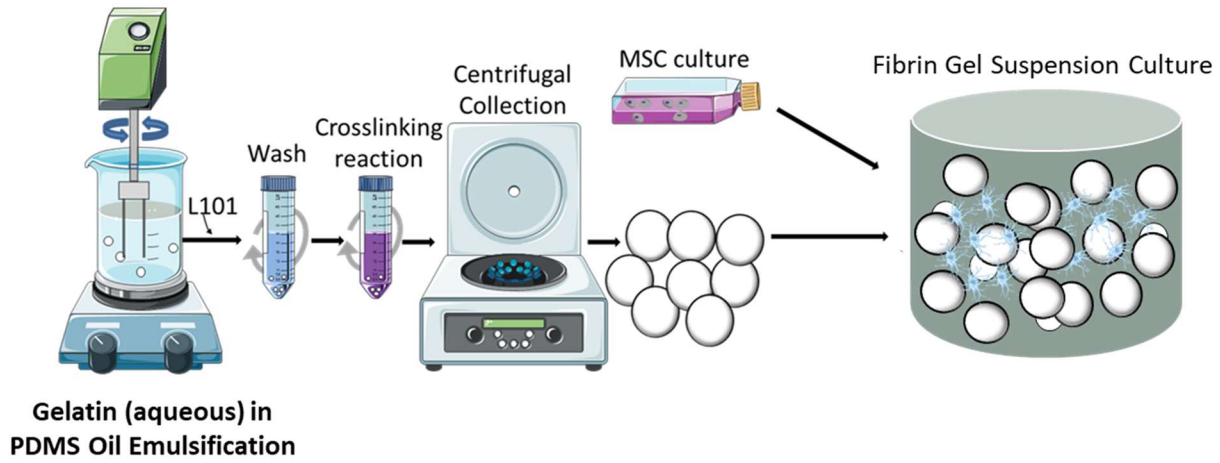

Figure 5.1: Scheme showing gelatin microcarrier (GmC) production by water-in-oil emulsification, crosslinking, and subsequent co-suspension with cells (MSC) within fibrinous environment.

5.2.3 Genipin crosslinking of gelatin microcarriers

Gelatin microparticles were admixed to 1.0% (wt/vol) genipin in PBS solution with continuous rotational suspension to facilitate the crosslinking process. The degree of crosslinking was time-dependent and mixed at 23 °C for a duration of 48 hours in order to totally saturate reactive amine functional groups (Solorio et. al., 2010). Genipin aldehyde groups crosslink gelatin macromolecules by catalytically reacting with available lysine residue amine moieties. Previous work has demonstrated that hydrogels crosslinked in this way reach an optimum degree of crosslinking equal to approximately 90 %, imparting a red autofluorescence to gelatin materials (Hwang et. al., 2011; Turner et. al., 2017). Physical gels of gelatin are understood to solidify at a melting temperature around 32 °C, allowing for room temperature crosslinking without great risk of microparticle fusion. Genipin-crosslinked gelatin microcarriers (GmC) were successively washed in ethanol and deionized (DI) water in order to eliminate unreacted genipin molecules. Prior to use in culture, microcarriers were sterilized through 10 minutes of ethanol submersion and UV exposure (Sylvania UV-C 255 nm germicidal T8 30W lamp).

5.2.4 Particle size analysis

GmC dimensions were visually characterized throughout 3 weeks of MSC culture using confocal microscopy. Micrographs were taken with a confocal microscope (Nikon A1Si Confocal) and analyzed with NIS Elements viewer software (Nikon). Automated particle size analysis was accomplished through laser diffraction (Malvern Mastersizer 2000S, Westborough, MA). GmC in

DI water sample dispersions were agitator-suspended within the equipment reservoir at 1750 rpm. Count median diameters for GmC populations were determined at recorded laser obscurations exceeding 5%. Mie light scattering theory, which assumes all particles to be generally spherical, was employed, with gelatin and water refractive indices of 1.52 and 1.33, respectively. The resulting particle diameter distributions were generated after the capture of 30,000 snapshots within 30 second time windows.

5.2.5 Mechanical characterization of gelatin materials

Rheological analysis of gelatin hydrogel mechanical properties were characterized on a rotational rheometer (AR-G2, TA Instruments, Newcastle DE) with an 8 mm parallel plate measurement head. Measurements were taken on 10 mm diameter 6.0-14.0% (wt/vol) gelatin discoid samples using a Peltier temperature-controlled stage set at 25 °C at a pre-load of 0.5 N and a gap height of 3 mm. A 0.1-10 radian/second (rad/s) oscillating frequency sweep test was conducted at a constant oscillating strain of 0.1% to identify the linear viscoelastic region (LVER). And a 0.1 - 10% oscillating strain sweep test was then administered at a constant oscillating frequency of 1 rad/s to establish a modulus-strain relationship for the specified concentrations of gelatin hydrogels.

5.2.6 Cell culture

Human bone marrow-derived mesenchymal stem cells (MSC, RoosterBio, Frederick MD) were expanded to passage 4-6 in defined growth medium (RoosterNourishTM, RoosterBio, Frederick MD). Control medium (CTRL) consisted of Dulbecco's Modified Eagle's Medium (DMEM) supplemented with 10% (vol/vol) fetal bovine serum (FBS) and 1% (vol/vol) penicillin-streptomycin. Osteogenic (OST) medium was prepared by adjusting CTRL medium to final

concentrations of 0.2 mM L-ascorbic acid 2-phosphate, 10 mM β-glycerophosphate, and 100 nM dexamethasone. All cell culture was performed in a standard incubator at 37 °C in a 5% CO2. Upon reaching 70–80% confluence in T-175 polystyrene culture flasks, MSC were trypsinized and either pre-seeded onto GmC in ultra-low attachment plates for a duration of approximately 18 hours prior to fibrin suspension or simultaneously-mixed along with GmC into fibrin suspension without pre-seeding, at a cell density of 640,000 MSC/ml in all cell culture experiments. Nutrient medium was changed every 3-4 days over the span of a three-week culture period.

5.2.7 Cell number, ALP activity, and calcium deposition

On day 1 after seeding of 6.0-14.0% (wt/vol) gelatin GmC, and subsequently on day 7, day 14, and day 21 of culture, MSC were assayed for DNA content, ALP activity, and calcium deposition. These assays were used to characterize the number, proliferation rate, and differentiated state of the MSC. Additionally, confocal microscopy was performed on days 7, 14, and 21 to determine the number, cytoskeletal shape, and distribution of MSC in GmC-embedded fibrin culture.

GmC- and MSC-loaded fibrin gels were fixed in buffered formalin (Z-fix, Anatech), stained with 0.1% (wt/vol) DAPI and 2.5% (wt/vol) phalloidin in PBS for 45 minutes prior to rinsing and resuspension in PBS for subsequent visual inspection. Fluorescence imaging of stained samples was administered on a confocal microscope (Nikon) to capture cell number and distribution. Phalloidin-stained cytoskeletal features were captured in the green fluorescence channel while the red channel of the same field of view was imaged to capture any dead cells and microcarrier autofluorescence. DAPI-stained cell nuclei were captured in the blue channel.

The quantity of cellular DNA in samples was assayed as a measure of relative cell numbers, which were used to normalize ALP activity and calcium deposition, using the commercially

available Quanti-iT™ PicoGreen double-stranded DNA assay kit kit (Invitrogen, Grand Island, NY) as described previously (Annamalai et. al., 2018). Briefly, total DNA was isolated from packed-bed culture samples through solubilization in 0.1% (wt/vol) sodium dodecyl sulfate 10 mM Tris-HCL solution (0.1%SDS TBS) adjusted to a pH of 7.5. Samples were subsequently centrifuged at 10,000 × G for 10 minutes before aspiration of supernatants for further use in quantifying DNA content by PicoGreen assay using the manufacturer's protocol and reagents. Briefly, lysate samples, alongside reference samples of Lambda-DNA standards, were admixed with 0.5% (vol/vol) PicoGreen 1mM ethylenediaminetetraacetic acid (EDTA) TBS for 5 minutes of reaction time. Fluorescence signal from each reacted sample, pipetted into a 96-well plate, was read with an excitation wavelength of 485 nm at an emission wavelength of 528 nm.

ALP activity was quantified as described previously (Annamalai et. al., 2018) by first lysing MSC in 0.1 % SDS TBS, centrifuging at 10,000 × G for 10 minutes, and then collecting the respective supernatants. Sample supernatants were each admixed with 1.5 M 2-amino-2-methylpropanol-buffered 5 mM p-nitrophenyl phosphate substrate solution in a 96-well plate for 30 minutes of reaction on shaker plate. This reaction was stopped with the addition of 3.0 N NaOH to all sample wells. Sample absorbance was measured at 405 nm.

Calcium deposition was measured using an orthocresolphthalein complex one (OCPC) method described in earlier studies (Babur et. al., 2015; Saito et. al., 2013). Briefly, sample sediments from 10,000 × G centrifugation were digested in 1.0 N acetic acid overnight on a 37°C shaker plate. These were each then admixed with a 5:5:2:88 volume ratio blend of 14.8 M ethanolamine-boric acid buffer (pH 11), 1 mg/ml OCPC solution, 50 mg/ml 8-hydroxyquinoline in 95% ethanol solution, and deionized water in a 96-well plate for 10 minutes of reaction on shaker plate. Sample absorbance was then measured at 575 nm.

5.2.8 Statistical analysis

Microcarrier sizes, mechanical data, ALP activities, calcium levels, and DNA are all reported as numerical mean ± standard deviation with n=3. For these data sets, groups were compared and analyzed by ANOVA and t-test. A resulting F-value of greater than F-critical and a p-value of less than 0.05 between groups were considered statistically significant.

5.3 Results and Discussion

5.3.1 Characterization of microparticle size

The effect of gelatin content on the average size of gelatin microparticles was assessed through automated particle size analysis in Figure 5.2A. All batch-emulsified gelatin microparticles exhibited generally smooth-surfaced, spheroidal forms. Microcarrier diameter is functionally significant in determining available surface area for cell attachment. (Man et. al., 2005; Baule et. al., 2014).

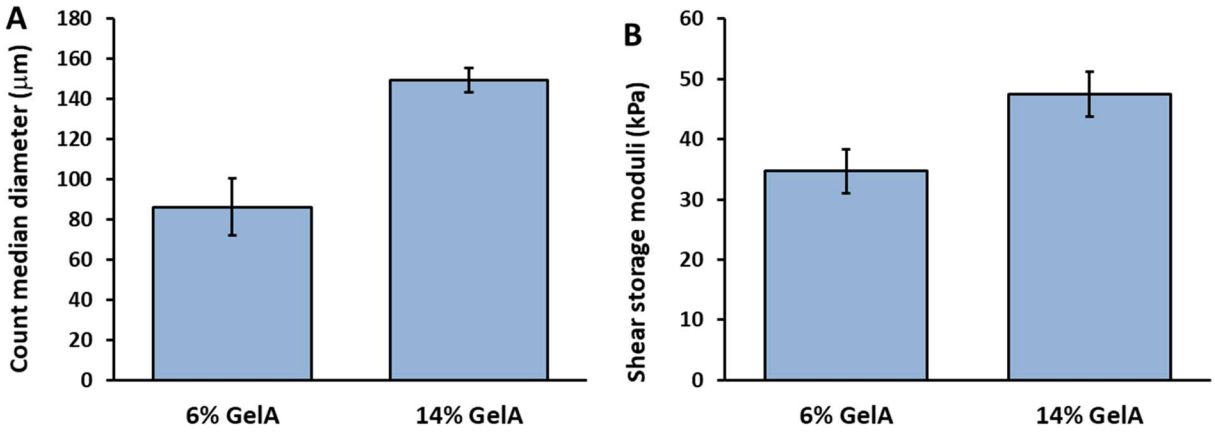

Figure 5.2: Particle (a) size analysis of emulsified 6.0-14.0% wt/vol gelatin (GelA) microparticles and (b) viscoelastic mechanical analysis of 6.0-14.0% wt/vol GelA hydrogel.

Batch to batch reproducibility was very high for both GmC types. The general size range of GmC made in this study, approximately 80-150 μm in diameter, is large enough to support the attachment of multiple MSC, and small enough to be passed through the 514 μm inner diameter of a 21 gauge needle, and have been shown to be osteoconductive to bone progenitor cells (Shapoff et. al., 1980; Leiblein et. al., 1980). Figure 5.2A, specifically, shows the effects of gelatin concentration on the size of gelatin microparticles created at a stirring rate of 500 rpm. Increasing gelatin concentration from 6.0 % to 14.0 % (wt/vol) resulted in a change in median particle diameter from 86.2 ± 14.2 to 149.6 ± 6.2 μm. (Sart et. al., 2013). Generally, microparticle size exhibits a positive relationship with an increase in solid content. Stable, spherical particles are preferred in cell delivery applications since their flow and packing properties are more predictable.

5.3.2 Mechanical properties of gelatin materials

A range of mechanobiology studies have identified a link between cell culture substrate stiffness and the differentiation capacity of progenitor cells (Handorf et. al., 2015; Vining et. al., 2017; Butcher et. al., 2009; Cox et. al., 2011). And though considerably less robust than the hydroxyapatite-reinforced collagen of natural bone, gelatin has been deployed broadly as a stiff, cytocompatible scaffold material for cell culture. Additionally, even substrate moduli on the order of those typical to gelatin-based materials have been found to demonstrate some level of osteoconduction to bone progenitor cells (Ruiz et. al., 2008).

The oscillatory shear moduli of 6.0-14.0% (wt/vol) GelA material, as shown in Figure 5.2B, suggest a positive relationship between solid gelatin content and shear storage modulus. Hydrogels of 6.0% and 14.0% (wt/vol) gelatin were shown to exhibit shear storage moduli (G') of 34.7 ± 3.7 kPa and 47.5 ± 3.7 kPa, respectively. This direct relationship is seemingly due to the increased polymer entanglement and inter-chain dispersion forces associated with greater gelatin

mass. These shear moduli were generally typical of mechanical values previously reported as having an osteogenic effect similar to other crosslinked collagen-based substrates (Handorf et. al., 2015; Vining et. al., 2017; Butcher et. al., 2009; Cox et. al., 2011; Engler et. al., 2006).

5.3.3 Proliferative and osteogenic effect of matrix properties

Cells in both GmC-preseeded and matrix-simultaneously-mixed control media culture conditions showed a general behavior of increasing up to day 14, followed by a levelling off thereafter, while osteogenic conditions behaved similarly, but plateauing after 7 days of culture. This is more clearly evidenced by the DNA data, as seen in Figure 5.3, but fairly concurs with confocal imaging, as shown in Figure 5.4. In both control and osteogenic media, the simultaneously-mixed conditions appear to lag the GmC-preseeded conditions in cell number early on, but eventually overtake them slightly by day 21 of culture. This effect appears more pronounced in DNA levels than in confocal imaging. Overall, the data from this experiment on 6.0% (wt/vol) GelA GmC-cultured MSC reflected a relatively stable cell number over the duration of the culture period. This behavior fits with gelatin's record of high cell attachment and support, as well as genipin's demonstrably lower cytotoxicity relative to more widely researched crosslinkers like glutaraldehyde and 1-ethyl-3-(3-dimethyl aminopropyl) carbodiimide (EDC) (Bello et. al., 2020; Lau TT, Wang C, & Wang DA, 2010).

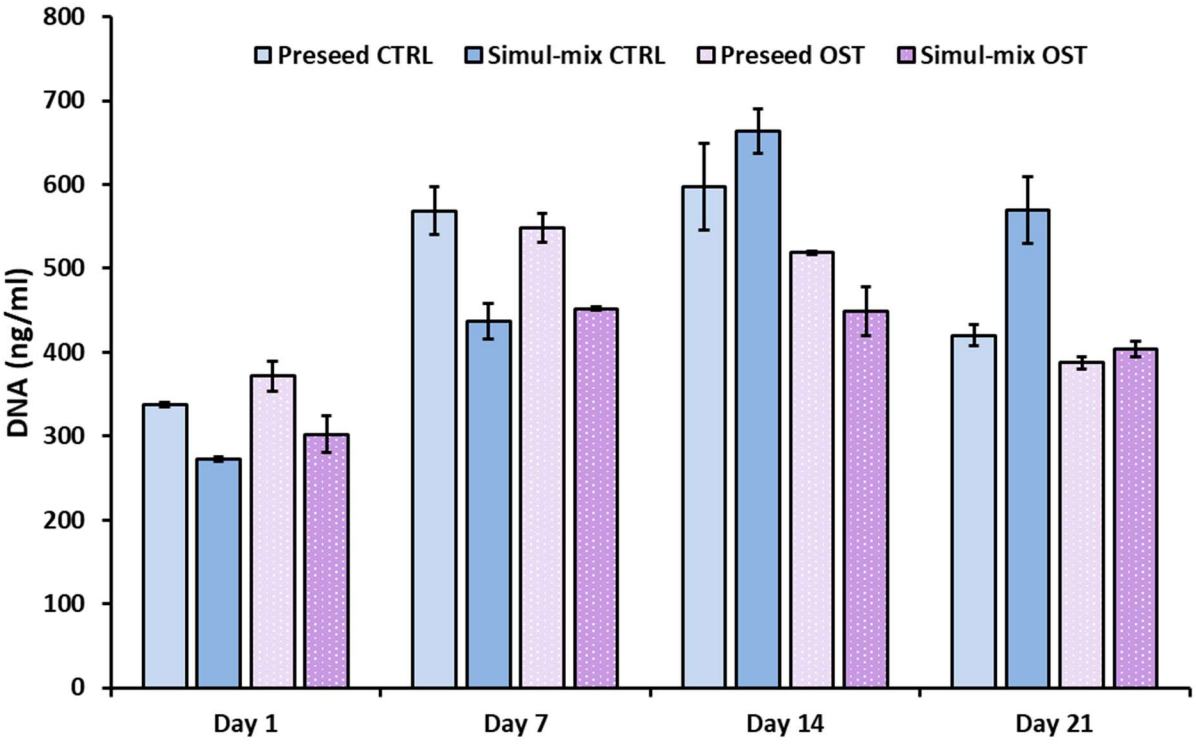

Figure 5.3: DNA levels of GmC-preseeded or matrix-mixed MSC cultured at 640,000 cells/ml amidst fibrin-embedded 6.0% wt/vol GelA GmC in control and osteogenic media.

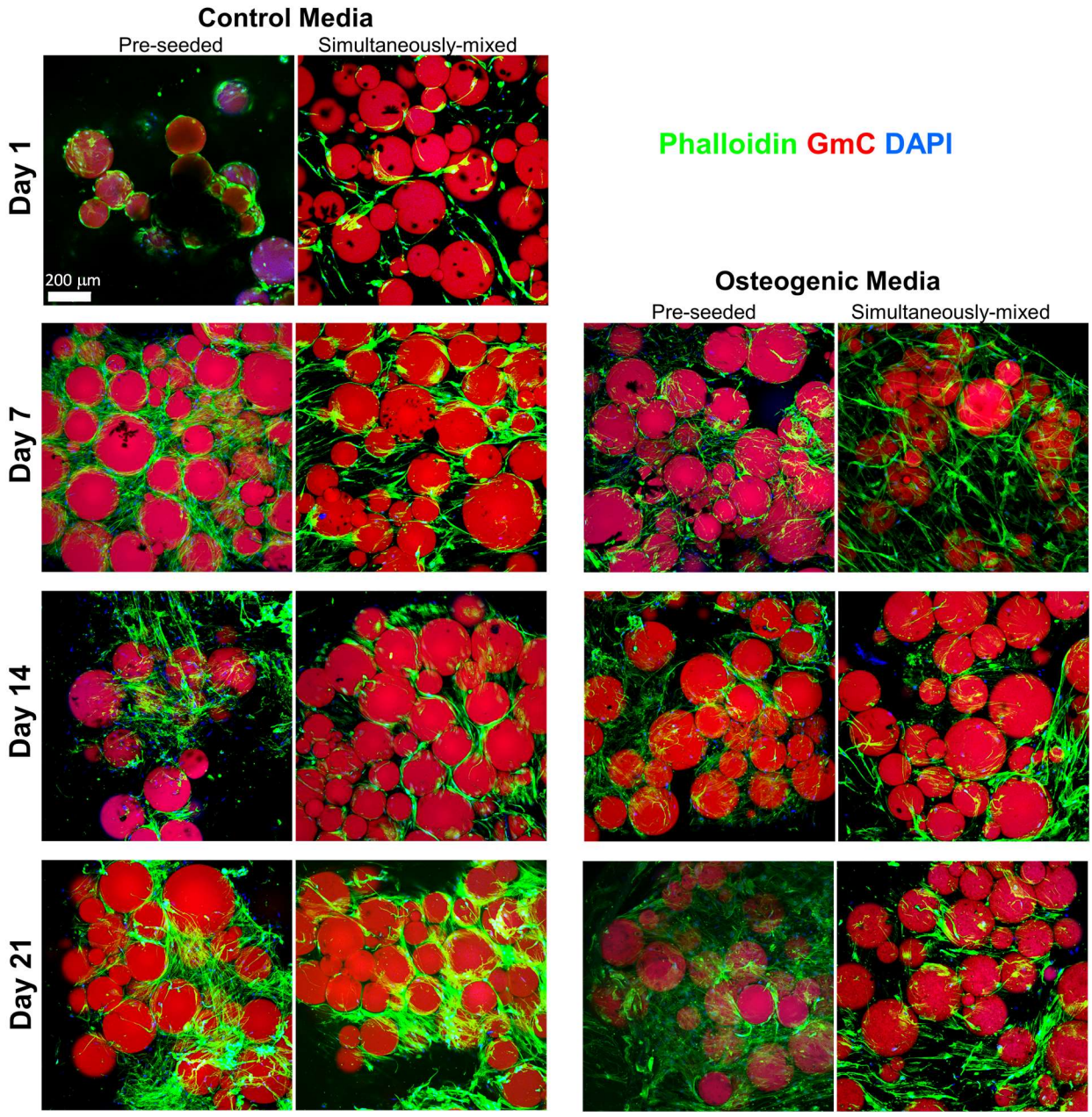

Figure 5.4: Confocal microscopy images of GmC-preseeded or matrix-mixed MSC cultured at 640,000 cells/ml amidst fibrin-embedded 6.0% wt/vol GelA GmC. MSC were cultured for three weeks on GmC in either control (CTRL) or osteogenic (OST) media. Fluorescent images were taken on day 1 to day 21 of culture. Phalloidin staining shows cell cytoskeletal features, DAPI staining shows nuclei, and genipin-crosslinked gelatin matrix autofluoresces in the red channel. Scale bar represents 200 µm.

Figure 5.5 shows the alkaline phosphatase (ALP) levels of GmC-preseeded and simultaneously-mixed MSC cultured on 6.0% (wt/vol) GelA GmC at a nominal cell density of 640,000 cells/ml. MSC were cultured for 21 days in either control or osteogenic media. In both total (Fig. 5.5A) and relative (Fig. 5.5B) numbers, ALP levels for both GmC-preseeded and simultaneously-mixed MSC were shown to increase to their respective maxima on day 14 and maintain a significantly upregulated amount of ALP on day 21, relative to day 1 of culture in the presence of osteogenic media. The same could not be said for control conditions, which remained relatively unchanged through the culture period. Because elevated ALP levels are regarded as a strong indicator of osteogenic activity, among many things, this data set simply confirms the osteoconductive behavior of GmC-embedded fibrin hydrogel as an MSC culture environment. Notably, GmC-preseeded MSC ALP levels exceeded those of simultaneously-mixed MSC at the early time-points only to be overtaken for the later time-points. A similar trend could be seen in DNA levels.

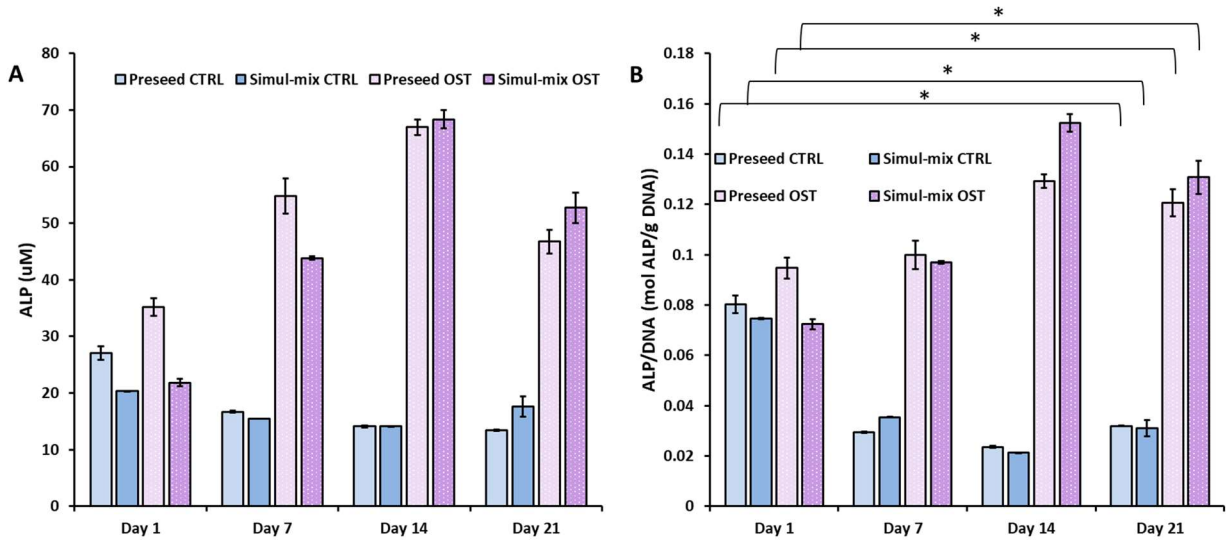

Figure 5.5: ALP (a) total and (b) DNA-normalized levels of GmC-preseeded or matrix-mixed MSC cultured at 640,000 cells/ml amidst fibrin-embedded 6.0% wt/vol GelA GmC in control and osteogenic media.

Calcium deposition serves as a more functional indicator of osteogenic differentiation. Figure 5.6A and 5.6B show total and DNA-normalized calcium amounts in GmC-preseeded and simultaneously-mixed MSC cultured in 6.0% (wt/vol) GelA GmC-mixed fibrin. Similar to ALP activity levels, only conditions cultured with osteogenic media demonstrated osteogenic activity. There were significant increases in calcium from day 1 to day 21 in total and relative numbers for both GmC-preseeded and simultaneously-mixed MSC cultures. This further suggests the osteoconductive effect of a GmC-suspended fibrin hydrogel environment, with or without MSC preseeding.

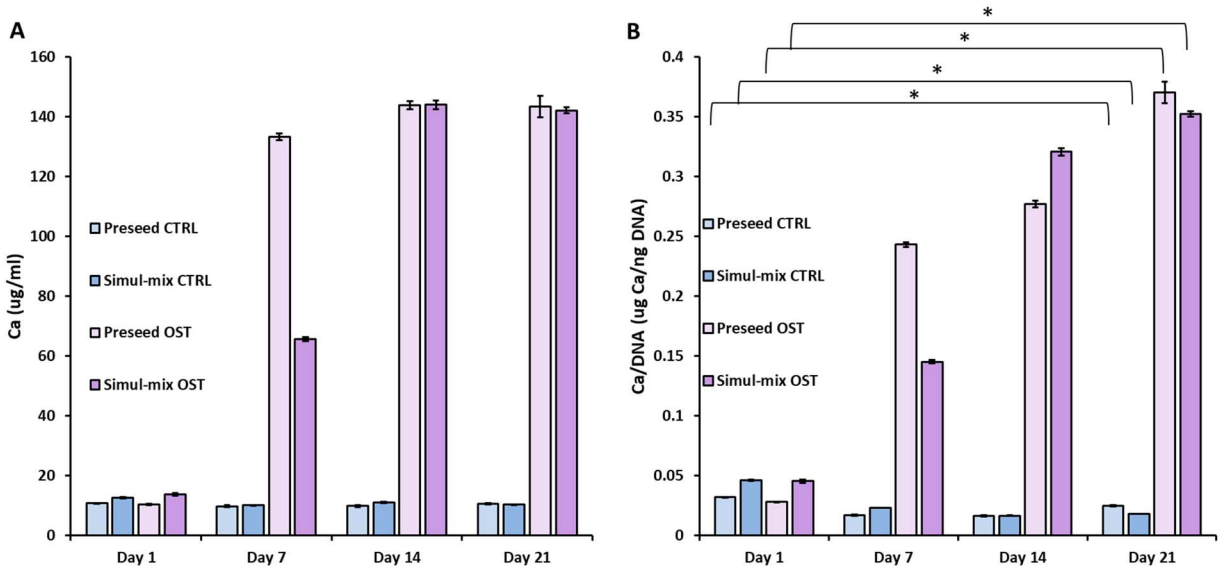

Figure 5.6: Calcium (a) total and (b) DNA-normalized levels of GmC-preseeded or matrix-mixed MSC cultured at 640,000 cells/ml amidst fibrin-embedded 6.0% wt/vol GelA GmC in control and osteogenic media.

Cell number for 6.0% and 14.0% (wt/vol) GelA GmC-MSC simultaneously-mixed fibrin samples, both in control and osteogenic media, showed a general stability throughout 3 weeks of culture. DNA levels, as seen in Figure 5.7, remains remarkably consistent from day 1 to day 21 of culture. Confocal imaging data, as shown in Figure 5.8, reveals broadly spread and distributed

cells by day 7 at the latest. Even more so than in the previous data sets from seeding experimentation, the data from MSC culture on 6.0-14.0% (wt/vol) GelA GmC-cultured MSC showed a largely unchanged cell number throughout culture.

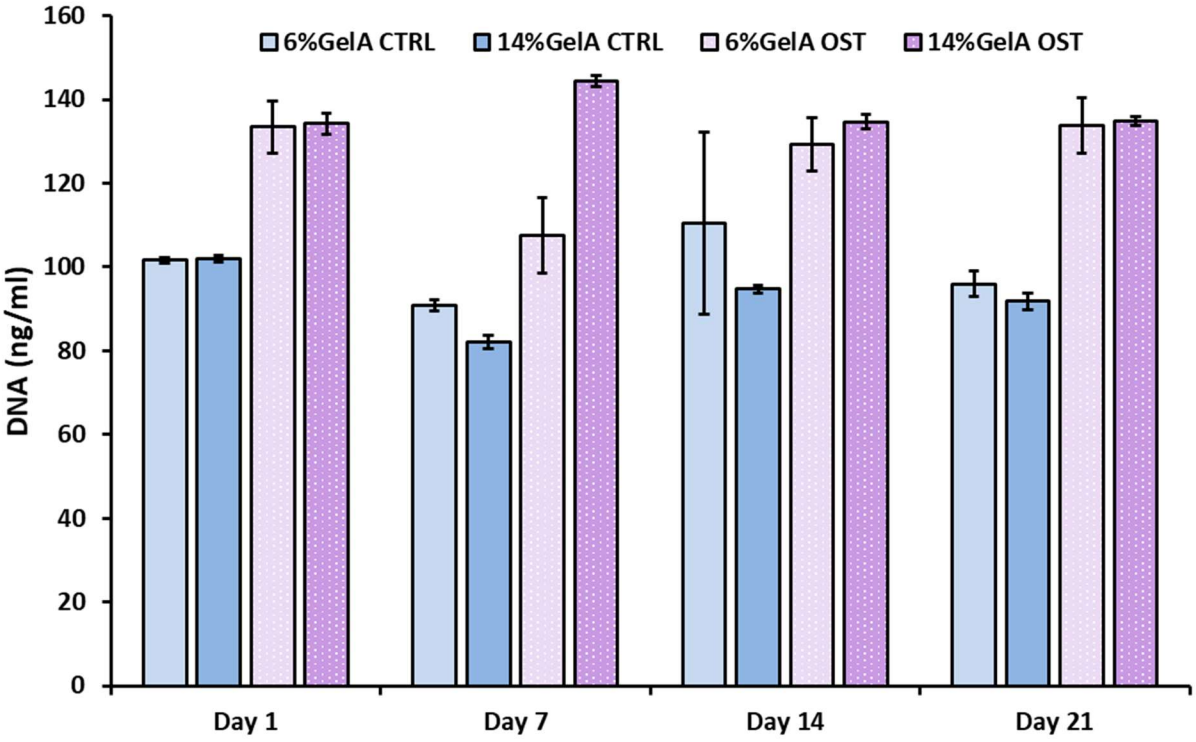

Figure 5.7: DNA levels of matrix-mixed MSC cultured at 640,000 cells/ml amidst fibrin-embedded 6.0-14.0% wt/vol GelA GmC in control and osteogenic media.

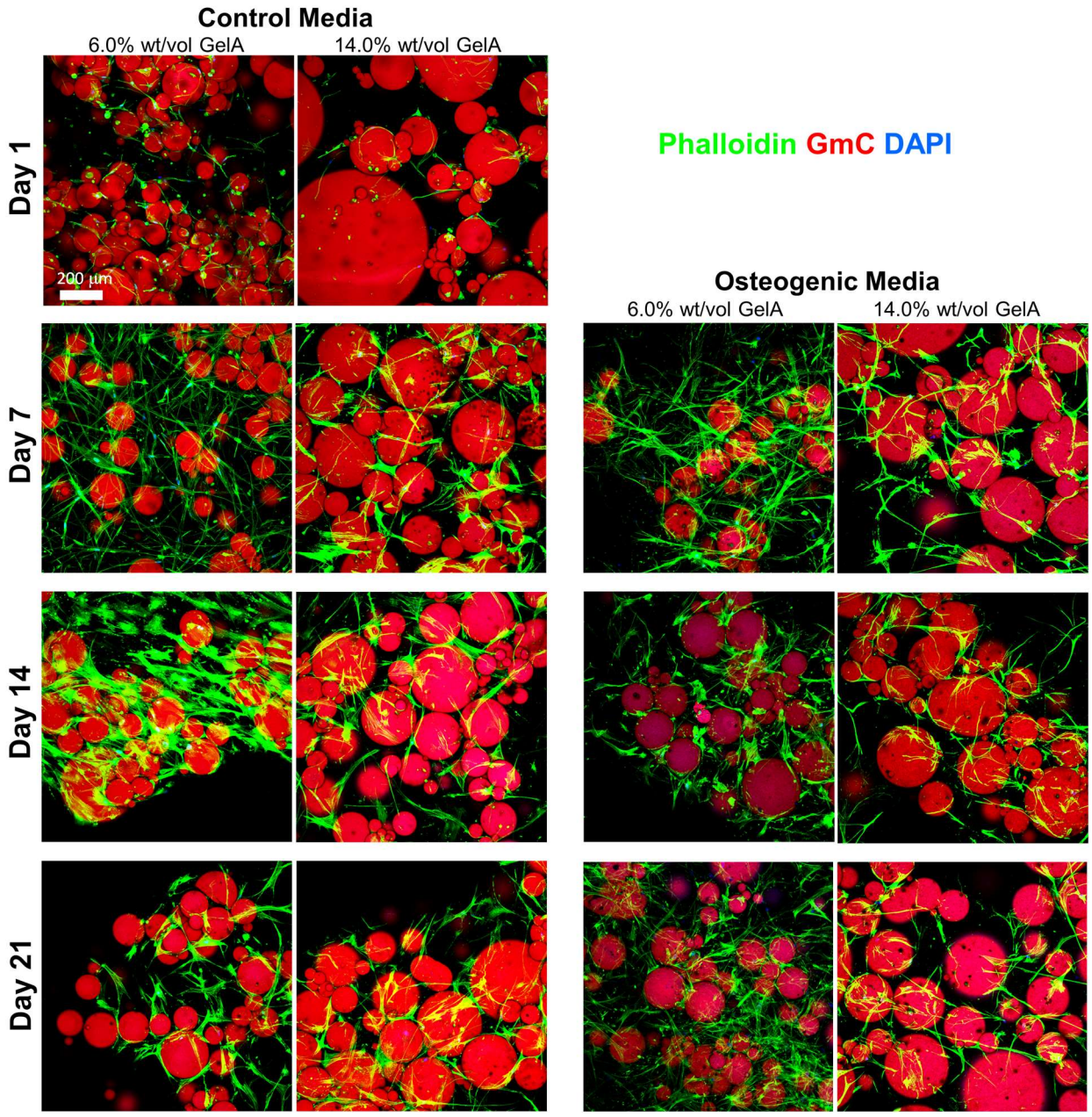

Figure 5.8: Confocal microscopy images of matrix-mixed MSC cultured at 640,000 cells/ml amidst fibrin-embedded 6.0-14.0% wt/vol GelA GmC. MSC were cultured for three weeks on GmC in either control or osteogenic media. Fluorescent images were taken on day 1 to day 21 of culture. Phalloidin staining shows cell cytoskeletal features, DAPI staining shows nuclei, and genipin-crosslinked gelatin matrix autofluoresces in the red channel. Scale bar represents 200 µm.

Figure 5.9A and 5.9B show ALP activity in cells cultured amid fibrin-embedded 6.0-14.0% (wt/vol) gelatin GmC in absolute numbers and in DNA-normalized numbers, respectively.

Although DNA-normalized ALP activity levels are most appropriate for quantification of osteogenic function in the average cell, it can be instructive to determine how much change in ALP activity is due to abnormal DNA effects. Both quantities show a general decrease in ALP activity levels overtime, in almost all GmC culture conditions, which taken alone might indicate a downregulation in osteogenic impact.

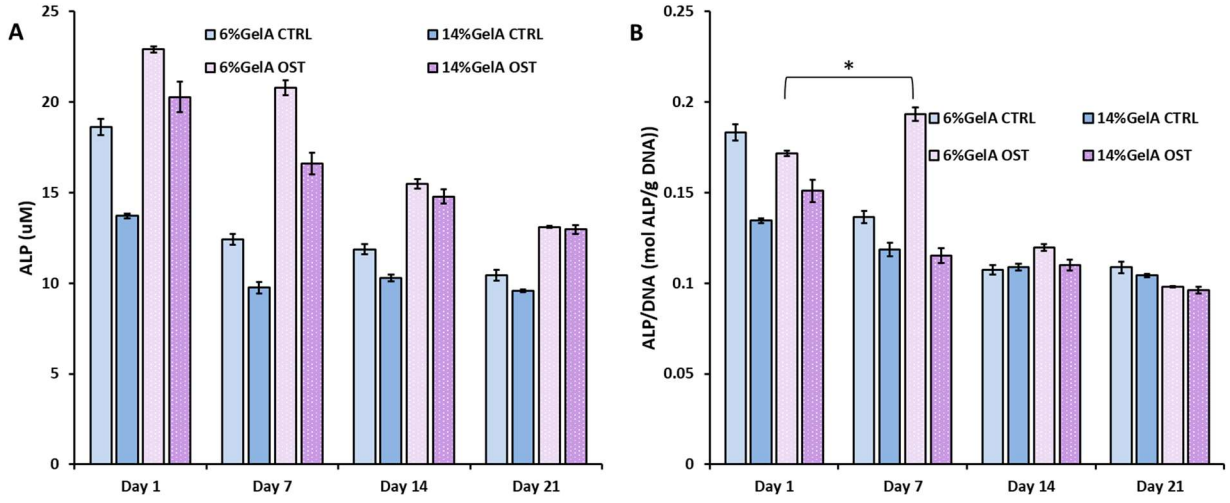

Figure 5.9: ALP (a) total and (b) DNA-normalized levels of matrix-mixed MSC cultured at 640,000 cells/ml amidst fibrin-embedded 6.0-14.0% wt/vol GelA GmC in control and osteogenic media.

Total and DNA-normalized calcium deposition, seen in Figure 5.10A and Figure 5.10B, respectively, show significant increases in calcium deposition over the experiment period in all culture conditions. Total calcium deposition numbers, specifically, increase progressively from day 1 levels to significantly heightened day 21 levels. DNA-normalized numbers, similarly, show significant enhancement from day 1 to day 21 of culture.

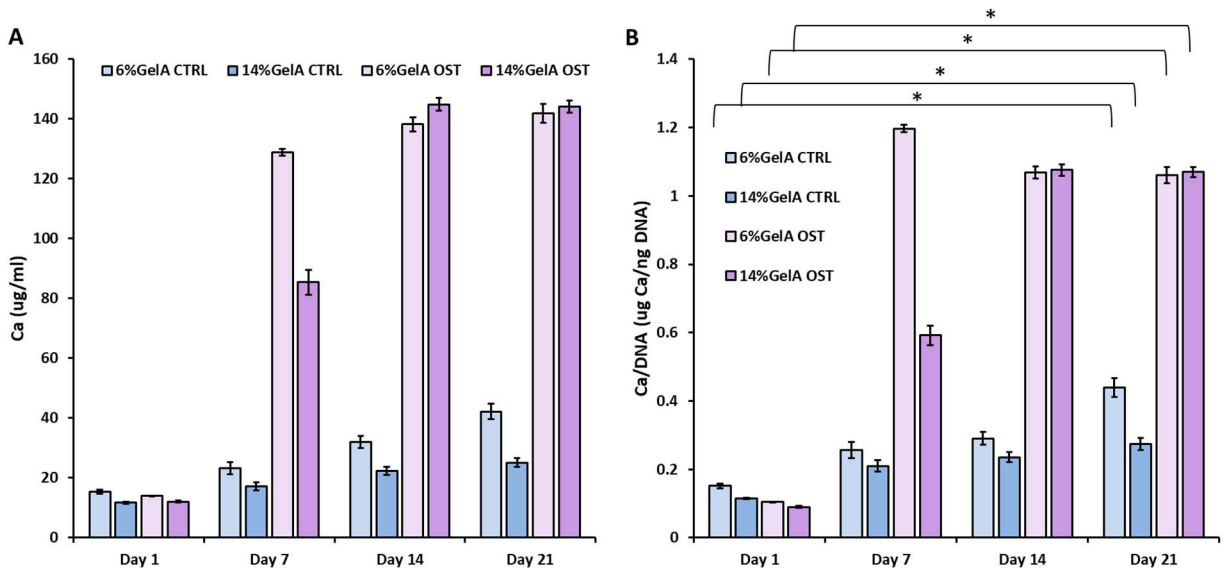

Figure 5.10: Calcium (a) total and (b) DNA-normalized levels of matrix-mixed MSC cultured at 640,000 cells/ml amidst fibrin-embedded 6.0-14.0% wt/vol GelA GmC in control and osteogenic media.

Summarily, fibrin-embedded culture of MSC intermixed with or preseeded onto 6.0% or 14.0% (wt/vol) GelA GmC was not strongly proliferative, but did display some potential for osteo-conductivity. Differing seeding methods resulted in similar ALP upregulation in the presence of osteogenic media. Calcium deposition mirrored this behavior. However, MSC cultured in fibrin alongside 6.0% or 14.0% (wt/vol) GelA GmC showed a divergence between ALP and calcium deposition data. While ALP behavior suggested a downregulation in osteogenic function, calcium levels increased monotonically, indicating an increase in osteogenic function, in all culture conditions. Taken together, these properties would appear to conflict, but as was stated earlier, calcium deposition is a more functional assay for osteogenesis, and thus should be regarded as stronger evidence of differentiative capacity.

5.4 Conclusions

This study demonstrates that batch-emulsified gelatin microsphere particles can be generated with controlled median diameter and shear moduli with a simple high through-put procedure. Greater gelatin content is associated with growing median diameter for particles generated through gelatin (aqueous) solution in polydimethylsiloxane (PDMS) oil emulsification. Shear moduli was similarly related with increasing gelatin solids content. Both preseeding of MSC onto or intermixing with GmC within a fibrin hydrogel culture environment showed both 6.0% and 14.0% (wt/vol) gelatin microsphere-infused fibrin to be cytocompatible, non-proliferative, in terms of quantified DNA levels, and osteoconductive, in terms of calcium deposition and, in some cases, ALP activity.

Chapter 6 Summary and Future Directions

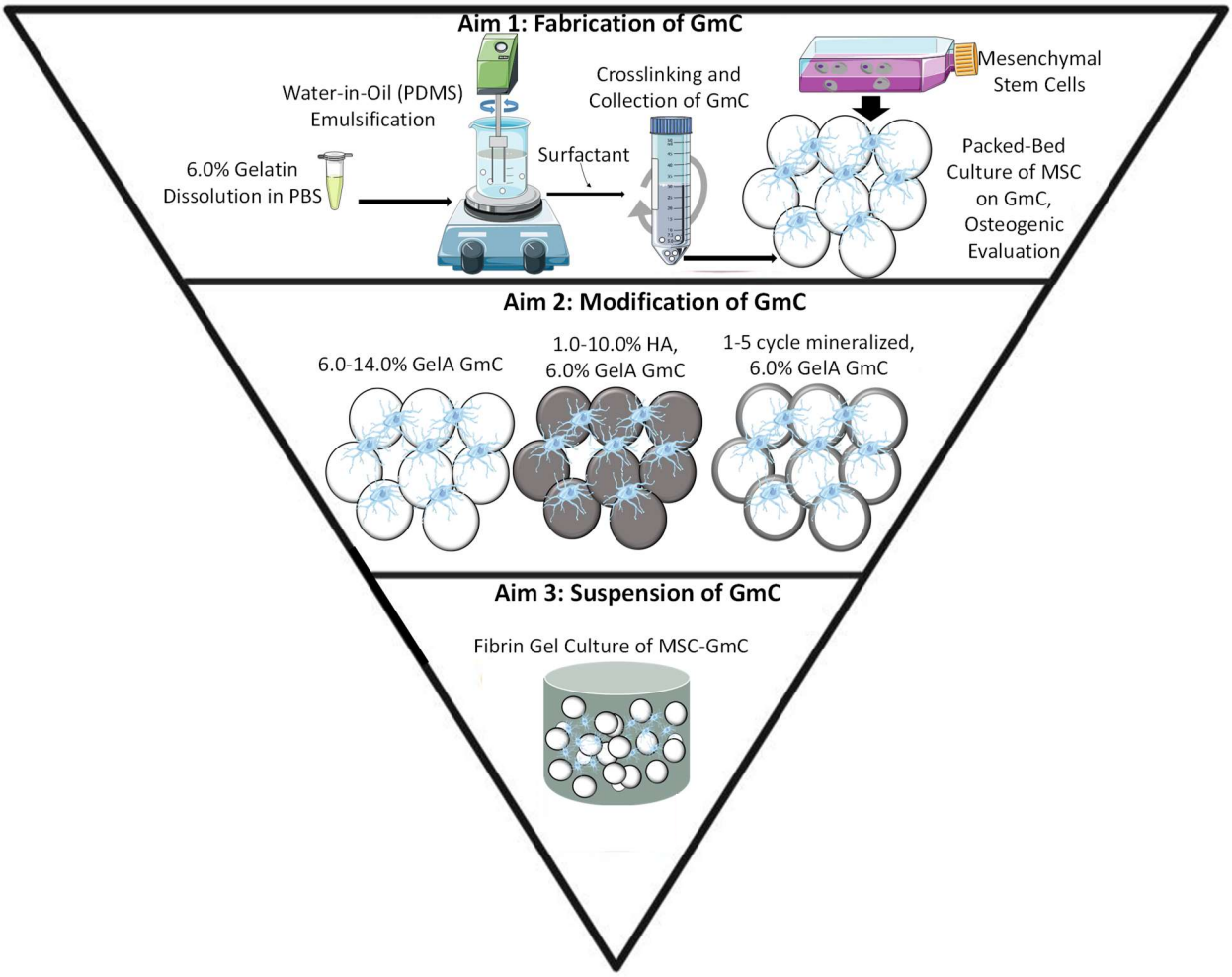

Figure 6.1: Schematic map of evaluated strategies in this developmental project.

6.1 Summary and Conclusions

In this dissertation work, genipin-crosslinked GmC were designed and fabricated to address incomplete bone defect regeneration constrained by metabolite diffusion and spatiotemporal limits to the distribution of osteogenic cues. The GmC developed and evaluated in this project were found to be suitable for MSC attachment and culture, and were determined to

have an osteogenic effect under some conditions. The project consisted of a series of studies to progressively examine GmC formulation and culture parameters, and to evaluate their potential as a cellularized, modular bone filler material, as shown schematically in Figure 6.1. In Aim 1, GmC size was found to be partially regulated through control over relevant emulsification process parameters. In particular, the effects of impeller geometry and stirring rate were characterized rigorously to determine the range of GmC morphologies that could be achieved. Axial impeller geometries were employed to confine critical shearing radial forces and the subsequent distribution of GmC sizes. These studies also examined a range of MSC seeding densities and their effect on cell attachment and osteogenic function. The studies in Aim 2 examined the benefits of mechanobiological stimulation to improve osteogenic function by increasing the biopolymer content and adding an exogenous mineral phase. In Aim 3, suspension culture of MSC-GmC populations in a fibrin carrier gel was examined to determine the effect on MSC localization and phenotype, as a simple model of GmC delivery as packed-bed populations.

The genipin-crosslinked, spheroidal GmC in this work were designed to achieve injectability and conformal defect infill. Water-in-oil emulsification was used to generate large batches of microparticles rapidly and reproducibly. The count median diameter of these particles was controllable through the adjustment of impeller blade geometry and impeller rotations per minute. The average diameter of emulsion-generated particles was found to be positively correlated with axial impeller blade dimensions (0.33-1.0 mm blade cross-sectional diameter). It was also found to be negatively correlated with impeller rotations per minute (250-500 rpm). Osteogenic performance was also modulated through MSC seeding density (5,000-50,000 MSC/cm^2) and all conditions, both in control and osteogenic media, were found to exhibit increased DNA-normalized calcium deposition over three weeks of culture. However, DNA levels

in all conditions was found to have declined or plateaued after one week of static packed-bed GmC culture. In addition, DNA-normalized calcium deposition also was shown to be negatively related to seeding density, with diminishing levels of calcium deposition resulting from additional increases in cell seeding density. Previous studies have documented these early increases, while missing the post-7-day declines (Lau TT, Wang C, & Wang DA, 2010; Lau TT, Wang C, Peng SW, Su K, & Wang DA, 2010; Lau et. al., 2012). The reasons for this phenomenon also tie into findings from the subsequent research aims, as discussed further below.

In the subsequent research of Aim 2, GmC were compositionally modified by increasing gelatin content, adding emulsified HA, and applying solution-crystalized apatite mineralization to enhance a sustained, stiffness-based osteogenic influence. Shear modulus (G') was found to be clearly and positively correlated with increased gelatin (6.0-14.0% (wt/vol)), HA (1.0-10.0% (wt/vol)), and apatite mineralization (1-5 cycles). GmC diameter was found to be positively correlated with increased gelatin or HA content, as is often the relationship between microgel size and increasing solid content (Kim et. al., 2007). Viable cell area coverage and DNA levels were found to negatively correlate with calcium content and generally peaked at one week into culture. The subsequent decline in cell number is likely to have resulted from increasing GmC-surface calcium deposition through the culture period. DNA-normalized ALP and calcium deposition were found to be upregulated on all modified GmC, indicating osteogenicity even without osteogenic solution supplements.

These findings were supported by a related study pre-surface-mineralized GmC, in which DNA levels remained low relative to unmineralized GmC throughout culture. Viable cell coverage area was similarly diminished on pre-surface-mineralized GmC relative to unmineralized GmC. The 6.0% (wt/vol) GelA GmC-cultured MSC exhibited the greatest absolute and DNA-normalized

calcium deposition on the final day of culture. They also exhibited the greatest DNA-normalized ALP activities on the final day of culture, which contributes to an osteogenic profile with and without osteogenic supplement. Hydroxyapatite-containing conditions also displayed an osteogenic effect, with 5.0% (wt/vol) HA GmC-cultures showing greatest final DNA-normalized calcium levels. For these reasons, subsequent fibrin-embedding experiments in Aim 3 were done exclusively with pure gelatin GmC, due to their higher ALP activity upregulation, as well as to prevent interference of HA in measuring calcium deposition.

In Aim 3 of the project, MSC-GmC populations were suspended in a fibrin matrix to promote localization of GmC and retention of cells, and to determine whether osteogenic influence is retained within a simple simulated implant environment. In these studies, MSC were either pre-seeded onto GmC or were added simultaneously with their co-suspension in fibrin. Osteogenic function was observed in both seeding methods, and 6.0% gelatin GmC exhibited greater osteogenic impact than 14.0% gelatin GmC within fibrin, just as was found to be the case in the absence of fibrin. Notably, fibrin matrix was found to successfully counteract the post-7-day DNA decline routinely seen on the GmC, indicating gradual cell loss. The fibrin carrier gel, in addition to simulating the implant environment and a delivery system for cellularized GmC, also restrains cell loss. This is reflected in more stable DNA levels. And calcium level increases over the duration of culture indicated osteogenic activity.

GmC have been shown to be multifunctional osteogenic cell microcarrier platforms. Much of the benefit to these microspheres stems from their low toxicity genipin crosslinking. This makes them cytocompatible to MSC, resulting in the exceptionally high seeding efficiencies in this study, consistently exceeding 90%. Genipin is also a small and aromatic molecule, which promotes stiff, tightly bound gelatin chains. This stiffness creates a microenvironment which has been shown to

induce ALP upregulation and sustained calcium deposition without need of exogenous osteogenic bio-chemicals. GmC have also been shown, in this study, to be rapidly producible within a controllably, microscale size envelope. This study has shown the potential for these compositionally-modifiable micro-modules to harbor MSC in packed bone-filler-like configurations and in fibrinous tissue-like environments while retaining osteogenic impact on localized bone progenitor cells. The findings of this work present a useful platform for researching and developing more osseointegrative bone defect therapeutics.

6.2 Future Directions

Emulsification methods used in the fabrication of GmC used for this study were sufficient for high-throughput generation of syringe-injectable modular microspheres (80-350 μm in diameter). In the future, it may be useful to experiment with more combinations of gelatin and hydroxyapatite hybrids in the interest of establishing more options in mechanically and chemically tuning GmC products. These complex relationships were not prioritized in this developmental project in the interest of establishing more one-to-one relationships. Also, while mechanical enhancement of gelatin was accomplished in this study, the stiffness of GmC remained much lower than values reported to be extremely osteogenic (Tseng et. al., 2011).

Further work could also be performed with spectroscopic analysis methods in order to more clearly identify the morphology and chemical structure of the solution-crystalized apatite as well as the cell deposited calcium compounds over the span of culture. This structure could potentially be further related to cell viability, DNA level, and how they change over time. Emulsion-generated solid-collagen microcarriers are also an option. Such carriers, as well as a traditional hydrogel GmC, may be taken at specified culture time-points and subjected to multiple forms of analysis. Scanning electron microscopy and Fourier transform infrared spectroscopy, in particular, would

be useful for identifying surface mineralization and possible time-lapsed cell detachment. However, based on the findings of this study, the best options for addressing the issue of gradual surface-mineralized cell detachment would likely involve more experiments with carrier gel encapsulation

Altering the relative compositions of the fibrin carrier gel system will be a critical follow-up to this research. Fibrinogen and thrombin concentrations could be further optimized for adjusted hydrogel density and mixing time for varied compositions of GmC. Appropriate pre-gelation viscosities, gelation times, and post-gelation stiffnesses will need to be validated through the performance of a set of non-cellular viscoelastic mechanical tests, cellular in-vitro experiments, and osteoporotic mouse distal femoral metaphysis defect in-vivo model experimentation (Xie et. al., 2017). Additionally, increased HA causes faster settling of microcarriers, which can be countered with faster gelling systems. Embedding GmC within a more compliant matrix may allow greater mass transport while a stiffer matrix could provide necessary mechanobiological reinforcement.

Near future experiments for a future graduate student in this line of research will include a number of cell/GmC/carrier gel trials meant to complement the studies already undertaken. Additional gelatin and HA compositions for GmC along with their hybridized variants could be fabricated and used in in-vitro MSC culture, with the intent of tuning the material parameters to further promote osteogenic function.

Carrier gel system optimization to extend the preliminary work done with fibrin represents the next important steps in the development of this project, as the composition and GmC:carrier-gel ratio could be tailored for greater control over pre-gelation viscosities, gelation kinetics, post-gelation shear moduli, and functional impacts. Preliminary experimentation similar to the previous

cellular in-vitro packed-bed GmC experimentation should be done with a murine cell line like the transgenic C57BL/6 ROSA$^{mT/mG}$ mouse mesenchymal stromal cell (Annamalai et. al., 2019) due to the chosen eventual in-vivo model. This cell line has been used in the CMITE lab with success in previous in vivo studies. Concurrently or subsequently, non-cellular viscoelastic mechanical testing would be administered on fibrin concoctions mixed with 2.5 mg/mL clottable fibrinogen, 10% (wt/vol) FBS, and a range of thrombin concentrations going from 0.1 U/mL to 20 U/mL. The change in thrombin concentration is meant to more sufficiently mechanically stimulate and retain anchorage-dependent stromal cells. Pure fibrin has been shown to reach a stable viscosity of approximately 80-650 Pa*s from a starting viscosity of approximately 7-20 Pa*s in a gelation time of around 200-500 seconds (G'-G" crossover between 6.5 and 13 seconds), but future studies will definitively establish the benchmark values for the proposed formulations. Similarly, the post-gelation shear modulus reached a value of around 1300 Pa. The 3 mm diameter defect size allows for the use of a 12 to approximately 23 gauge needle for the application phase. In addition, other biopolymer options or additives for the carrier gel phase could be explored, including laponite, alginate, or collagen. Taken together, these studies would build on the current MSC-GmC culture, differentiation, and delivery system to create new options for cellularized bone fillers, particularly for large and recalcitrant defects.

Appendix

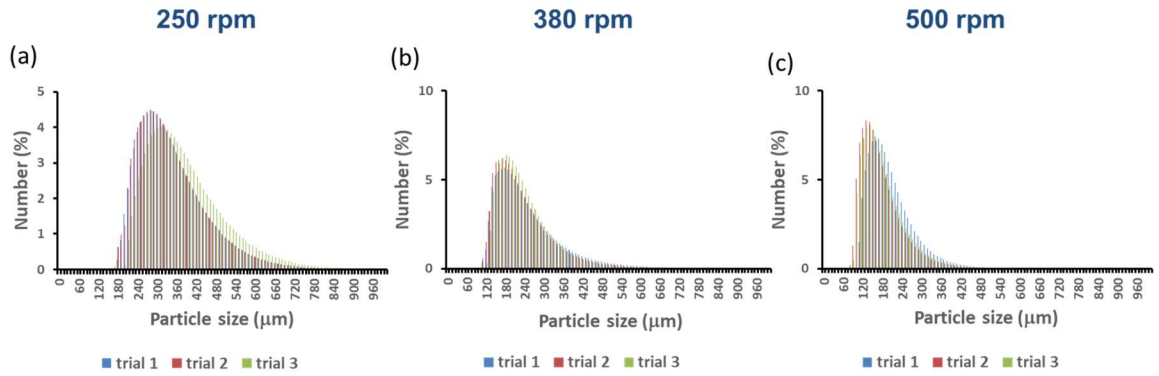

Figure S1: Effect of stirring rate on microparticle size using the Axial-1.0 impeller geometry, demonstrating very good batch-to-batch reproducibility. Histograms show three separate batches of microparticles at each stirring rate of a) 250 rpm, b) 380 rpm, and c) 500 rpm.

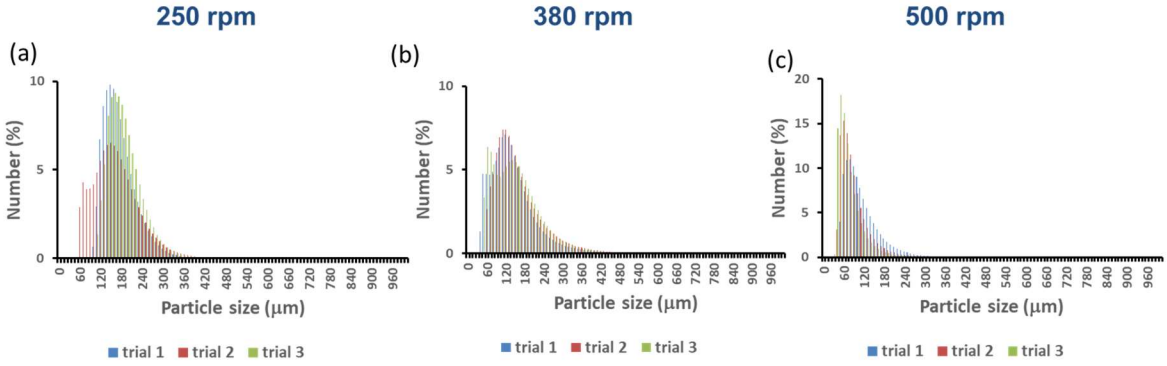

Figure S2: Effect of stirring rate on microparticle size using the Axial-0.3 impeller geometry, demonstrating very good batch-to-batch reproducibility. Histograms show three separate batches of microparticles at each stirring rate of a) 250 rpm, b) 380 rpm, and c) 500 rpm.

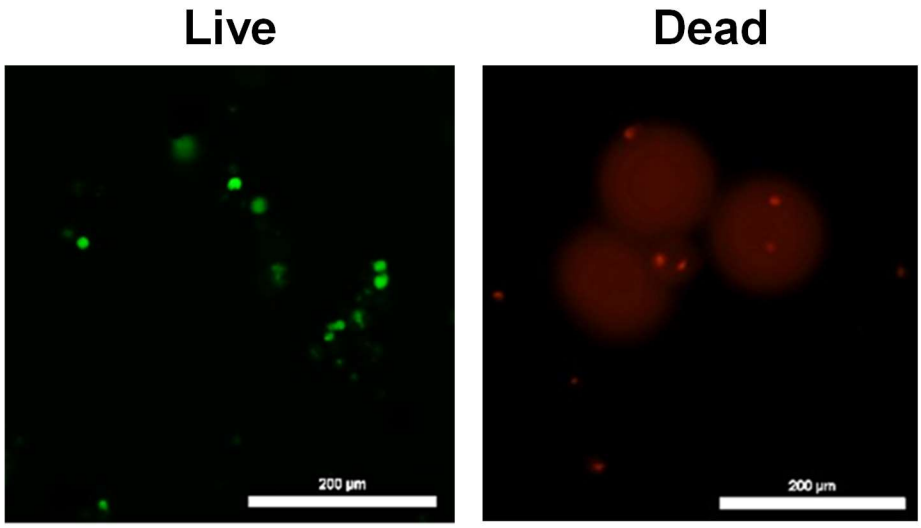

Figure S3: Fluorescence microscopy of human lung fibroblasts cultured on GmC at day 1 after seeding. Image at left shows green cytoplasm of living cells under control conditions. Image at right shows red-stained nuclei of dead cells after 20 min of ethanol treatment, showing that dead nuclei can be clearly distinguished from the autofluorescence of the gelatin matrix. Scale bar represents 200 µm.

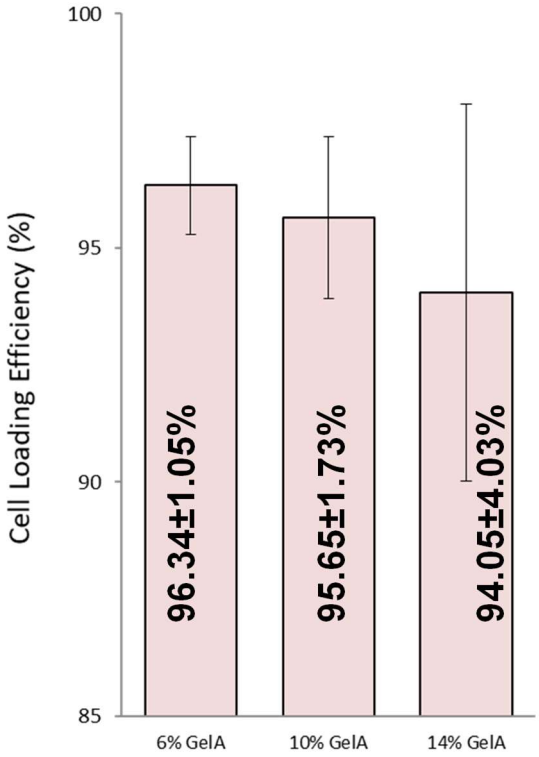

Figure S4: Cell loading efficiency for MSC seeded at 15,000 cells/cm^2 on microcarriers of 6.0 %, 10.0 %, or 14.0 % wt/vol gelatin at day one after seeding. Approximately,14.27 ± 0.16 cells were determined to have attached to each 6.0 % wt/vol gelatin GmC.

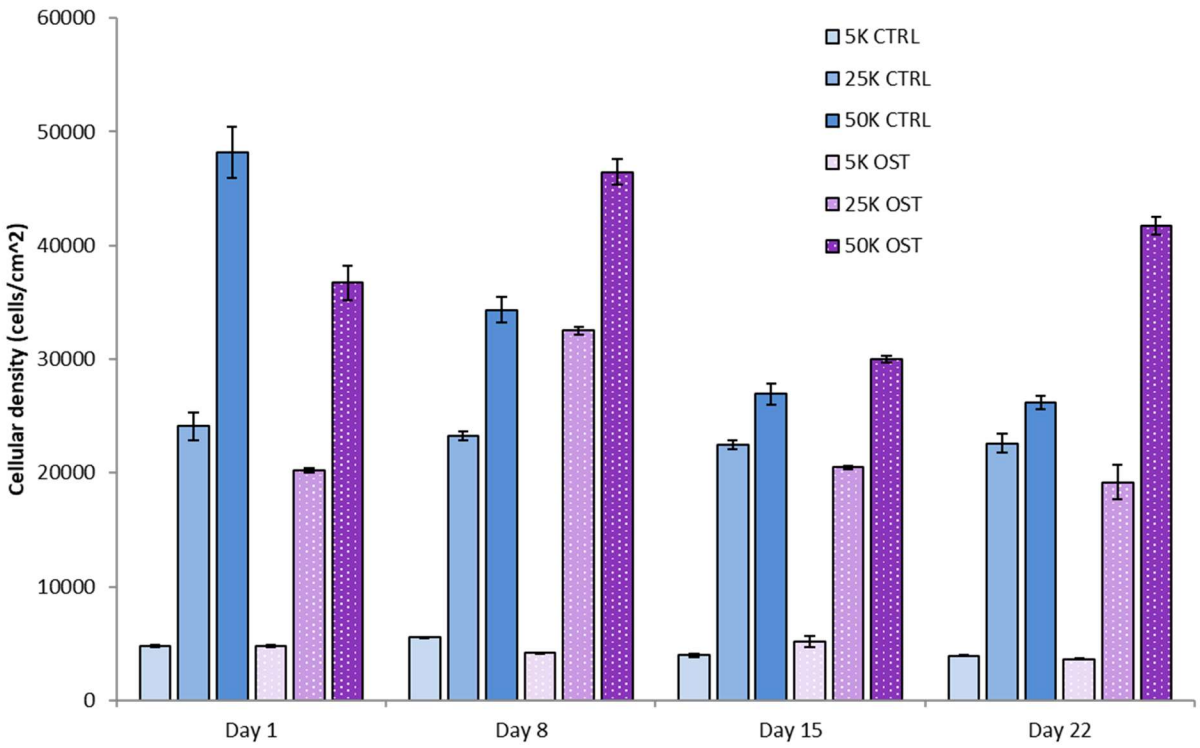

Figure S5: Cellular density of MSC seeded at 5,000-50,000 cells/cm^2 on 6.0 % wt/vol gelatin GmC and cultured in control and osteogenic media.

Bibliography

Annamalai RT, Naik T, Prout H, Putnam AJ, and Stegemann JP. Biofabrication of injectable fibrin microtissues for minimally-invasive therapies: application of surfactants. Biomed Mater 2018; **13(4):** 045005.

Annamalai RT, Turner PA, Carson IV WF, Levi B, Kunkel S, Stegemann JP. Harnessing macrophage-mediated degradation of gelatin microspheres for spatiotemporal control. *Biomaterials.* 2018; **161**: 216-227.

Aydogdu H, Keskin D, Baran ET, Tezcaner A. Pullulan microcarriers for bone tissue regeneration. *Materials Science and Engineering: C.* 2016; **63**: 439-449.

Babur BK, Futrega K, Lott WB, Klein TJ, Cooper-White J, Doran MR. High-throughput bone and cartilage micropellet manufacture, followed by assembly of micropellets into biphasic osteochondral tissue. *Cell Tissue Res.* 2015; **361**: 755-768.

Baino F, Hamzehlou S, Kargozar S. Bioactive glasses: where are we and where are we going?. *Journal of functional biomaterials*. 2018 Mar; **9(1)**:25.

Ballouze R, Marahat MH, Mohamad S, Saidin NA, Kasim SR, Ooi JP. Biocompatible magnesium-doped biphasic calcium phosphate for bone regeneration. *J. Biomed. Mater. Res. B.* 2021.

Barrias CC, Ribeiro CC, Barbosa MA. Adhesion and proliferation of human osteoblastic cells seeded on injectable hydroxyapatite microspheres. In *Key Engineering Materials* 2004 (Vol. 254, pp. 877-880). Trans Tech Publications Ltd.

Baule A, Makse HA. Fundamental challenges in packing problems: from spherical to non-spherical particles. *Soft Matter*. 2014; **10**: 4423-4429.

Bello AB, Kim D, Kim D, Park H, Lee SH. Engineering and functionalization of gelatin biomaterials: From cell culture to medical applications. *Tissue Eng. Part B: Rev.* 2020; **26**: 2.

Butcher DT, Alliston T, Weaver VM. A tense situation: forcing tumour progression. *Nat. Rev. Cancer.* 2009; **9**: 108-122.

Chao SC, Wang MJ, Pai NS, Yen SK. Preparation and characterization of gelatin–hydroxyapatite composite microspheres for hard tissue repair. *Mater. Sci. Eng. C*. 2015; **57**: 113-122.

Chen AKL, Reuveny S, Oh SKW. Application of human mesenchymal and pluripotent stem cell microcarrier cultures in cellular therapy: achievements and future direction. *Biotechnol. Adv.* 2013; **31**: 1032-1046.

Chen XY, Chen JY, Tong XM, Mei JG, Chen YF, Mou XZ. Recent advances in the use of microcarriers for cell cultures and their ex vivo and in vivo applications. *Biotechnol. Lett.* 2020; **42(1)**: 1-10.

Cox TR, Erler JT. Remodeling and homeostasis of the extracellular matrix: implications for fibrotic diseases and cancer. *Dis. Model. Mech.* 2011; **4(2)**: 165-178.

Cuzmar E, Perez RA, Manzanares MC, Ginebra MP, Franch J. In vivo osteogenic potential of biomimetic hydroxyapatite/collagen microspheres: comparison with injectable cement pastes. *PLoS One*. 2015 Jul 1; **10(7)**:e0131188.

Dosta P, Ferber S, Zhang Y, Wang K, Ros A, Uth N, Levinson Y, Abraham E, Artzi N. Scale-up manufacturing of gelatin-based microcarriers for cell therapy. *J Biomed Mater Res B Appl Biomater*. 2020; **108**: 2937-2949.

Ducheyne P, Livingston T, Shapiro I, Ayyaswamy P, Gao H, Radin S. Surface-modified bioactive glass particles as microcarriers in a microgravity environment. *Tissue Engineering*. 1997 Sep 1; **3(3)**:219-29.

Engler AJ, Sen S, Sweeney HL, Discher DE. Matrix elasticity directs stem cell lineage specification. *Cell*. 2006; **126**: 677-689.

Fernandez de Grado G, Keller L, Idoux-Gillet Y, Wagner Q, Musset AM, Benkirane-Jessel N, Bornert F, Offner D. Bone substitutes: a review of their characteristics, clinical use, and perspectives for large bone defects management. *J. Tissue Eng.* 2018; **9**: 1-18.

Fischer EM, Layrolle P, Van Blitterswijk CA, de Bruijn JD. Bone formation by mesenchymal progenitor cells cultured on dense and microporous hydroxyapatite particles. *Tissue engineering*. 2003 Dec 1;**9(6)**:1179-88.

Ghomi ER, Nourbaksh N, Kenari MA, Zare M, Ramakrishna S. Collagen-based biomaterials for biomedical applications. *J. Biomed. Mater. Res. B.* 2021.

Handorf AM, Zhou Y, Halanski MA, Li WJ. Tissue stiffness dictates development, homeostasis, and disease progression. *Organogenesis*. 2015; **11(1)**: 1-15.

Hayashi K, Tabata Y. Preparation of stem cell aggregates with gelatin microspheres to enhance biological functions. *Acta Biomater.* 2011; **7**: 2797-2803.

Hong SJ, Yu HS, Kim HW. Preparation of porous bioactive ceramic microspheres and in vitro osteoblastic culturing for tissue engineering application. *Acta Biomaterialia*. 2009 Jun 1; **5(5)**:1725-31.

Hsu FY, Chueh SC, Wang YJ. Microspheres of hydroxyapatite/reconstituted collagen as supports for osteoblast cell growth. *Biomaterials*. 1999; **20**: 1931-1936.

Humbert P, Brennan MA, Davison N, Rosset P, Trichet V, Blanchard F, Layrolle P. Immune modulation by transplanted calcium phosphate biomaterials and human mesenchymal stromal cells in bone regeneration. *Front. Immunol.* 2019; **10**: 663.

Hwang YJ, Larsen J, Krasieva TB, Lyubovitsky JG. Effect of genipin crosslinking on the optical spectral properties and structures of collagen hydrogels. *ACS Appl. Mat. & Interfaces*. 2011; **3**: 2579-2584.

Kim HW, Gu HJ, Lee HH. Microspheres of Collagen-Apatite Nanocomposites with Osteogenic Potential for Tissue Engineering. *Tissue Eng*. 2007; **13**: 965-973.

Kim HW, Yoon BH, Kim HE. Microsphere of apatite-gelatin nanocomposite as bone regenerative filler. *J. Mater. Sci.: Mater. Med.* 2005; **16**: 1105-1109.

Lau TT, Lee LQP, Leong W, and Wang DA. Formation of model hepatocellular aggregates in a hydrogel scaffold using degradable genipin crosslinked gelatin microspheres as cell carriers. Biomed Mater 2012; **7:** 065003.

Lau TT, Wang C, Png SW, Su K, and Wang DA. Genipin-crosslinked microcarriers mediating hepatocellular aggregates formation and functionalities. J Biomed Mater Res A 2010; **96(1):** 204-211.

Lau TT, Wang C, Wang DA. Cell delivery with genipin crosslinked gelatin microspheres in hydrogel/microcarrier composite. *Compos. Sci. Technol.* 2010; **70(13)**: 1909-1914.

Leiblein M, Koch E, Winkenbach A, Schaible A, Nau C, Buchner H, Schroder K, Marzi I, Henrich D. Size matters: Effect of granule size of the bone graft substitute (Herafill®) on bone healing using Masquelet's induced membrane in a critical size defect model in the rat's femur. *J. Biomed. Mater. Res. Part B Appl. Biomater.* 1980; **29**: 33-41.

Lin H, Sohn J, Shen H, Langhans MT, Tuan RS. Bone marrow stem cells: Aging and tissue engineering applications to enhance bone healing. *Biomaterials.* 2019; **203**: 96-110.

Malda J, Frondoza CG. Microcarriers in the engineering of cartilage and bone. *Trends in biotechnology*. 2006 Jul 1; **24(7)**:299-304.

Man W, Donev A, Stillinger FH, Sullivan MT, Russel WB, Heeger D, Inati S, Torquato S, Chaikin PM. Experiments on random packings of ellipsoids. *Phys. Rev. Lett*. 2005; **94**: 198001.

Mankani MH, Kuznetsov SA, Wolfe RM, Marshall GW, Robey PG. In vivo bone formation by human bone marrow stromal cells: reconstruction of the mouse calvarium and mandible. *Stem cells*. 2006 Sep; **24(9)**:2140-9.

Mateus, A.Y.P., Barrias, C.C., Ribeiro, C., Ferraz, M.P. and Monteiro, F.J., 2008. Comparative study of nanohydroxyapatite microspheres for medical applications. *Journal of Biomedical Materials Research Part A: An Official Journal of The Society for Biomaterials,*

The Japanese Society for Biomaterials, and The Australian Society for Biomaterials and the Korean Society for Biomaterials, **86(2)**:483-493.

McLaren JS, Macri-Pellizzeri L, Hossain KM, Patel U, Grant DM, Scammell BE, Ahmed I, Sottile V. Porous phosphate-based glass microspheres show biocompatibility, tissue infiltration, and osteogenic onset in an ovine bone defect model. *ACS applied materials & interfaces*. 2019 Apr 16; **11(17)**:15436-46.

Nweke CE, Stegemann JP. Modular microcarrier technologies for cell-based bone regeneration. *J. Mater. Chem. B.* 2020; **8(18)**: 3972-3984.

Ornelas-Gonzalez A, Gonzalez-Gonzalez M, Rito-Palomares M. Microcarrier-based stem cell bioprocessing: GMP-grade culture challenges and future trends for regenerative medicine. *Crit. Rev. Biotechnol.* 2021; 1-15.

Overstreet M, Sohrabi A, Polotsky A, Hungerford DS, Frondoza CG. Collagen microcarrier spinner culture promotes osteoblast proliferation and synthesis of matrix proteins. *In Vitro Cell. Dev. Biol. Animal*. 2003; **39**: 228-234.

P. V. Braun *Nanocomposite Science and Technology*. P. M. Ajayan, L. S. Schadler and P. V. Braun, Wiley-VCH, Weinheim, 2003, pp. 155–207.
Pajarinen J, Lin T, Gibon E, Kohno Y, Maruyama M, Nathan K, Lu L, Yao Z, Goodman SB. Mesenchymal stem cell-macrophage crosstalk and bone healing. *Biomaterials*. 2019; **196**: 80-89.

Park JH, Lee EJ, Knowles JC, Kim HW. Preparation of in situ hardening composite microcarriers: calcium phosphate cement combined with alginate for bone regeneration. *Journal of Biomaterials Applications*. 2014 Mar; **28(7)**:1079-84.

Park JH, Lee GS, Shin US, Kim HW. Self-hardening microspheres of calcium phosphate cement with collagen for drug delivery and tissue engineering in bone repair. Journal of the American Ceramic Society. 2011 Feb; **94(2)**:351-4.

Park JH, Pérez RA, Jin GZ, Choi SJ, Kim HW, Wall IB. Microcarriers designed for cell culture and tissue engineering of bone. *Tissue Engineering Part B: Reviews*. 2013 Apr 1; **19(2)**:172-90.

Park JS, Hong SJ, Kim HY, Yu HS, Lee YI, Kim CH, Kwak SJ, Jang JH, Hyun JK, Kim HW. Evacuated calcium phosphate spherical microcarriers for bone regeneration. *Tissue Engineering Part A*. 2010 May 1; **16(5)**:1681-91.

Perez JR, Kouroupis D, Li DJ, Best TM, Kaplan L, Correa D. Tissue engineering and cell-based therapies for fractures and bone defects. *Front. Bioeng. Biotechnol.* 2018; **6**: 105.

Perez RA, Altankov G, Jorge-Herrero E, Ginebra MP. Micro-and nanostructured hydroxyapatite–collagen microcarriers for bone tissue-engineering applications. Journal of tissue engineering and regenerative medicine. 2013 May; **7(5)**:353-61.

Perez RA, Del Valle S, Altankov G, Ginebra MP. Porous hydroxyapatite and gelatin/hydroxyapatite microspheres obtained by calcium phosphate cement emulsion. Journal of Biomedical Materials Research Part B: Applied Biomaterials. 2011 Apr; **97(1)**:156-66.

Perez RA, Riccardi K, Altankov G, Ginebra MP. Dynamic cell culture on calcium phosphate microcarriers for bone tissue engineering applications. *J. Tissue Eng.* 2014; **5**: 2041731414543965.

Petruskevicius J, Nielsen S, Kaalund S, Knudsen PR, Overgaard S. No effect of Osteoset®, a bone graft substitute, on bone healing in humans: A prospective randomized double-blind study. *Acta Orthop. Scand.* 2002; **73**: 575-578.

Presen DM, Traweger A, Gimona M, Redl H. Mesenchymal stromal cell-based bone regeneration therapies: From cell transplantation and tissue engineering to therapeutic secretomes and extracellular vesicles. *Front. Bioeng. Biotechnol*. 2019; **7**: 352.

Qiu Q, Ducheyne P, Gao H, Ayyaswamy P. Formation and differentiation of three-dimensional rat marrow stromal cell culture on microcarriers in a rotating-wall vessel. *Tissue engineering*. 1998 Mar 1; **4(1)**:19-34.

Qiu QQ, Ducheyne P, Ayyaswamy PS. 3D bone tissue engineered with bioactive microspheres in simulated microgravity. *In Vitro Cellular & Developmental Biology-Animal*. 2001 Mar; **37(3)**:157-65.

Qiu QQ, Ducheyne P, Ayyaswamy PS. New bioactive, degradable composite microspheres as tissue engineering substrates. *Journal of biomedical materials research*. 2000 Oct; **52(1)**:66-76.

Rao RR, Stegemann JP. Cell-based approaches to the engineering of vascularized bone tissue. *Cytotherapy.* 2013; **15(11)**: 1309-1322.

Rao RR, Vigen ML, Peterson AW, Caldwell DJ, Putnam AJ, Stegemann JP. Dual-phase osteogenic and vasculogenic engineered tissue for bone formation. *Tissue Eng. Part A.* 2015; **21(3-4)**: 530-540.

Roberts TT, Rosenbaum AJ. Bone grafts, bone substitutes and orthobiologics: the bridge between basic science and clinical advancements in fracture healing. *Organogenesis*. 2012; **8**: 114-124.

Ruiz SA, Chen CS. Emergence of patterned stem cell differentiation within multicellular structures. *Stem Cells*, 2008; **26**: 2921-2927.

Sadowska JM, Wei F, Guo J, Guillem-Marti J, Zhengmei L, Maria-Pau G, Xiao Y. The effect of biomimetic calcium deficient hydroxyapatite and sintered β-tricalcium phosphate on osteoimmune reaction and osteogenesis. *Acta biomaterialia*. 2019 Sep 15; **96**:605-618.

Saito E, Suarez-Gonzalez D, Rao RR, Stegemann JP, Murphy WL, Hollister SJ. Use of micro-computed tomography to nondestructively characterize biomineral coatings on solid freeform fabricated poly (L-lactic acid) and polycaprolactone scaffolds in vitro and in vivo. *Tissue Eng. Part C Methods.* 2013; **19(7)**: 507-517.

Saltz A, Kandalam U. Mesenchymal stem cells and alginate microcarriers for craniofacial bone tissue engineering: A review. *J. Biomed. Mater. Res. B.* 2016; **104(5)**: 1276-1284.

Sart S, Errachid A, Schneider YJ, Agathos SN. Modulation of mesenchymal stem cell actin organization on conventional microcarriers for proliferation and differentiation in stirred bioreactors. *J. Tissue Eng. Regen. Med.* 2013; **7**: 537-551.

Shadjou N, Hasanzadeh M. Silica-based mesoporous nanobiomaterials as promoter of bone regeneration process. *J. Biomed. Mater. Res. B.* 2015; **103(11)**: 3703-3716.

Shapoff CA, Bowers GM, Levy B, Mellonig JT, Yukna RA. The effect of particle size on the osteogenic activity of composite grafts of allogeneic freeze-dried bone and autogenous marrow. *J. Periodontol.* 1980; **29**: 33-41.

Shen S, Fu D, Xu F, Long T, Hong F, Wang J. The design and features of apatite-coated chitosan microspheres as injectable scaffold for bone tissue engineering. *Biomed. Mater*. 2013; **8**: 025007.

Sobacchi C, Erreni M, Strina D, Palagano E, Villa A, Menale C. 3D bone biomimetic scaffolds for basic and translational studies with mesenchymal stem cells. *Int. J. Mol. Sci.* 2018; **19(10)**: 3150.

Solorio L, Zwolinski C, Lund AW, Farrell MJ, Stegemann JP. Gelatin microspheres crosslinked with genipin for local delivery of growth factors. *J. Tissue Eng. Regen. Med.* 2010; **4(7)**: 514-523.

Tsai HH, Yang KC, Wu MH, Chen JC, Tseng CL. The effects of different dynamic culture systems on cell proliferation and osteogenic differentiation in human mesenchymal stem cells. *Int. J. Mol. Sci.* 2019; **20(16)**: 4024.

Tseng PC, Young TH, Wang TM, Peng HW, Hou SM, Yen ML. Spontaneous osteogenesis of MSCs cultured on 3D microcarriers through alteration of cytoskeletal tension. *Biomaterials.* 2011; **33(2)**: 556-564.

Turner PA, Thiele JS, Stegemann JP. Growth factor sequestration and enzyme-mediated release from genipin-crosslinked gelatin microspheres. *J. Biomaterials Sci., Polym. Ed.* 2017; **28**: 1826-1846.

Verrier S, Alini M, Alsberg E, Buchman SR, Kelly D, Laschke MW, Menger MD, Murphy WL, Stegemann JP, Schütz M, Miclau T. Tissue engineering and regenerative approaches to improving the healing of large bone defects. *Eur. Cell Mater.* 2016; **32**: 87-110.

Vimalraj S. Alkaline phosphatase: Structure, expression and its function in bone mineralization. *Gene.* 2020; **754**: 144855.

Vining KH, Mooney DH. Mechanical forces direct stem cell behavior in development and regeneration. *Nat. Rev. Mol. Cell Biol.* 2017; **18**: 728-742.

Winkler T, Sass FA, Duda GN, Schmidt-Bleek K. A review of biomaterials in bone defect healing, remaining shortcomings and future opportunities for bone tissue engineering: The unsolved challenge. *Bone & joint research*. 2018 Mar; **7(3)**:232-43.

Wissemann KW, Jacobson BS. Pure gelatin microcarriers: synthesis and use in cell attachment and growth of fibroblast and endothelial cells. *In vitro Cellular & Dev. Biology*. 1985; **21**: 391-401.

Xie Z, Weng S, Li H, Yu X, Lu S, Huang K, Wu Z, Bai B, Boodhun V, Yang L. Teriparatide promotes healing of critical size femur defect through accelerating angiogenesis and degradation of β-TCP in OVX osteoporotic rat model. *Biomedicine & Pharmacotherapy*. 2017 Dec 1; **96**: 960-7.

Yang G, Xiao Z, Long H, Ma K, Zhang J. Assessment of the characteristics and biocompatibility of gelatin sponge scaffolds prepared by various crosslinking methods. *Sci. Rep.* 2018; **8(1)**: 1-3.

Yang Y, Rossi FM, Putnins EE. Ex vivo expansion of rat bone marrow mesenchymal stromal cells on microcarrier beads in spin culture. *Biomaterials*. 2007; **28**: 3110-3120.

Yao L, Phan F, Li Y. Collagen microsphere serving as a cell carrier supports oligodendrocyte progenitor cell growth and differentiation for neurite myelination in vitro. *Stem Cell Res. Ther.* 2013; **4**: 109.

A. Ethirajan, U. Ziener, A. Chuvilin, U. Kaiser, H. Cölfen and K. Landfester, *Adv. Funct. Mater.*, **18**, 2221-2227.

C. C. Barrias, C. C. Ribeiro, M. Lamghari, C. S. Miranda and M. A. Barbosa, *J. Biomed. Mater. Res. A*, 2005, **72**, 57-66.

H. A. Declerq, T. L. Gorski, S. P. Tielens, E. H. Schecht and M. J. Cornelissen, *Biomacromolecules,* 2005, **6**, 1608-1614.

J. G. Calcei and S. A. Rodeo, *Clin. Sports Med.,* 2019, **38**, 79-95.

S. Sart and S. N. Agathos, in *Bioreactors in Stem Cell Biology*, Humana Press, New York, NY, 2015, pp. 87-102.

G. Blüml, in *Animal Cell Biotechnology*, Humana Press, 2007, pp. 149-178.

A. V. Goncharenko, M. S. Kotlyarova, A. M. Moisenovich, A. Y. Arkhipova, D. A. Kulikov, A. S. Konkov, A. V. Kulikov, A. E. Mashkov, I. I. Agapov, M. M. Moisenovich and M. P. Kirpichnikov, in *Doklady Biochemistry and Biophysics*, Pleiades Publishing, 2017, pp. 345-348.

K. A. Luetchford, J. B. Chaudhuri and A. Paul, *Mater. Sci. Eng. C*, 2020, **106**, 110116.

C. C. Ribeiro, C. C. Barrias and M. A. Barbosa, *J. Mater. Sci.: Mater. Med.*, 2006, **17**, 455-463.

C. C. Barrias, C. C. Ribeiro, D. Rodrigues, S. Miranda and M. A. Barbosa, in *Key Engineering Materials*, Trans Tech Publications, 2005, pp. 689-692.

A.H. Lourenço, N. Neves, C. Ribeiro-Machado, S.R. Sousa, M. Lamghari, C.C. Barrias, A.T. Cabral, M.A. Barbosa and C.C. Ribeiro, *Sci. Rep.*, 2017, **7**, 5098.
S. M. Oliveira, C. C. Barrias, I. F. Almeida, P. C. Costa, M. R. P. Ferreira, M. F. Bahia and M. A. Barbosa, *J. Biomed. Mater. Res. B*, 2008, **87**, 49-58.
T. J. Wu, H. H. Huang, C. W. Lan, C. H. Lin, F. Y. Hsu and Y. J. Wang, *Biomaterials*, 2004, **25**, 651-658.
E. Boanini and A. Bigi, *J. Colloid Interface Sci.*, 2011, **362**, 594-599.
H. Maeda, T. Kasuga and M. Nogami, in *Key Engineering Materials*, Trans Tech Publications, 2004, pp. 533-536.
X. Shi, J. Jiang, L. Sun and Z. Gan, *Colloids Surf. B*, 2011, **85**, 73-80.
K. Du, X. Shi and Z. Gan, *Langmuir*, 2013, **29**, 15293-15301.
H. S. Yu, S. J. Hong, J. H. Park, I. Jeong and H. W. Kim, *Adv. Eng. Mater.*, 2009, **11**, B162-B168.
S. Mann, Biomineralization: principles and concepts in bioinorganic materials chemistry, Oxford University Press on Demand, 2001, **5**.
X. Wang, M. Ackermann, S. Wang, E. Tolba, M. Neufurth, Q. Feng, H.C. Schröder and W.E. Müller, *Biomed. Mater.*, 2016, **11**, 035005.
K. Kamiya, K. Yanagida and J. Shirokaze, in *Animal Cell Technology: Developments Towards the 21st Century*, Springer, Dordrecht, 1995, pp. 759-763.
G. A. Howard, R. T. Turner, J. E. Puzas, F. Nichols and D. J. Baylink, *JAMA*, 1983, **249**, 258-259.
M. Shima, Y. Seino, H. Tanaka, H. Kurose, M. Ishida, H. Yabuuchi and H. Kodama, *Calcif. Tissue Int.*, 1988, **43**, 19-25.
J. M. Sautier, J. R. Nefussi and N. Forest, *Calcif. Tissue Int.*, 1992, **50**, 527-532.
T. K. P. Goh, Z. Y. Zhang, A. K. L. Chen, S., Reuveny, M. Choolani, J. K. Y. Chan and S. K. W. Oh, *BioResearch Open Access*, 2013, **2**, 84-97.
P. L. Granja, A. I. N. Silva, J. P. Borges, C. C. Barrias and I. F. Amaral, in *Key Engineering Materials*, Trans Tech Publications, 2004, pp. 573-576.
R. S. Singh, N. Kaur, V. Rana and J. F. Kennedy, *Carbohydr. Polym.*, 2017, **171**, 102-121.
Y. Yang, F. M. Rossi and E. E. Putnins, *Biomaterials*, 2007, **28**, 3110-3120.
Y. Yang, F. M. Rossi and E. E. Putnins, *Biomaterials*, 2010, **31**, 8574-8582.
T.N. Vo, S.R. Shah, S. Lu, A.M. Tatara, E.J. Lee, T.T. Roh, Y. Tabata and A.G. Mikos, *Biomaterials*, 2016, **83**, 1-11.
F. Y. Hsu, S. W. Tsai, C. W. Lan and Y. J. Wang, *J. Mater. Sci.: Mater. Med*, 2005, **16**, 341-345.
A. W. Lund, J. A. Bush, G. E. Plopper and J. P. Stegemann, *J. Biomed. Mater. Res. B*, 2008, **87**, 213-221.
L. Wang, R. R. Rao and J. P. Stegemann, *Cells Tissues Organs*, 2013, **197**, 333-343.
J. K. Wise, A. I. Alford, S. A. Goldstein and J. P. Stegemann, *Connect. Tissue Res.*, 2016, **57**, 516-525.

R. T. Annamalai, X. Hong, N. G. Schott, G. Tiruchinapally, B. Levi and J. P. Stegemann, *Biomaterials*, 2019, **208**, 32-44.
Q. Q. Qiu, P. Ducheyne and P. S. Ayyaswamy, *Biomaterials*, 1999, **20**, 989-1001.
Q. Q. Qiu, P. Ducheyne and P. S. Ayyaswamy, *Ann. N. Y. Acad. Sci.*, 2002, **974**, 556-564.
N. J. Lakhkar, R. M. Day, H. W. Kim, K. Ludka, N. J. Mordan, V. Salih and J. C. Knowles, *J. Tissue Eng.*, 2015, **6**, 2041731415617741.
M. E. L. B. A. Navarro, M. P. Ginebra, J. A. Planell, C. C. Barrias and M. A. Barbosa, *Acta Biomater.*, 2005, **4**, 411-419.
H. H. Lee, S. J. Hong, C. H. Kim, E. C. Kim, J. H. Jang, H. I. Shin and H. W. Kim, *J. Mater. Sci.: Mater. Med*, 2008, **19**, 3029-3034.
Y. M. Kong, H. E. Kim and H. W. Kim, *J. Biomed. Mater. Res. B*, 2008, **84**, 334-339.
S. Guruvenket, G. M. Rao, M. Komath and A. M. Raichur, *Appl. Surf. Sci.*, 2004, **236**, 278-284.
A. Zühlke, B. Röder, H. Widdecke and J. Klein, *J. Biomater. Sci. Polym. Ed.*, 1994, **5**, 65-78.
B. Röder, A. Zühlke, H. Widdecke and J. Klein, *J. Biomater. Sci. Polym. Ed.*, 1994, **5**, 79-88.
H. Shen, X. Hu, F. Yang, J. Bei and S. Wang, *Acta Biomater.*, 2010, **6**, 455-465.
E. A. Botchwey, S. R. Pollack, E. M. Levine and C. T. Laurencin, *J. Biomed. Mater. Res.*, 2001, **55**, 242-253.
S. W. Kang, H. S. Yang, S. W. Seo, D. K. Han and B. S. Kim, *J. Biomed. Mater. Res. A*, 2008, **85**, 747-756.